AD-A166 320 SUBMERGED ARC WELDING CONTROL VIA ARC SENSING(U) 1/2
CRC-EVANS AUTOMATIC WELDING HOUSTON TX
M D RANDALL ET AL. 31 JAN 86 CRCAW-0001AC
UNCLASSIFIED N00014-85-C-0750 F/G 13/8 NL

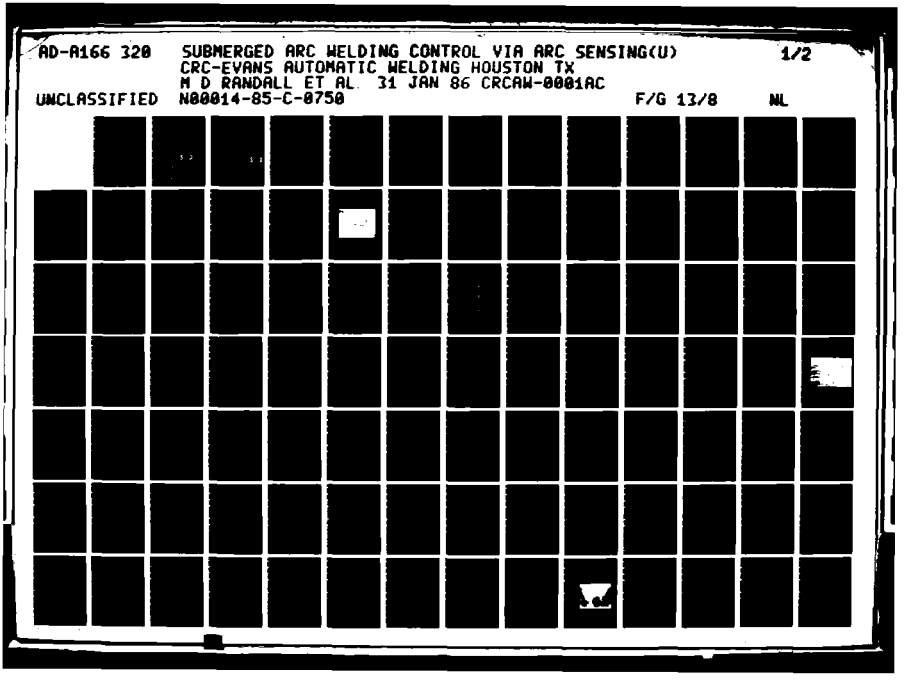

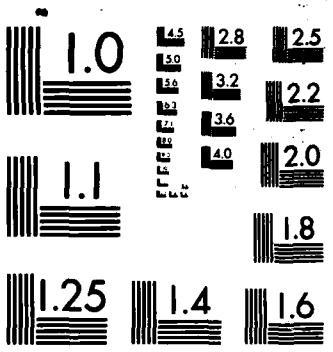

MICROCOPY RESOLUTION TEST CHART
NATIONAL BUREAU OF STANDARDS-1963-A

(2)

NR-SR1-032

Code 1131

DTIC FILE COPY

AD-A166 320

FINAL REPORT CRCAW-0001AC

on

SUBMERGED ARC WELDING CONTROL VIA
ARC SENSING - PHASE I
CONTRACT NUMBER N00014-85-C-0750

DTIC
ELECTE
APR 0 2 1986
S D
D

CRC-EVANS AUTOMATIC WELDING

PIPELINE INTERNATIONAL, INC.

DISTRIBUTION STATEMENT A
Approved for public release;
Distribution Unlimited

86 3 20 015

(12)

FINAL REPORT CRCAW-0001AC

on

SUBMERGED ARC WELDING CONTROL VIA ARC SENSING - PHASE I

CONTRACT NUMBER N00014-85-C-0750

by

MILTON D. RANDALL, GEORGE E. COOK, AND MARK E. SHEPARD

to

OFFICE OF NAVAL RESEARCH
DEPARTMENT OF THE NAVY

from

CRC-EVANS AUTOMATIC WELDING

DTIC
ELECTE
APR 0 2 1986
S D
D

DISTRIBUTION STATEMENT A
Approved for public release:
Distribution Unlimited

31 JANUARY 1986

TABLE OF CONTENTS

QUALITY INSPECTED 3

Dist Avail and/or Special

A-1

LIST OF FIGURES

LIST OF FIGURES CON'T.

LIST OF FIGURES CON'T.

LIST OF FIGURES CON'T.

LIST OF FIGURES CON'T.

LIST OF FIGURES CON'T.

LIST OF FIGURES CON'T.

LIST OF TABLES

FINAL REPORT CRCAW-0001AC
on
SUBMERGED ARC WELDING CONTROL VIA
ARC SENSING - PHASE I
CONTRACT NUMBER N00014-85-C-0750
to
OFFICE OF NAVAL RESEARCH
from
CRC-EVANS AUTOMATIC WELDING

INTRODUCTION

This program was funded by the Office of Naval Research as Phase I of the Defense Small Business Innovation Research (SBIR) Program. The overall objective of this Phase I research was to establish the feasibility of using intelligence gleaned from the electrical arc signals of the submerged arc welding (SAW) process to adaptively control the position and geometry of the weld head relative to the weld joint. By so doing, it was expected that the weld joint could be tracked accurately and that proper fusion into the joint sidewall (and/or adjacent weld beads in a multipass per layer weld) and uniform fill could be adaptively maintained in real time.

The research was conducted from 13 September, 1985 through 31 January, 1986. The effective start date of the contract was 1 August, 1985, although the contract was not received at CRC-Evans until 12 September, 1985.

This Final Report discusses the materials and equipment used, the experimental procedures followed, the analysis and results, a discussion of results, conclusions, and recommendations for continuing Phase II experimental work.

SUMMARY

Submerged-arc welds were deposited in 19.1 mm thick plain-carbon steel plate with two different joint designs: (1) single-vee groove weld with 45-dgree included angle, and (2) Narrow Gap, single-vee groove weld with 15-degree included angle. Plain-carbon steel backing bars were used with both joints. Both flame-cut and machined test plates were used.

The experimental welding equipment was instrumented to record the following instantaneous welding parameters: (1) arc voltage, (2) arc current, (3) wire feed rate, and (4) cross-seam position of the electrode. The parameters were processed using an analog-to-digital converter and appropriate filters and recorded on double-sided, double-density floppy discs.

A controlled series of welds were made representing different spatial relationships between the welding electrode and the weld joint as it affects the dynamic welding arc signals (voltage and amperage) produced. Welds were made with the axis of weld torch travel aligned with the weld joint and other welds skewed to the weld joint. Welds were made to study the effect of inclining the weld joint on contact tube-to-work (CTWD) variation.

The dynamic welding data recorded on the floppy discs were analyzed using the I*S*P analysis software system. The data were analyzed in a large variety of ways to study the power spectrum of the instantaneous voltage, current, power and impedance wareforms. A number of potential electrode centering control algorithms were investigated.

A number of important conclusions were made:

- The current and voltage signal variations that result from the lateral cross-seam oscillation are very robust and quite indicative of weld joint geometry and electrode placement relative to the joint.

- This robustness of signal should make through-the-arc sensing control of the SAW process even more sensitive than the already-established through-the-arc control of the GMAW and FCAW processes.

- The dynamics of the SAW process are substantially different than the dynamics of the other consumable electrode processes. As a result, the voltage and current variations as a function of changes in the CTWD are greater by nearly an order of magnitude as compared to the other processes.

- The lateral cross-seam oscillation of the electrode does not have a detrimental effect on the SAW weld; instead, it may offer advantages in terms of bead geometry, sidewall fusion, and perhaps strength and toughness.

° Digital data acquisition and analysis of the current and voltage signals can serve as an excellent diagnostic tool for better understanding, monitoring, and control of the SAW process.

° Unlike the other consumable electrode processes, process dynamics plays a major role in the operation of the SAW process with through-the-arc sensing for purposes of monitoring and control. While steady-state conditions have been discussed at length in the literature, the dynamic characteristics and development of dynamic models of the SAW process have not been previously addressed.

The limited research effort of the Phase I research program has shown that through-the-arc sensing and control methodology offers excellent promise for the SAW process. Indeed, the results achieved suggest that through-the-arc sensing will be potentially more powerful as a diagnostic and control tool for the SAW process than the other consumable electrode processes, where it has already met with high success. The results of this Phase I research indicates that the the SAW process may prove to be the most applicable for through-the-arc methodologies. Therefore, additional Phase 2 research is necessary and very important and is strongly recommended.

MATERIALS

The steel base material purchased for the welding experiments was 19.0 mm-thick A516 Grade 70-S4.1 PVQ, heat number 3G2070, made by United States Steel Corporation. The back up bar material was 9.5 mm- by 38.1-mm- hot-rolled A36 steel, heat number 59018. The ladle analysis provided by the mill was as follows:

Steel Type	Heat Number	Chemical Composition, Weight Percent C	Mn	Si	S	P
A516	3G2070	0.21	1.09	0.22	0.015	0.006
A36	59018	0.15	0.70	0.22	0.032	0.018

The mill-provided mechanical properties of these steels was as follows:

Steel Type	Heat Number	Yield Strength, mPa	Ultimate Strength, mPa	Elongation in 203 mm percent
A516	3G2070	337	524	25.0
A36	59018	331	469	25.7

The submerged-arc flux and filler wire were purchased from Oerlikon. The combination flux-wire is designated F72EM12K. The filler wire is identified as 2.4 mm diameter SD3, Lot F0280. The composition of this heat of wire as provided by Oerlikon was as follows:

Element	Weight, Percent
C	0.10
Mn	1.67
Si	0.30
S	0.010
P	0.009
Cr	0.08
Ni	0.05
Cu	0.06
Al	0.01
Sn	0.02

The submerged arc flux was Oerlikon OP121TT which is a basic flux of the following approximate composition:

Compound	Weight, Percent
C_AO+MgO	40
SiO_2	15
C_AF_2	20
TiO_2+ZrO_2+Al_2O_3	5

EQUIPMENT

The welding and data acquisition equipment are described in the following sections.

Welding Equipment

The submerged-arc welding power supply was a Lincoln Electric Company Idealarc DC-600, 600-ampere constant-voltage or constant-current welder. The air-cooled welding torch was mounted on a motor-driven, X-Y slide fixture to provide lateral movement and oscillation to the torch and vertical control over contact tube-to-work distance. The overall welding equipment setup is shown in Figure 1.

Figure 1. Experimental submerged arc welding equipment.

Data Acquisition Equipment

The data acquisition equipment was assembled to record dynamic arc welding parameters. The dynamic welding parameters that were recorded were: (1) arc voltage measured at the contact tip, (2) arc current measured with a 100-millivolt shunt, 500-ampere, (3) wire feed rate, and (4) crossseam position of the electrode.

Instantaneous wire feed speed was measured using a Disc Instruments Model 835-125-OBLS-TTL Optical Shaft Encoder. The glass disc of the encoder contains 500 radial lines. Light passing through the slots in the disc are converted into voltage pulses. The time interval between pulses is a measure of the rotational speed of the shaft. The shaft is driven by a fixed-diameter rubber pressure roller riding against the filler wire. The wire feed speed resolution was $\pm$ 1 percent.

The cross-seam position signal was obtained from a Trans-Tek, Series 240 linear variable displacement transformer (LVDT). This displacement transformer is an integrated package consisting of a precision linear variable differential transformer, a solid state oscillator, and a phase-sensitive demodulator. The oscillator converts the DC input to AC, exciting the primary winding of the differential transformer. Voltage is induced in the secondary windings by the axial core position. The two secondary circuits consist of a winding, a full-wave bridge, and an RC filter. The circuits are connected in series opposition so that the resultant output is a DC

voltage proportional to core displacement from the electrical center. The polarity of the voltage is a function of the direction of the core displacement with respect to the electrical center.

This Model 0243-0000 LVDT has a working range of ± 12.7 mm with a measured ± 0.2 percent of full scale linearity over the total working range. The LVDT was mounted on the X-Y fixture controlling the oscillator.

The arc voltage, arc current wire feed speed, and cross-seam filler wire position were dynamically recorded using the following data acquisition equipment:

QUANTITY	DESCRIPTION
1	Model DT2818 Analog and Digital I/O System
1	Model DT750 Backplane/Chassis Assembly
1	Model DT6792 Power Supply
1	Model DT6711 High Level Input Module
1	Model DT6712 Low Level Input Module

The analog-to-digital converter was a model DT2818 system manufactured by Data Translation Inc. The DT2818 provides simultaneous sampling (at a maximum throughput rate of 27,500 samples per second) of 4 analog inputs. The DT2818 consists of a single board which fits into one of the expansion slots on a IBM XT computer. The principal reason for choosing the DT2818 board was its feature of simultaneous sampling. If sequential sampling

were used, voltage and current could not be sampled closer together than 36 microseconds [1/(27.5 KHz)]. This corresponds to approximately a 40-degree phase shift at the 3 KHz Nyquist frequency of a 6 KHz sample rate, and would make accurate calculations of instantaneous arc power, cross-correlation, or cross power spectral density impossible at high frequencies.

The sampling rate for the preliminary welds and Test Weld 1 was 6 KHz. However, it was observed that the Lincoln Electric welding power source produced a significant ripple at 360 Hz due to the 6-pulse-controlled rectifier circuitry. Even with a 250 Hz rolloff and third-order filter, the ripple amplitude was sufficiently large to cause an aliasing problem if the sampling rate was not sufficiently high to keep the Nyquist frequency above 360 Hz. Rather than losing information with a low-frequency, antibiasing filter, a 1 kilohertz sampling frequency was chosen for the remainder of the welds. Preliminary spectral analysis showed that this sample rate was well matched to the natural rolloff of the process combined with the 250 Hz anti-aliasing filter.

The anti-aliasing filter was an active Butterworth with a stopband attenuation rate of at least 18 dB per octave. The resolution of the DT2818 was 12 bits. Therefore, two bytes were used to store each sample. With samples accumulated at a 1 KHz rate, storage requirements per second were 1,000 x 4 x 2 = 8,000 bytes per second of data. Thus approximately 36 to 40 seconds of data was stored on a single 360-Kilobyte floppy disk.

The analysis software package that was used was I*S*P, manufactured by Bedford Research. This package contains an extensive set of signal processing and related functions. As an interpretive programming language, I*S*P can be used to generate additional special-purpose programs, such as is needed for nonlinear filtering of the current signal. I*S*P is also supported by a full range of graphics functions.

EXPERIMENTAL PROCEDURE

The 19.1 mm thick, A516 steel base plate was flame cut into 203.2 by 609.6 mm pieces for the weldments. Some of the pieces were machined to produce two joint designs shown in Figure 2. The A36 steel weld backup bars were 9.5 mm thick by 38.1 mm wide. The reason for machining some of the weld joint faces was to provide a precise joint opening for electrode lateral displacements measurements. The balance of the test pieces were welded in the flame-cut condition.

The plates were fitup and tack welded to produce the 406.4 by 609.6 mm weldments. Before and between weld passes, the weld surface profile was determined using a splined template made up of multiple wires that move relative to each other. The template was pressed against the weld surface and then used to reproduce the weld cross-section on paper. Transverse shrinkage after each weld pass was made using calipers to measure the distance between the two reference points on each side of the weld joint.

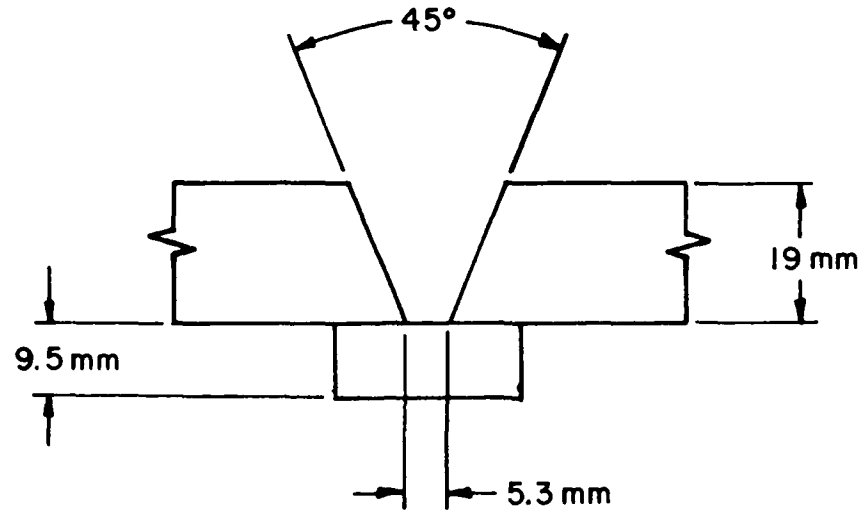

A. STANDARD JOINT DESIGN

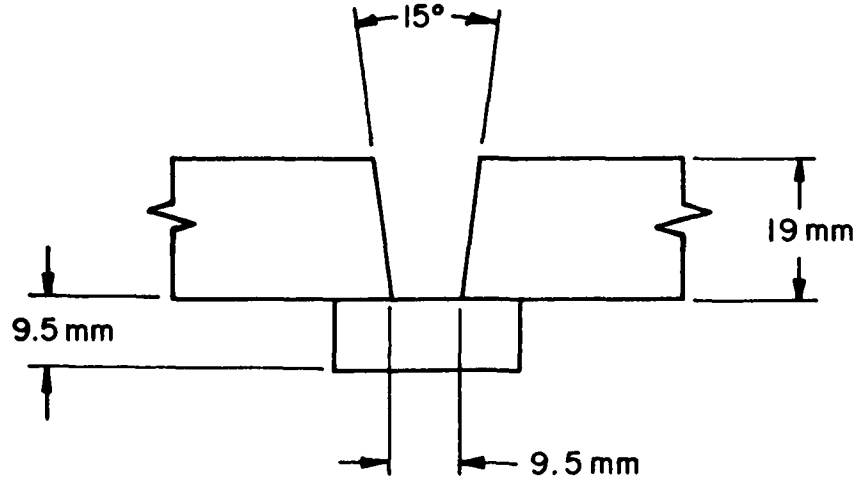

B. NARROW-GAP JOINT DESIGN

FIGURE 2. WELD JOINT DESIGNS

The welding parameters arc voltage, current, wire feed rate, and lateral displacement of the electrode were recorded dynamically on floppy discs as discussed before.

The program plan was to make a series of welds varying one welding parameter or weld joint condition or position with each weld. The root pass was deposited starting 25.4 mm from the end of the plate. Each subsequent weld pass was started 50.8 mm from the previous weld pass, thus producing a cascaded weld.

The welding parameters were recorded at various locations and under various conditions as will be discussed in the subsequent section, Analysis and Results. The experimental welds that were made in this program are summarized in Table 3.

TABLE 1. SUMMARY OF EXPERIMENTAL WELDS *

Weld No.	Pass No.	Joint Type	Arc Voltage volts	Arc Current amps.	Wire Feed Rate, mm/min.	Travel Speed mm/min.	CTWD, mm	Oscillation Width mm	Oscillation Frequency cycles/min.	Joint Skew, mm /610 mm	Data File**	Start Data, mm from start
1	1	45	31	550	3937	406	25	0	0	0	ONR011AS	25
	1										ONR011BF	407
	2					279					ONR012AS	102
	2										ONRO12BF	407
	3										ONR013AS	152
	3										ONR013BF	407
	4										ONR014AS	229
	4										ONRO14BF	432
	5										ONR015AS	254
2	1					406		3.3	240		ONR021AS	279
	2					279					ONR022AS	279
	3										ONR023AS	279
	4										ONR024AS	279
	5										ONR025AS	279
3	1					406				2.4	ONR031AS	25
	2					279					ONR032AS	76
	3										ONR033AS	127
	4										ONR034AS	178
	5										ONR035AS	229
4	1					406		Variable		0	ONR041AS	25
	2					279					ONR042AS	76
	3										ONR043AS	127
	4										ONR044AS	178
	5										ONR045AS	229
5	1	45-Inclined 6.4mm/610mm	29	500	3556	406		0	0		ONR051AS	25
	2		31	550	3937	279					ONR052AS	76
	3										ONR053AS	127
	4										ONR054AS	178
	5										ØNR055AS	229

* Blank spaces indicate repeat of previous parameter.

** Reference number of Data File: A = First data collection of weld; B = Second data collection of weld; S = Sample collection rate of 1 KHz; F = Sample collection rate of 6 KHz

TABLE 1. SUMMARY OF EXPERIMENTAL WELDS con't*

Weld No.	Pass No.	Joint Type	Arc Voltage volts	Arc Current amps.	Wire Feed Rate, mm/ min.	Travel Speed mm/min.	CTWD, mm	Oscillation Width mm	Oscillation Frequency cycles/min.	Joint Skew, mm /610 mm	Data File	Start Data, mm from start
6	1	Narrow Gap	28	425	3048	406					ONR061AS	25
	2		31	550	3937	279					ONR062AS	76
	3										ONR063AS	127
	4										ONR064AS	178
7	1	Narrow Gap	28	425	3048	406		3.3	240		ONR071AS	25
	2		31	550	3937	279					ONR072AS	76
	3										ONR073AS	127
	4										ONR074AS	178
8	1		28	425	3048	406				1.5	ONR081AS	25
	2		31	550	3937	279					ONR082AS	76
	3										ONR083AS	127
	4										ONR084AS	178
9	1		28	425	3048	406		Variable		Ø	ØNR091AS	25
	2		31	550	3937	279					ONR092AS	76
	3										ONR093AS	127
	4										ONR094AS	178
10	1	Narrow Gap Inclined 6.3mm/610mm	28	425	3048	406		Ø	Ø		ONR101AS	25
	2		31	550	3937	279					ONR102AS	76
	3										ONR103AS	127
	4										ONR104AS	178
11	1	45 Inclined 3.2mm/610mm				406		Variable	240		ONR111AS	305
	2					279						
	3											
12	1	45				406						
	2					279						
	3											
	4					239						
	5					156						

TABLE 1. SUMMARY OF EXPERIMENTAL WELDS con't*

Weld No.	Pass No.	Joint Type	Arc Voltage volts	Arc Current amps.	Wire Feed Rate, mm/min.	Travel Speed mm/min.	CTWD, mm	Oscillation Width mm	Oscillation Frequency cycles/min.	Joint Skew, mm /610 mm	Data File	Start Data, mm from start
13	1					419	12.7	10.2			ONR131AS	381
	2											
14	1			350	2413			Variable	250	2.5		
	2			550	3937							
	3					279		11.3	75		ONR143AS	
	4					216		15.9	250			
15	1			370	2667	419		6.3	250	Ø		
	2			500	3175			Variable	250			
	3			550	3937	279						
	4			540	3875	175		12.5	42		ONR154AS	76
	5			500	3175	76		25	250			
16	1			450	2413	406	19.0	Variable	250			
	2			460	3302	229						
	3			530	3810							
	4			550	3937							

ANALYSIS AND RESULTS

In this section the experimental and theoretical data analysis methods that have been investigated in the Phase I feasibility research program are described, and the results derived from these analyses are stated and discussed.

Data Acquisition and Signal Preprocessing Considerations

A major objective in this project has been the development of a computerbased data acquisition system to sample and store large amounts of welding data for later analysis using digital signal-processing methods.

Acquired signals

The four signals chosen for acquisition were voltage, current, cross-seam position, and wire feed rate. These signals provide both the arc signals (voltage and current) and information about changes in the electrode position to correlate with the arc signals. As explained earlier, voltage was measured between the torch and the workpiece. Current was obtained from a 100mV/500 A shunt in the workpiece ground lead. Cross-seam position was measured with a linear variable displacement transformer (LVDT) on the oscillating cross-slide carrying the torch. Wire feed rate was obtained with an optical encoder which was capstan-driven from the electrode wire. Figure 3 shows these transducers and the subsequent signal processing.

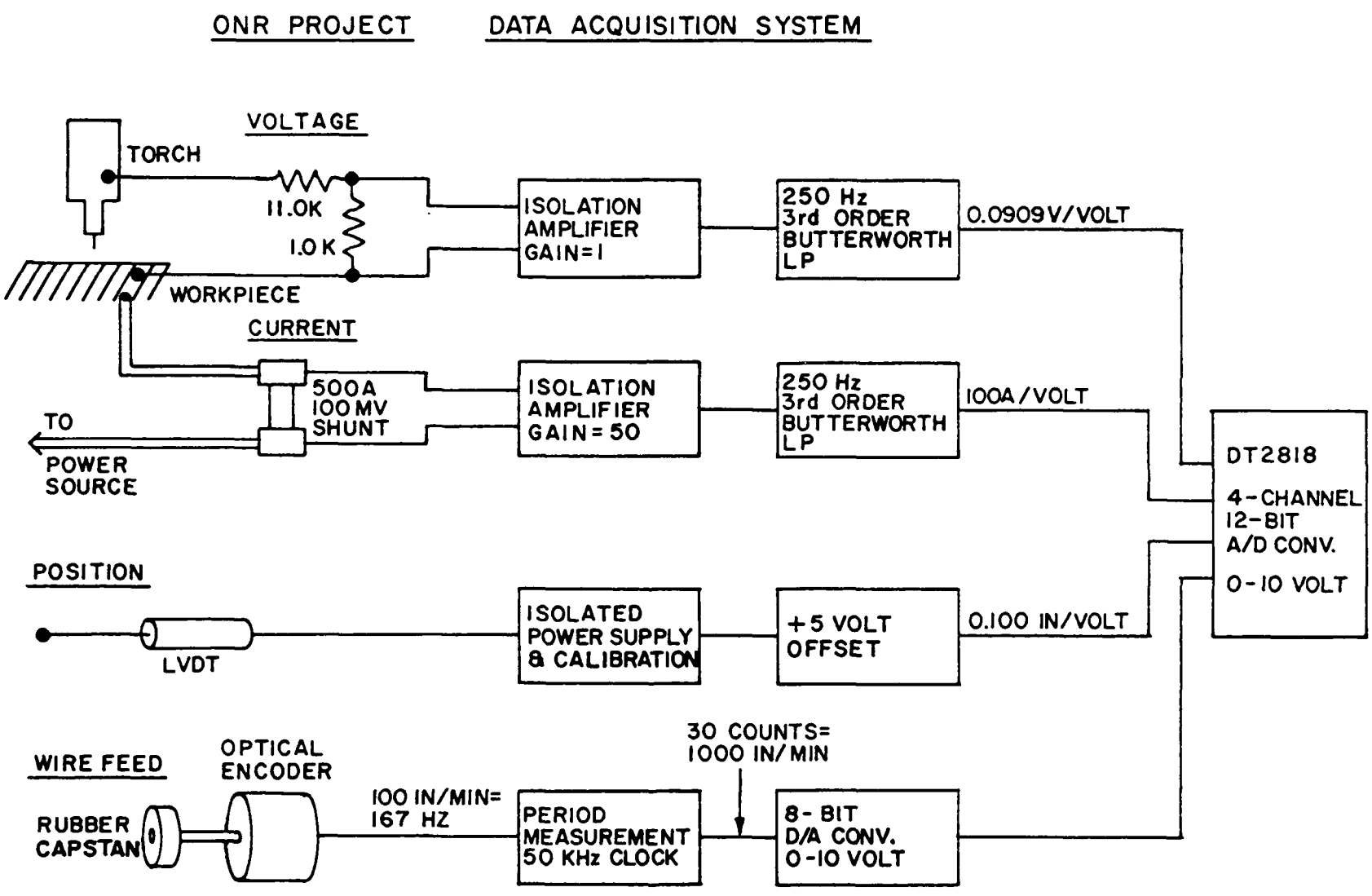

Fig. 3. Data acquisition system interconnection.

Considerable care was taken in the hardware design to avoid ground loops, multiple ground points, and the noise problems which they introduce. The voltage and current signals were taken directly from the output of the welding power supply, and were thus subject to its grounding system. To avoid having to consider grounding the computer as a part of the welding equipment, the voltage and current signals were passed through isolation amplifiers, producing signals referenced to the computer ground and separate from the welder ground. The LVDT has a separate, isolated, power supply, and its ground is tied only to the computer ground; the wire feed transducer and circuitry is also separately powered and connected only to ground at the computer.

Figure 4 shows the result of a test to assess the base noise level in the system induced by the welding equipment. The voltage input was connected to its ground reference, and the current input was connected to the low side of the shunt; both inputs thus experienced any common-mode signals present during data acquisition. A submerged-arc weld typical of those in this project was made, and data was acquired in the normal fashion. As can be seen in Fig. 4, any 60 Hz noise in the system is less than 1-bit in the A/D converters; occasional spikes are the only noise present, and they are quite small. The cross-seam oscillation is about 0.102 mm, and is the minimum setting of the oscillator. The feed rate signal represents the last value left in a counter, and is significant only in the fact that it is noise-free.

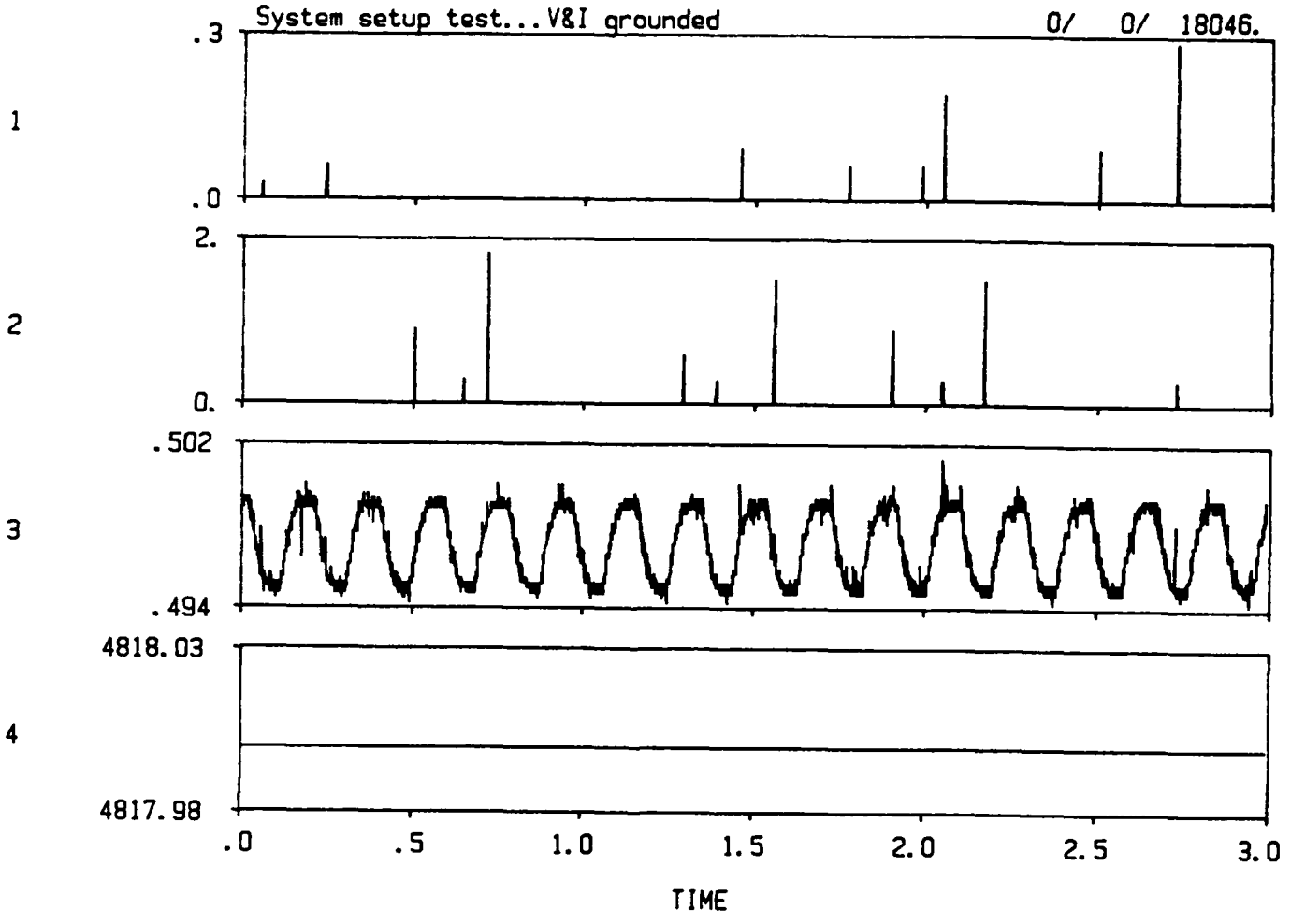

Fig. 4. Channel outputs for voltage (1), current (2), cross-seam position (3), and wire feed (4) for conditions of grounded inputs on voltage and current.

Analog Signal Processing

The voltage and current signals are processed through analog antialiasing filters. These filters have third-order Butterworth characteristics, and are implemented using operational amplifiers. The break frequency of the filters is based on the sample rate being used and the frequency content of the signals. This will be considered in more detail later.

The output signal from the LVDT is a DC voltage which swings both positive and negative around ground. The calibration of the signal is accomplished by adjusting the excitation voltage supplied to the LVDT, and it was set to give an output of 10.00 volt/inch. This was then offset by 5.00 V to give a 0-10 V swing compatible with the unipolar input range of the A/D board.

The output signal from the wire feed rate encoder is a logic signal whose frequency is proportional to feed rate. The capstan size and optical grating give a calibration factor such that 2540 mm/min feed rate produces a 166.7 Hz output signal. Simple frequency measurement techniques require counting the signal for approximately 1 second to produce 8-bit (0.25%) resolution. The objective of high-speed/wide-band width data acquisition cannot be met with a 1 Hz sample rate for feed rate. A scheme was devised in which the period of each pulse from the encoder is measured, and the resulting period converted to an analog voltage which is fed to the DT2818 A/D board in the computer. The frequency content of this signal is dependent

on feed rate, but is on the order of 200 Hz. Since the sampled signal is inversely proportional to feed rate, it must eventually be inverted numerically and scaled to provide useful results.

Calibration

The A/D converter produces an output between 0 and 4095 corresponding to input voltages of 0 and 10.00 volts. Figure 5 shows an example of raw data, with all signal values in the range 0-4095. By knowing the gains and attenuation of the various elements in the signal path, a theoretical calibration factor for each channel was determined. Actual calibration tests were done with voltage references on the voltage and current inputs, and by measuring the LVDT displacement with micrometers. The calculated scale constants produced recorded data values accurate to 0.5% of the actual voltages and currents. Figure 6 shows the same data record after scaling (and inverting the feed rate signal). Trace #1 is voltage in volts. Trace #2 is current in amperes. Trace #3 is cross-seam position in inches. Trace #4 is wire feed rate in inches/minute. Note that the cross-slide is barely moving.

Raw Data

Raw data is stored in files, each of which contains a contiguous set of samples from each of the four data signals. The size of a data file was chosen to fit onto one double-sided /double-density floppy disk, which holds

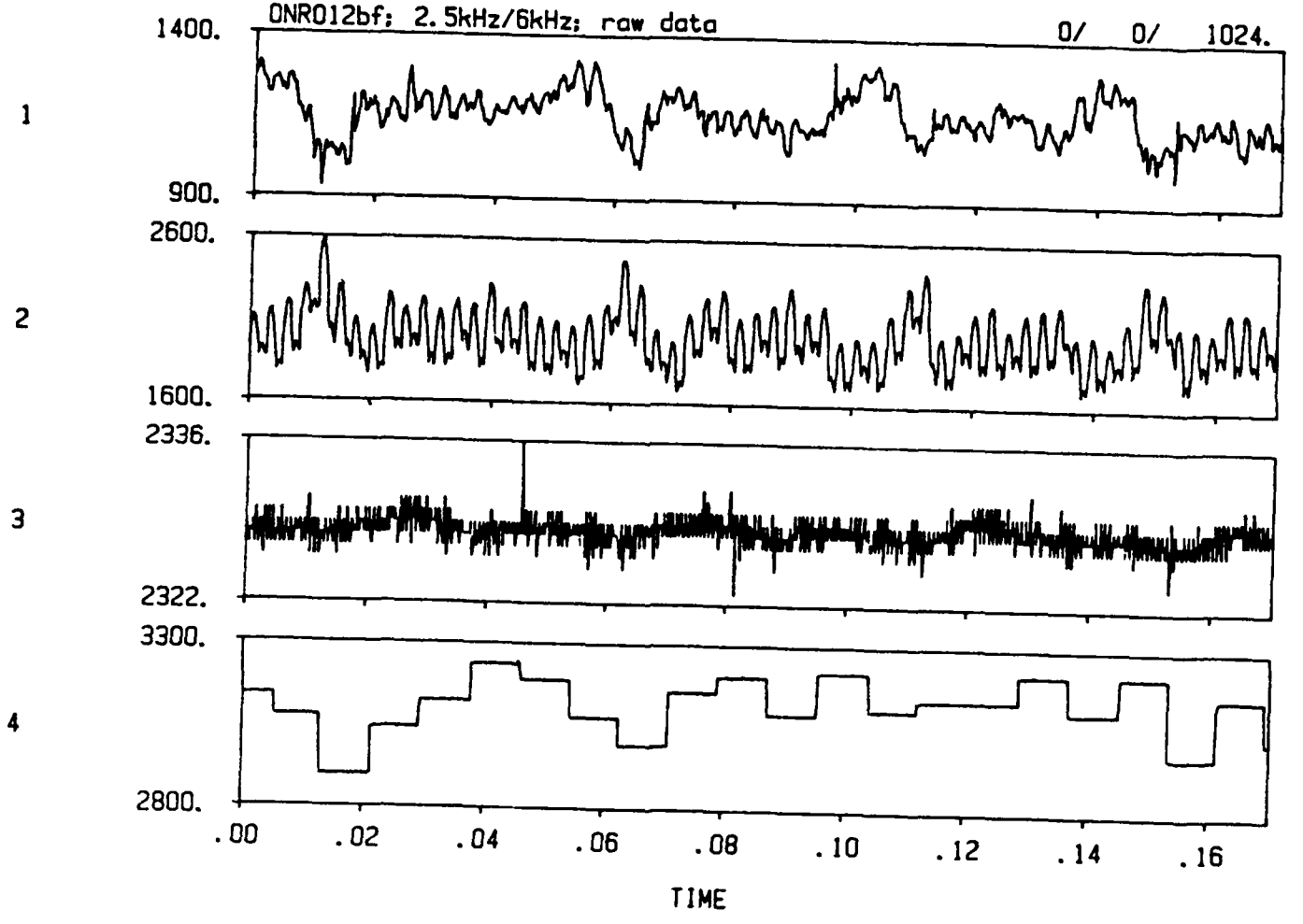

Fig. 5. Sample of unscaled signals of voltage (1), current (2), cross-seam position (3), and wire feed (4) acquired at data sampling rate of 6 kHz.

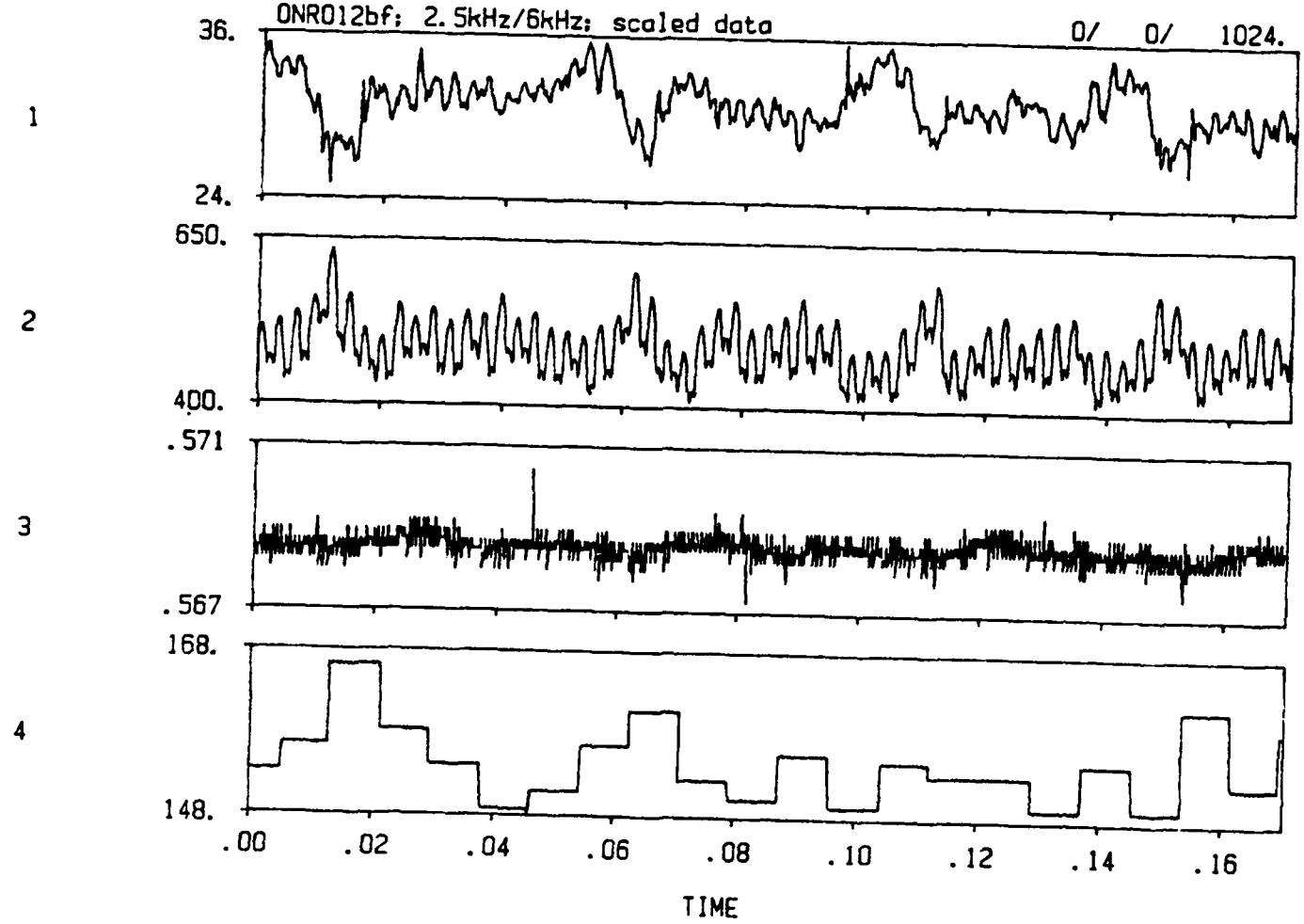

Fig. 6. Sample of scaled signals of voltage (1), current (2), cross-seam position (3), and wire feed (4) acquired at data sampling rate of 6 kHz.

360 kbytes on the IBM PC/XT. Data is acquired in the computer in blocks of 64 kbytes; five blocks are collected, giving a total of 327,680 bytes of data in a file. A 512 byte header is prepended to the data, for a total of 328,192 bytes in each raw data file.

The Data Translation DT2818 A/D board can be operated using one of the direct memory access (DMA) controllers in the PC. This mode allows data throughput rates of 27 kHz, or 6.7 kHz for each of four channels. However, because of limitations imposed by the architecture of the PC, the DMA controller cannot span 64 kbyte boundaries in memory, effectively limiting the amount of data acquired to 64 kbytes. The software distributed by Data Translation bears this limitation. To circumvent this problem, a data acquisition routine was written in assembly language to monitor the address register of the DMA controller. After the last byte of a 64K block has been written, it modifies the page register in the DMA controller to point into the next 64K block. To avoid loss of data, this operation must be accomplished in less than 37 microseconds, the conversion time of the DT2818. The program sets up the DT2818 board and DMA controller. Acquisition begins after a trigger signal is applied to the 2818. After five 64K blocks are filled, the program prompts the user for a file name and title for the data file and writes it to disk.

The format of the data files was chosen to be compatible with the data analysis software. The I*S*P software package supports data files with multiple data channels of 16-bit integer data. The required channel interleaving

for a four-channel I*S*P file is shown in Figure 7. It turns out that this is exactly the memory image of data placed in RAM by the DT2818 board in DMA mode. The only additional requirement is a header block containing information required by I*S*P about the file size, data type, sample rate, etc.

Sample Rate

With a fixed-length data file, choice of sample rate becomes a tradeoff between band width and total time of acquisition. On the one hand, it is desirable to have as many millimeters of weld bead as possible in digitized data; on the other hand, undersampling can result in aliasing problems, time skew from analog filters, and loss of important information. In this project, it was desired to acquire some data at the widest practical band width to permit evaluation of the high frequency characteristics of the arc signals, and some data at a much slower sample rate to provide long records for correlation with position information. The 6kHz sample rate yielded data records slightly less than seven seconds long, but with excellent high-frequency resolution.

The ripple components introduced by the SCR-based power source posed a problem in selecting a lower sample rate. Figure 8 is a Power Spectral Density plot of a typical SAW current signal; the sample rate is 6 kHz and a 2500 Hz analog antialiasing filter was used. The frequency axis is expanded because the frequency range from 1000-3000 Hz does not contain any significant peaks. It can be seen that a significant amount of spectral energy is

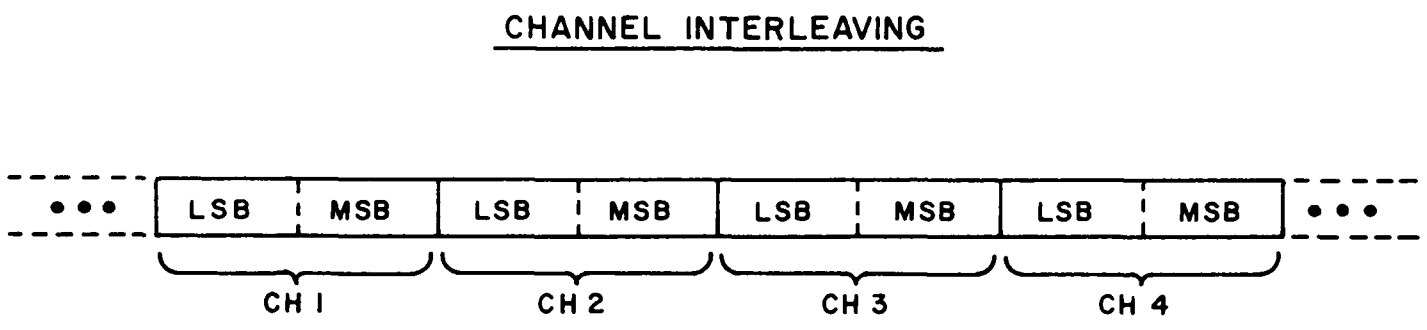

Fig. 7. Channel interleaving for 16-bit integer data (12-bits utilized for actual data).

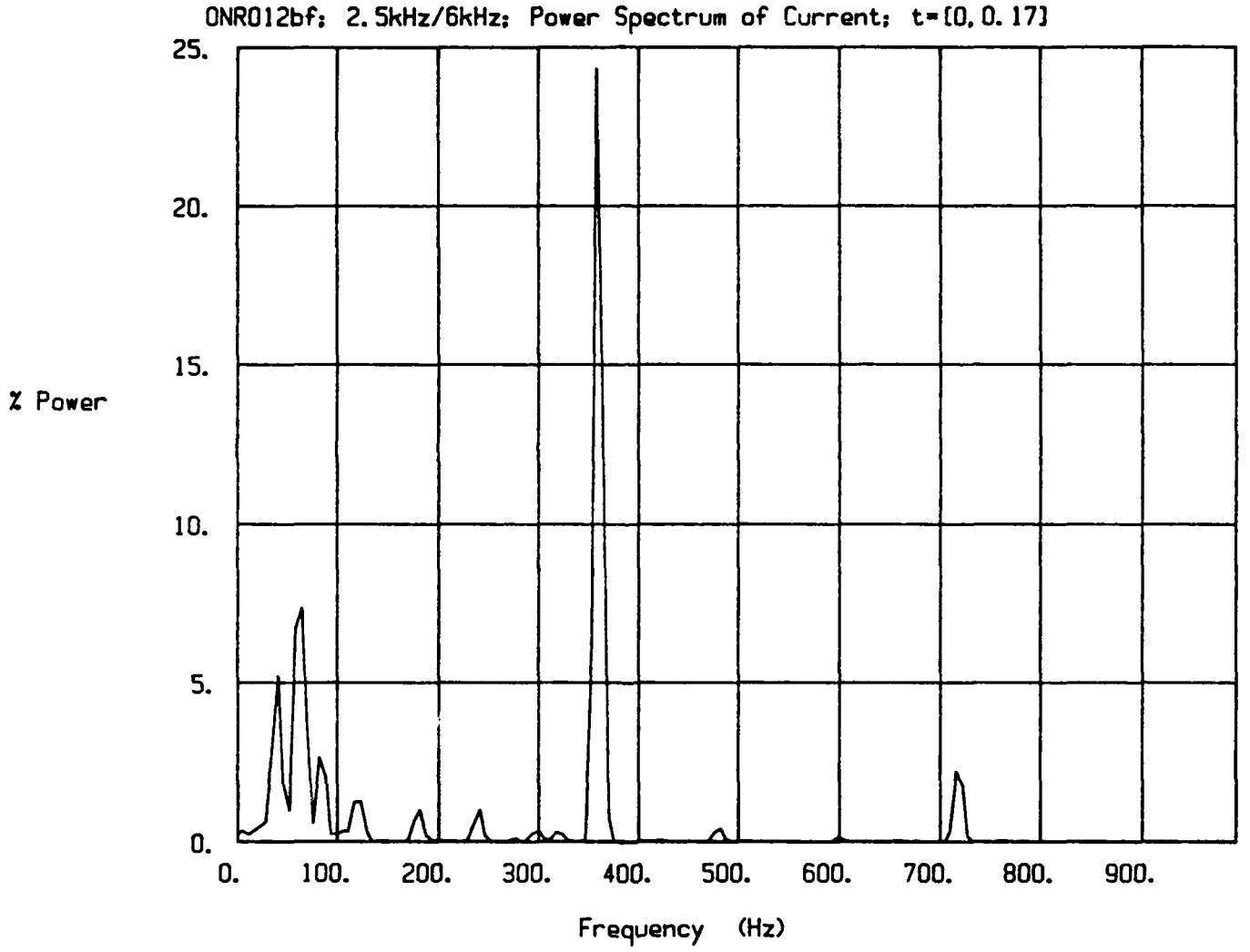

Fig. 8. Power spectrum of typical SAW current waveform with SCR type power source; sampling rate, 6 kHz, and analog antialiasing filter cutoff frequency, 2.5 kHz.

contained in the 360 Hz peak produced by the 6-pulse full-wave converter in the power source. Smaller peaks can be seen at 60, 120, 180, 240, 300, 480, 600 and 720 Hz. Figure 9 is another typical current signal sampled at 6kHz but with a 250 Hz third-order analog filter. The 360 Hz peak is seen to be attenuated when compared to the 120 Hz peak, but it is still the dominant feature of the spectrum. In Figure 10, a 250 Hz filtered current signal was sampled at 500 Hz. The 360 Hz ripple component, now above the Nyquist frequency, was not sufficiently attenuated by the antialiasing filter. It is aliased through the 500 Hz sample rate and produces the false signal at 140 Hz. Figure 11 shows the power spectrum of another current signal with the same 250 Hz filter, but sampled at 1 kHz. The 360 Hz peak is in the proper place, and the 140 Hz peak is gone. The vertical axis calibration in these plots is normalized to the total integrated power in the spectrum. Each spectrum represents the current signal from a different weld, and thus some features differ among the examples.

Data Reduction

For the purposes of extracting joint position information from the arc signals, it is desirable to reduce the amount of data which must be processed. The torch oscillation results in signals which are concentrated between 0.1 to 10 Hz. Power spectral analysis is limited by practical considerations to data blocks of 1024 samepls. At a 1 kHz sample rate, the 1024-point Discrete Fourier Transform (DFT) has a frequency resolution of 1 Hz. The most interesting spectral features are not recognizable at such poor resolution. By

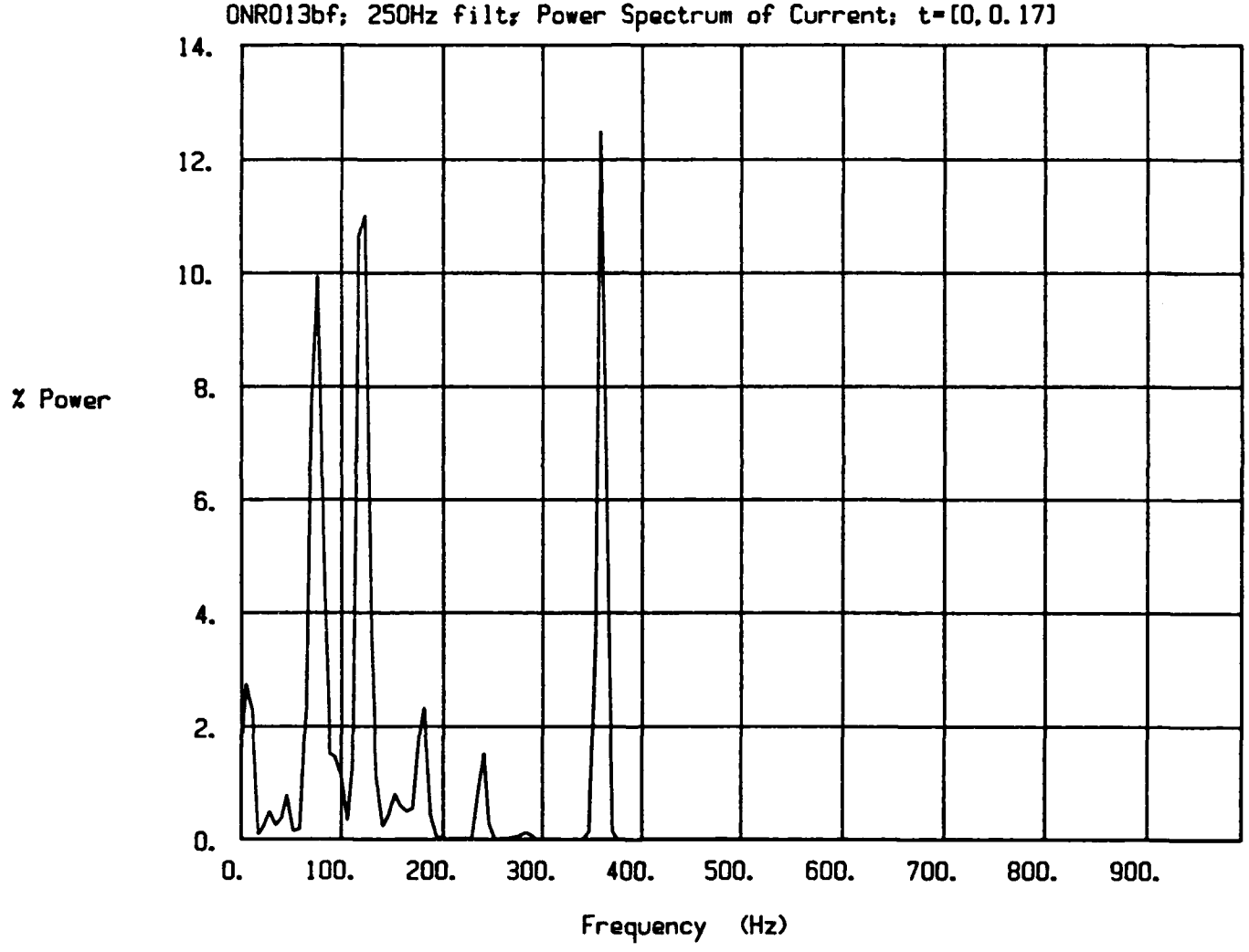

Fig. 9. Power spectrum of typical SAW current waveform with SCR type power source; sampling rate, 6 kHz, and analog antialiasing filter cutoff frequency, 250 Hz.

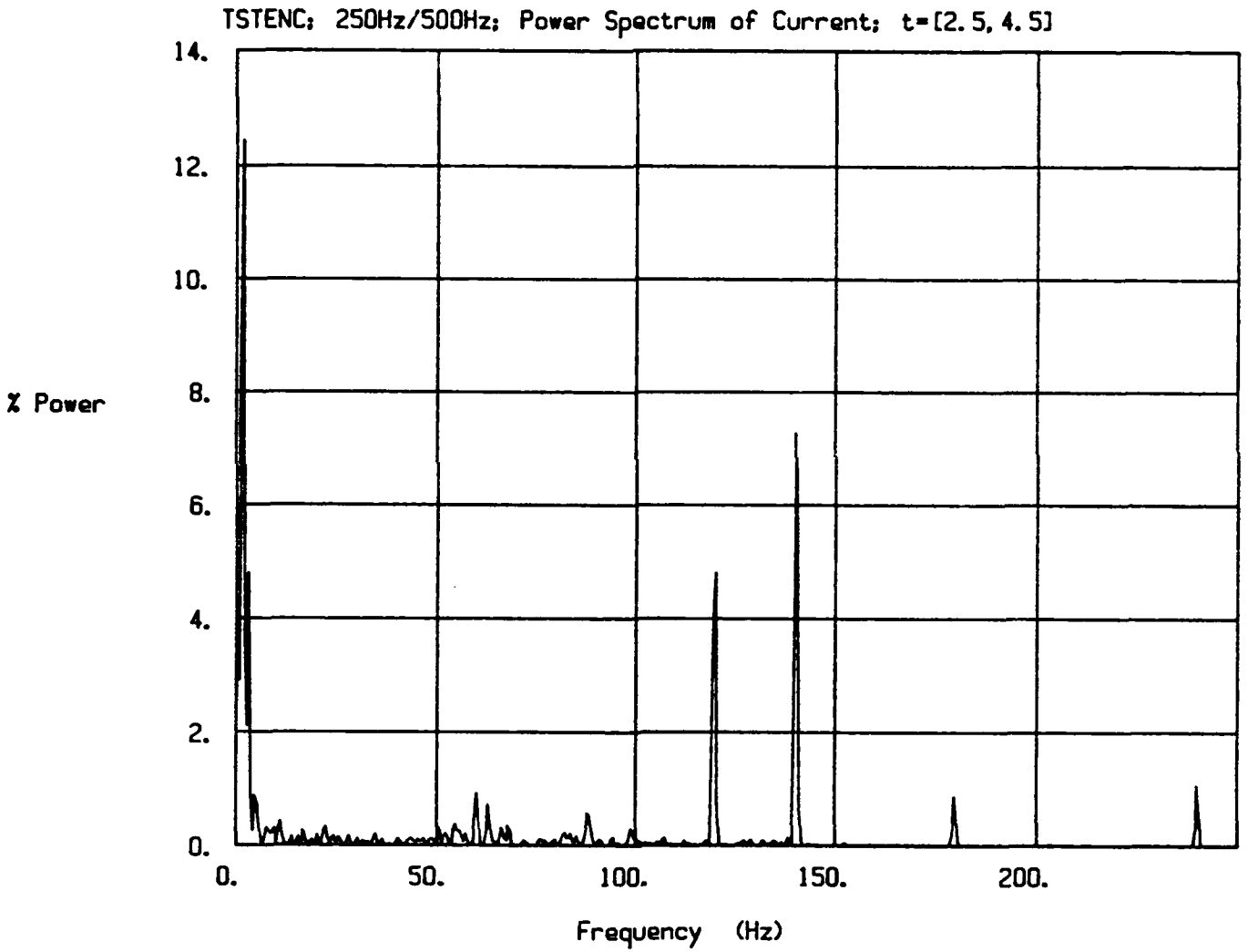

Fig. 10. Power spectrum of typical SAW current waveform with SCR type power soruce; sampling rate, 500 Hz, and analog antialiasing filter cutoff frequency, 250 Hz.

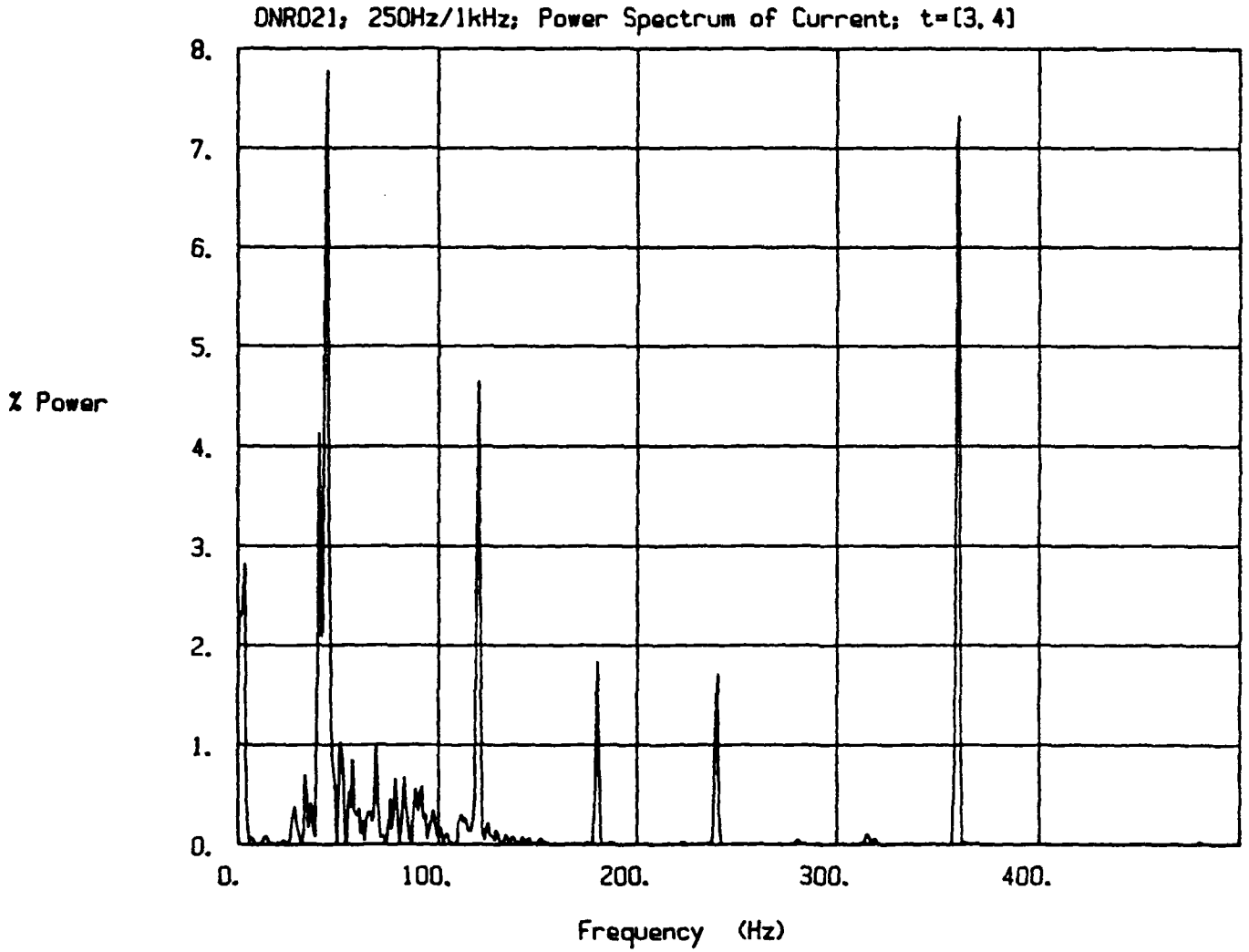

Fig. 11. Power spectrum of typical SAW current waveform with SCR type power soruce; sampling rate, 1 kHz, and analog antialiasing filter cutoff frequency, 250 Hz.

reducing the sample rate, spectral resolution can be improved with the same DFT size. A sample-rate-reduction procedure was developed and used to prepare the data for position information analysis.

The data reduction is done in two stages of filtering and decimation. Decimation is a process of reducing the sample rate by keeping every "Nth" sample in a data set. The procedure can only be used on an oversampled data set, however, or aliasing problems will occur. The solution is to filter the data to reduce its band width, then keep only the number of samples required to represent the lower-frequency data. Performing the band limiting operation with digital filters offers several advantages: (1) true linear-phase filters can be used; (2) much steeper cutoffs are realizable; and (3) exact matching of filters is possible.

The first stage reduces the sample rate from 1 kHz to 200 Hz. Figure 12 shows the 125th order FIR filter used to band limit the data. The filter is flat within 0.1 dB out to 80 Hz, and has 60 dB attenuation at 100 Hz. This is a transition band slope of almost 250 dB/octave, hardly realizable with analog components. The phase characteristic of the filter is linear, producing only a time delay in the output. If all data channels are filtered similarly, the time relationship of all data features is preserved exactly. The filter introduces no distortion and does not affect frequency components below 80 Hz. After the data is band-limited, every fifth sample is retained. Figure 13 is the power spectrum of a typical current signal, showing the effective band limiting of the filter.

	BAND 1	BAND 2	BAND
LOWER BAND EDGE	.0000E+00	1.0000E+02	
UPPER BAND EDGE	8.0000E+01	5.0000E+02	
DESIRED VALUE	1.000000	.000000	
WEIGHTING	1.000000	10.000000	
DEVIATION	.012434	.001243	
DEVIATION IN DB	-38.107850	-58.107850	

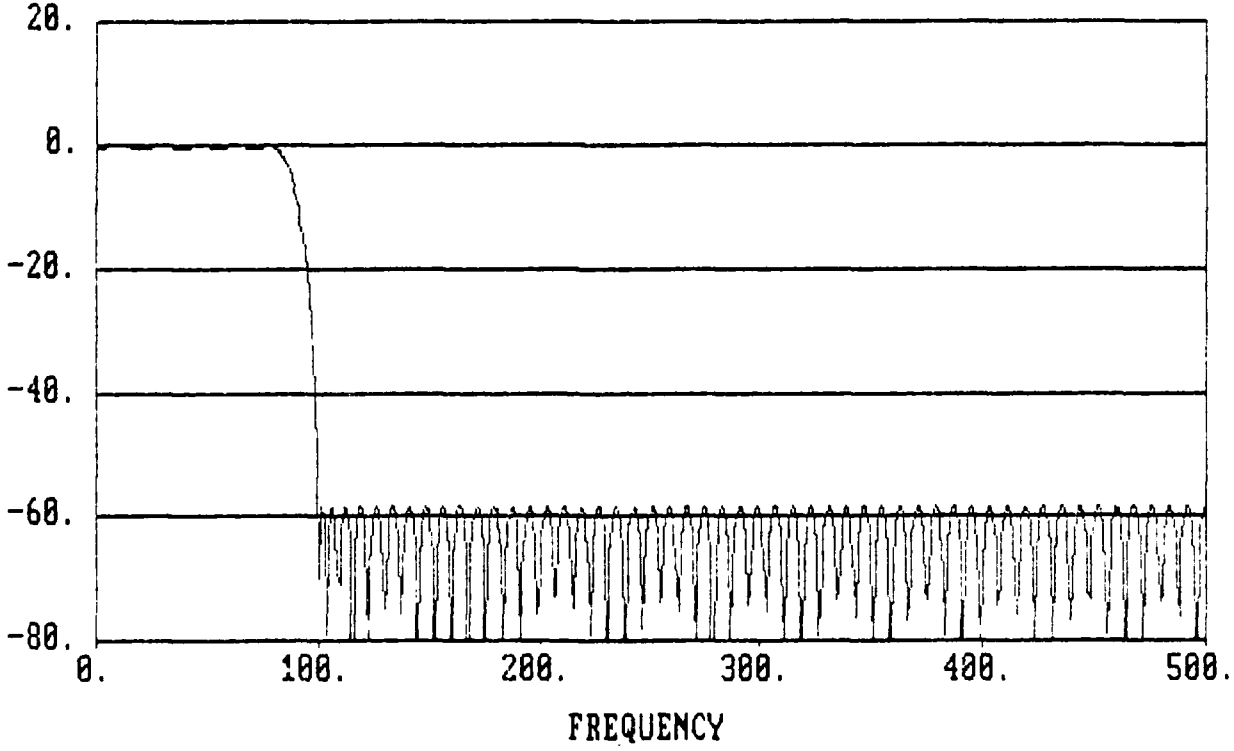

ISP>hard

Fig. 12. Frequency response of 125-th order finite impulse response (FIR) filter used in data reduction (first stage).

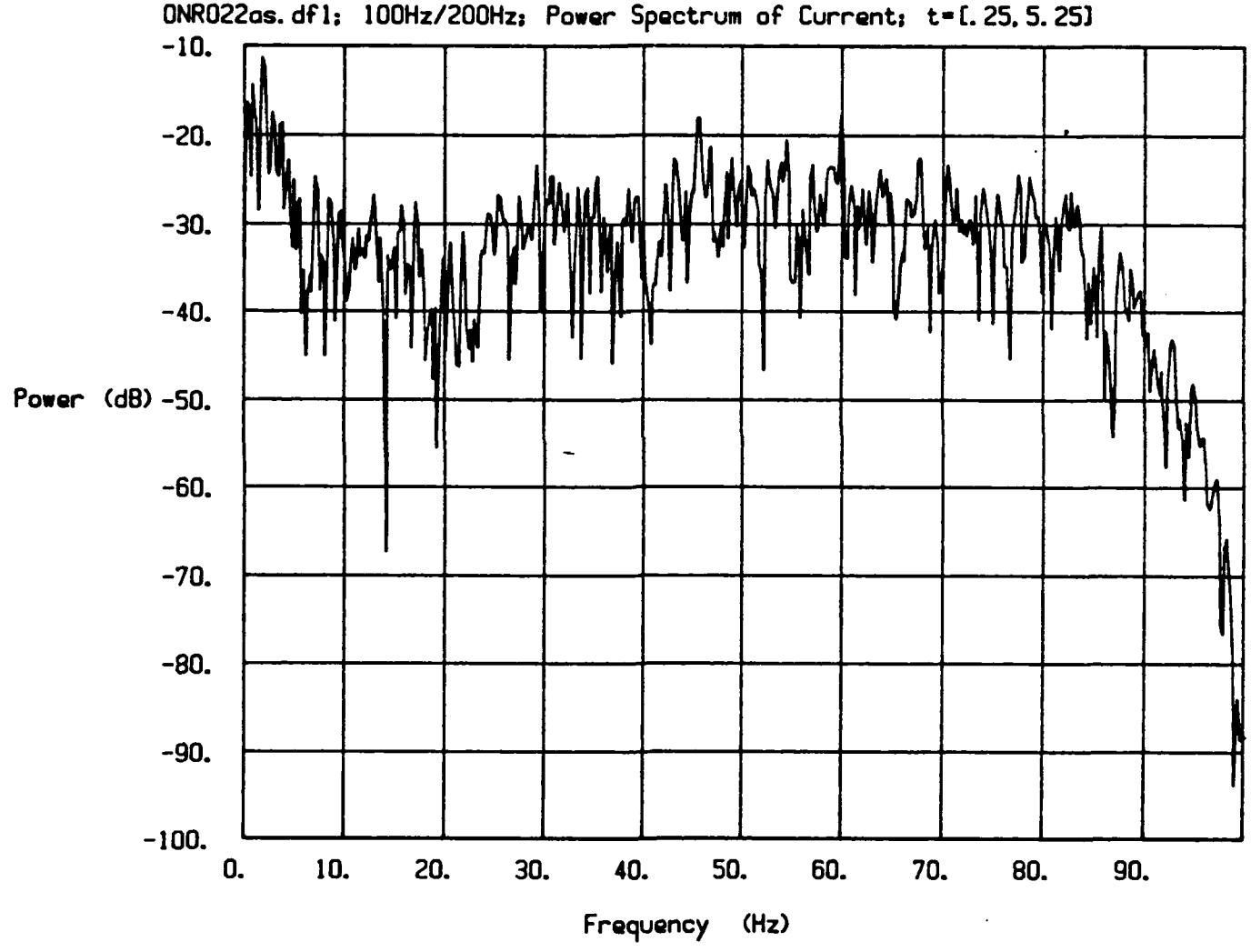

Fig. 13. Power spectrum of current waveform after filtering and decimation to 200 samples per second.

The second stage reduces the sample rate by a further factor of four by a similar filtering/decimation operation. Figure 14 shows the frequency response and ripple characteristics of the filter, and Figure 15 is a power spectrum of a current signal reduced to a 50 Hz sample rate. Figures 16 and 17 show the steps in the two stages of the procedure, including the number of samples and data file size at each step.

The decimation factor of 20 yields a data file with two 1024 sample records, simplifying FFT operations on the data. The 25 Hz band width appears adequate for initial analysis of seam-tracking information. By performing the sample-rate reduction operation on the 1 kHz sampled data, a data set is produced which retains the true time-relationship of all components of the signals.

Waveform Feature Recognition

Through-the-arc sensing is based on variations in the electrical signals as the electrode is oscillated back and forth across the welding joint. The variations in the electrical signals occur in response to the variations in the contact tip-to-work distance (CTWD), which varies as a function of the joint geometry. For a sudden change in the CTWD, there will be virtually an instantaneous change in the arc voltage and a corresponding change of opposite direction in the current. The new operating point that results from this sudden change will exist only momentarily. The wire feed rate (assumed constant) no longer equals the melting rate, and the system acts to reestablish

	BAND 1	BAND 2	BAND
LOWER BAND EDGE	.0000E+00	2.5000E+01	
UPPER BAND EDGE	2.0000E+01	1.0000E+02	
DESIRED VALUE	1.000000	.000000	
WEIGHTING	1.000000	10.000000	
DEVIATION	.004535	.000453	
DEVIATION IN DB	-46.869210	-66.869210	

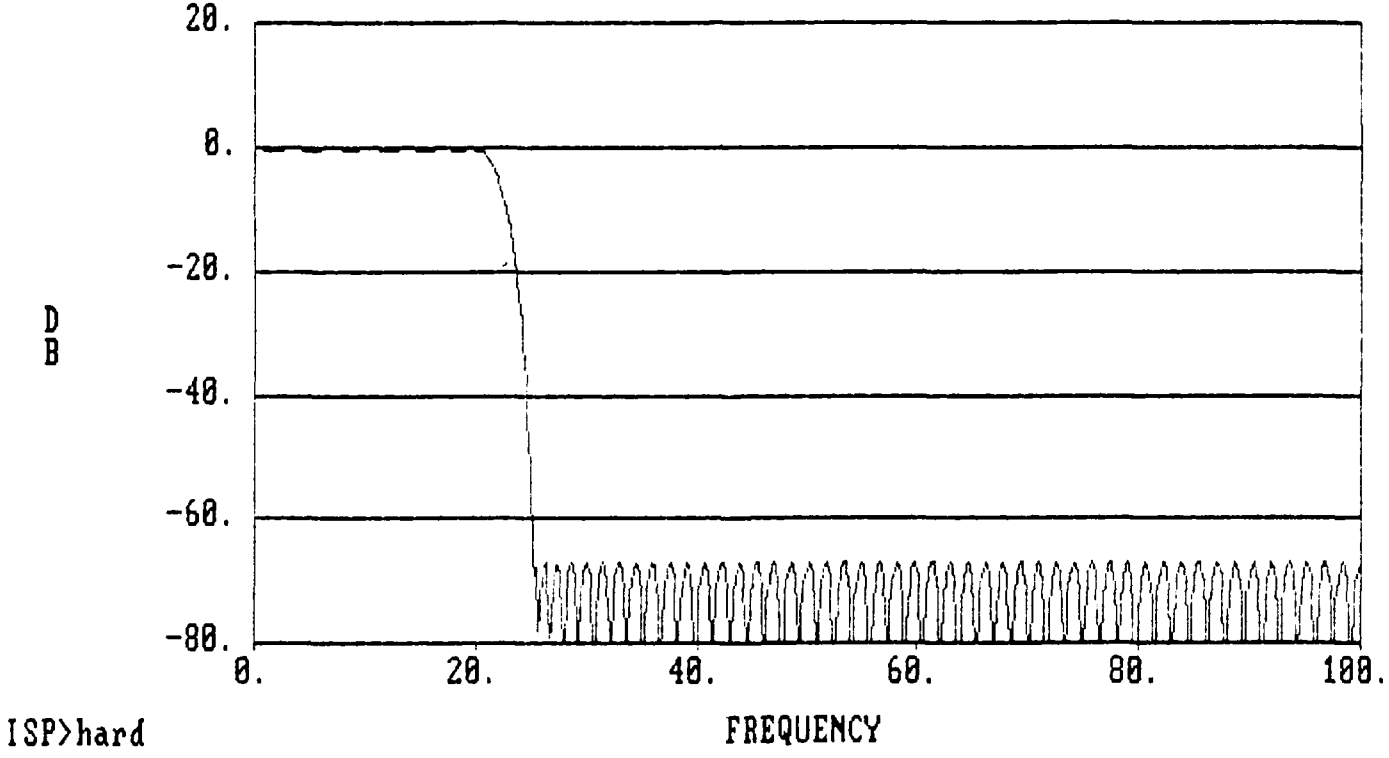

ISP>hard

Fig. 14. Frequency response of 125-th order finite impulse response (FIR) filter used in data reduction (second stage).

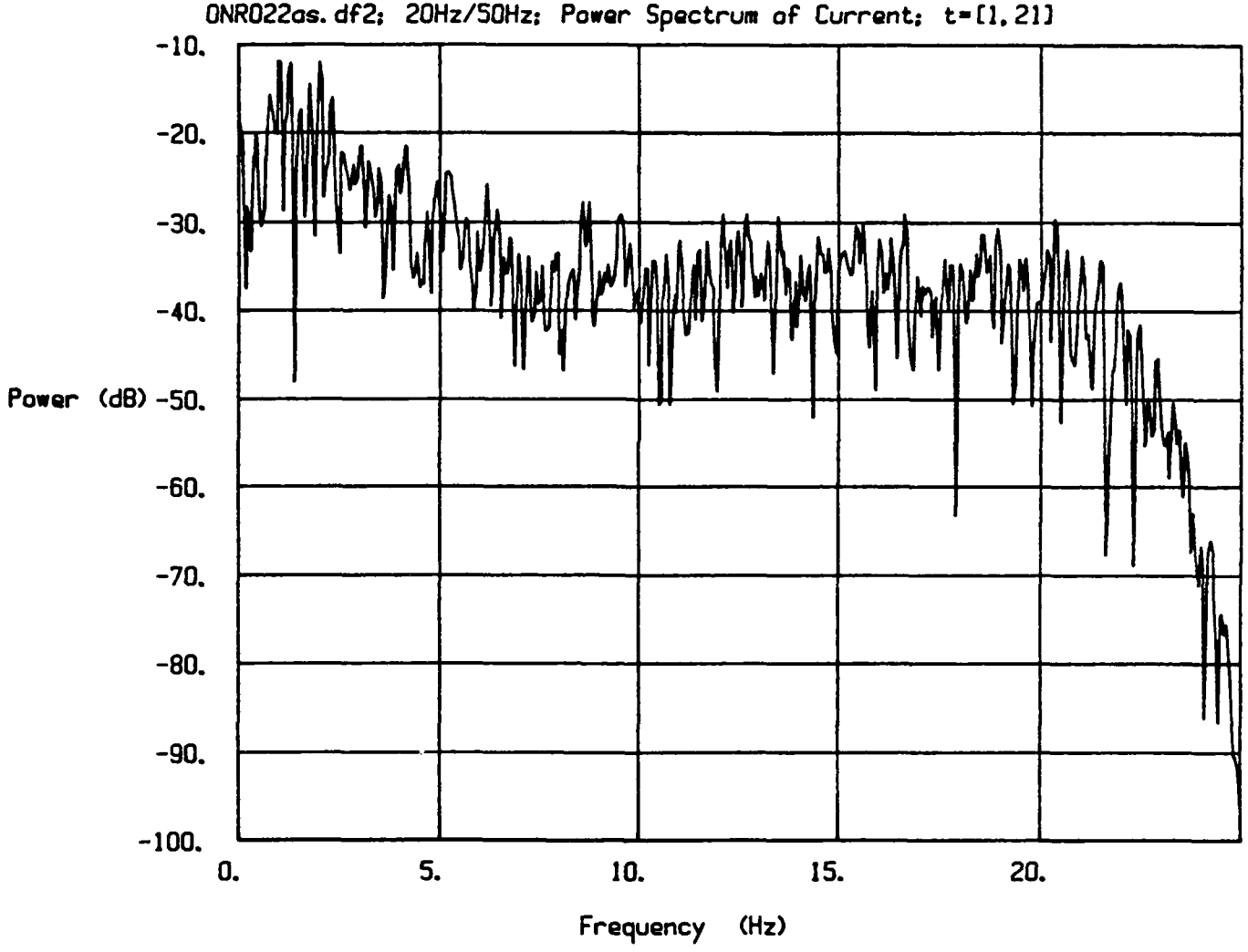

Fig. 15. Power spectrum of current waveform after filtering and decimation to 50 samples per second.

ONR PROJECT

PRELIMINARY DATA REDUCTION

(STAGE 1)

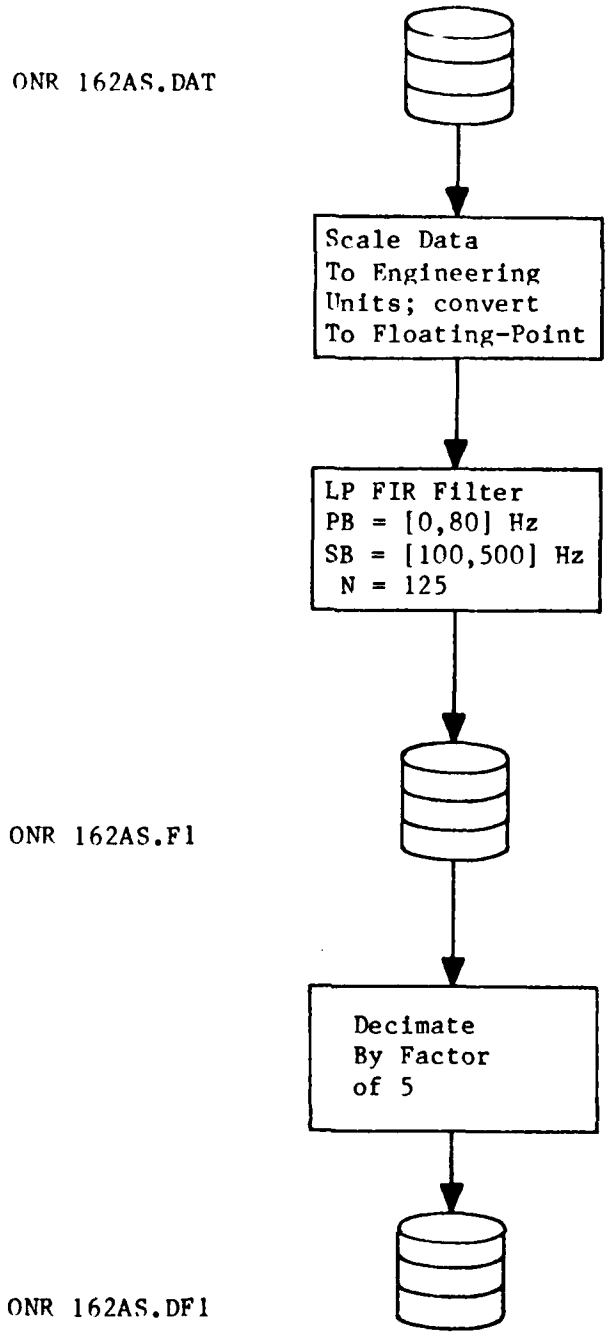

Raw Data
1 KHz Sample Rate
40960 16-bit Integer Samples
327,680 + 512 = 328,192 Bytes

Filtered and Scaled
1 KHz Sample Rate
100 Hz Bandwidth
40960 32-bit Floating Point Samples
655,360 + 512 = 655,872 Bytes

Filtered, Scaled and Decimated
200 Hz Sample Rate
100 Hz Bandwidth
8192 32-bit Floating Point Samples
131,072 + 512 = 131,584 Bytes

Fig. 16. Preprocessing data reduction method, stage 1.

4 DATA CHANNELS/SAMPLE

(STAGE 2)

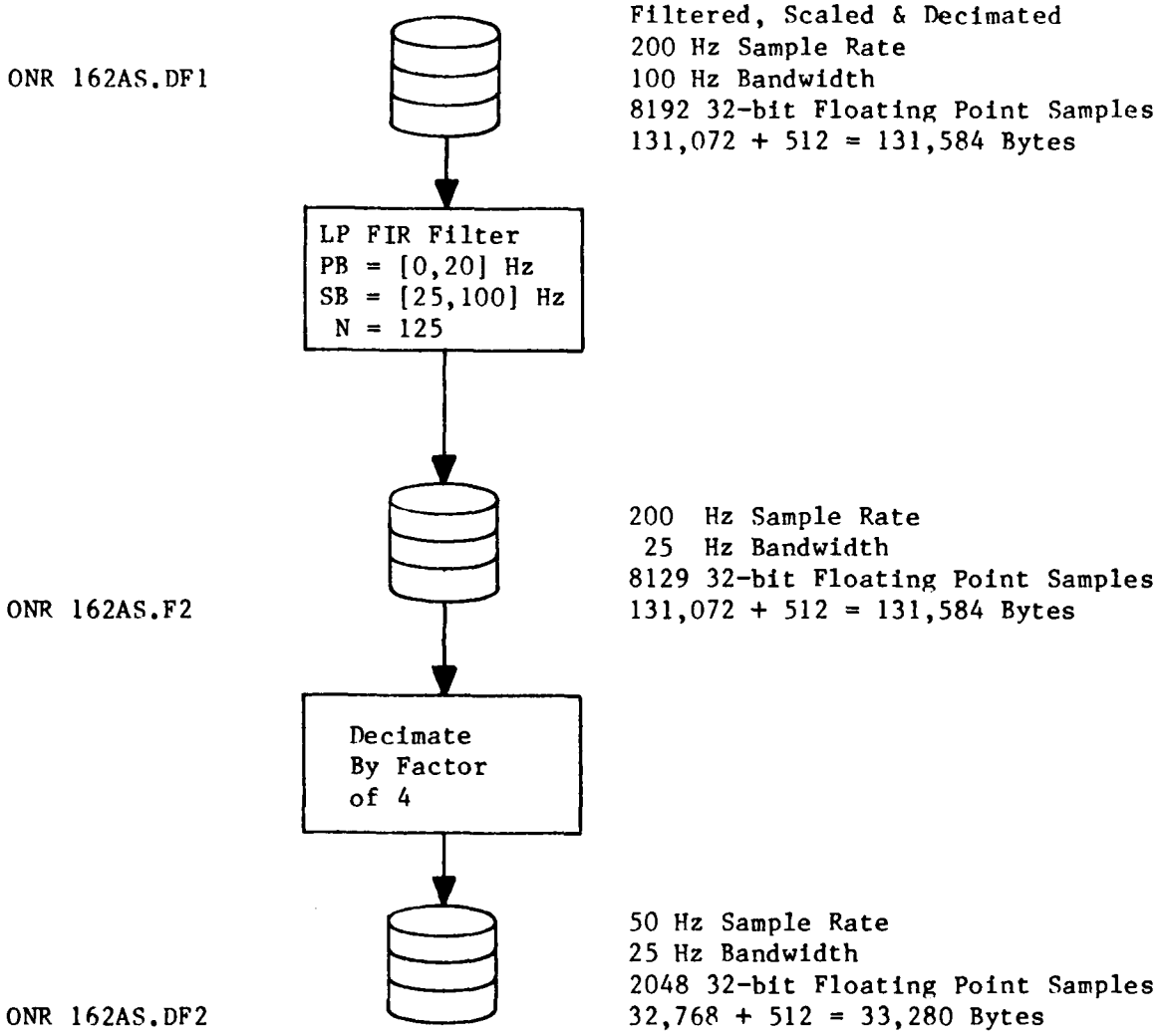

Fig. 17. Preprocessing data reduction method, stage 2.

an equilibrium. Assuming a constant potential, self-regulating system, the operating point will, in time, return to within a few percent of the voltage and current values that existed prior to the sudden change in the CTWD. The difference between the new steady state operating point and the old operating point will be reflected primarily in a small change in the electrode extension with the steady state arc length remaining essentially constant.

The rate at which the system reestablishes the new steady state operating point is a function of the power source characteristic, the arc characteristic, the electrode extension, the wire size, and the properties of wire material. For most applications of gas-metal-arc welding (GMAW) and flux-core-arc welding (FCAW), the desired welding conditions are such that the time constant of the self-regulating process is shorter than the oscillation rate. Hence, the steady state operating point "follows" the change in CTWD as the electrode traverses across the joint. The operation of these systems thus depends on the relatively small change in steady state operating conditions due to the change in the electrode extension.

For the SAW process, however, the larger size of the electrode results in a longer time constant for the self-regulating process. Indeed, the tests conducted in this Phase I research program have shown that the self-regulating time constant for the SAW process is comparable or slower to what would be considered reasonable and desirable oscillation rates. As a result, electrical signal variations that result from oscillation of the SAW electrode back and forth across the joint are transient in nature and hence,

considerably more robust than those that occur in steady state. This is advantageous from the standpoint of signal processing and maintenance of reliable control. However, to fully exploit the capabilities of this phenomenon, a more thorough understanding of the system and signal dynamics are required. (The Phase II research program will place considerable emphasis on these considerations).

Transient Considerations

To demonstrate the transient characteristics of the voltage and current signals of the SAW process, a series of bead-on-plate welds were made over a stepped plate constructed as shown in Figure 18. Each of the straps were 9.4 mm by 37.5 mm. The straps were tack welded in place prior to running the test. The nominal voltage was 31 volts, the nominal wire speed was 3750 mm/min, the CTWD was 25.4 mm, and the travel speed was 650 mm/min.

Representative results of the voltage and current transients are shown in Figure 19. The voltage waveform is labelled #1, and the current is labelled #2. As can be seen, as the weld moves onto the stepped transition, there is a rapid decrease in the voltage and a slightly delayed, large increase in the current. This is followed by a large transient in both the voltage and current with overshoot and undershoot. After the transient settles down, the steady state current is approximately 11% greater than the steady state current prior to the transition onto the strap. This corresponds to roughly 1.5% change in current per mm change in the CTWD.

Fig. 18. Stepped plate, bead-on-plate weld with SAW process.

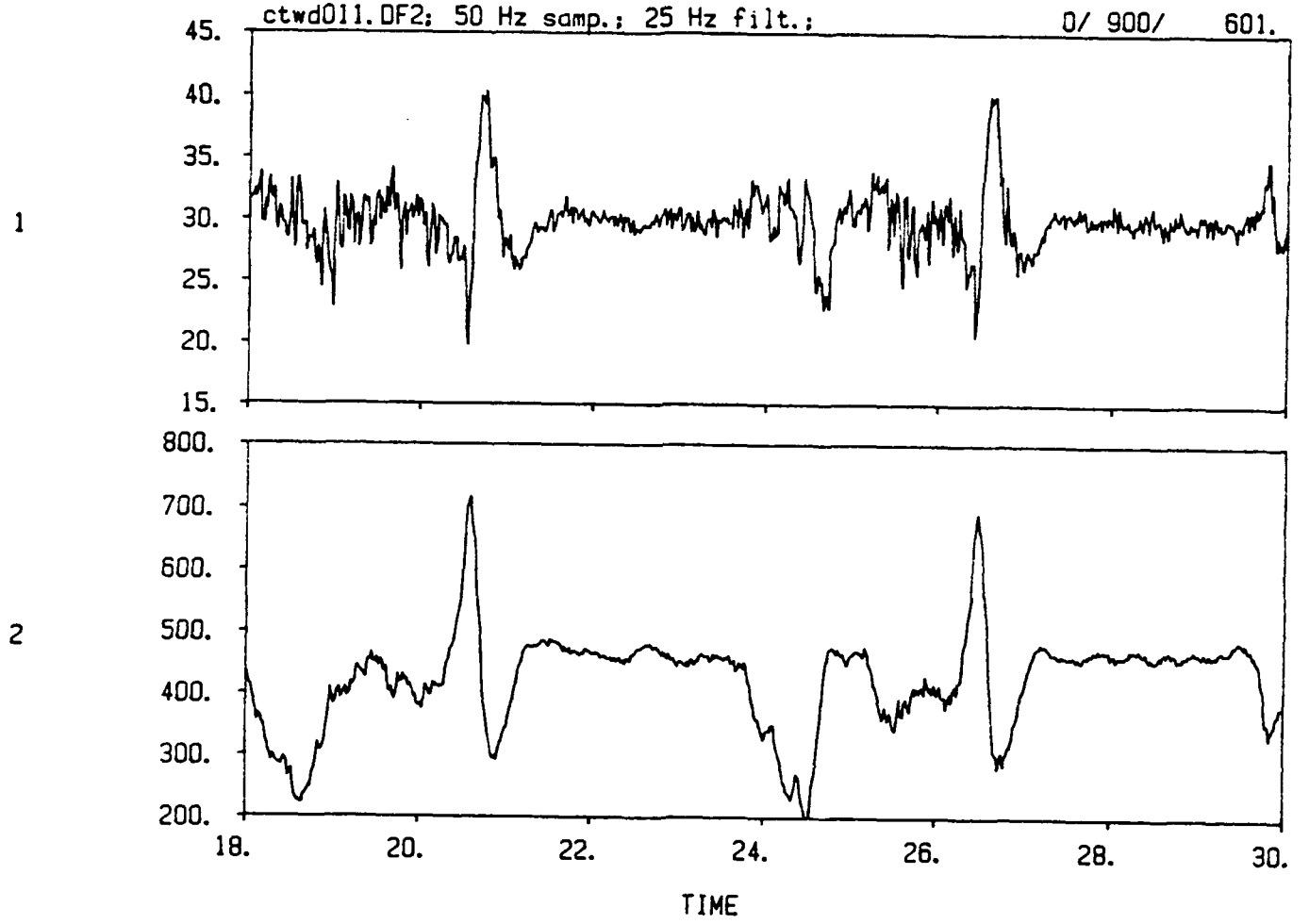

Fig. 19. Transient waveforms of voltage (1) and current (2) for SAW process test.

This steady state response is typical of the levels of current change normally anticipated with typical parameter settings (including cross-seam oscillation rate) for GMAW or FCAW, where the duration of the transient is considerably less.

For the SAW process, the experimental transient characteristics shown in Figure 19, show that the total transient time is roughly one second, which is typical of an entire cycle of cross-seam oscillation. As a result, for the SAW process, the rate of change of the CTWD, as the electrode approaches the sidewall, may be expected to be equal to or greater than the transient time of the self-regulation process. As stated previously, we may thus conclude that for typical welding conditions with the SAW process, the electrical signal variations will be captured in their transient mode, and as a result, will be considerably more robust than normally encountered with typical conditions of through-the-arc sensing as applied to GMAW or FCAW. (Once again, this points to considerable more work needed in the Phase II research program for both theoretical modeling of the process dynamics and representative power sources, and experimental testing under a much broader range of variables and conditions than time or resources permitted in the Phase I feasibility research program).

Waveform Feature Characterization on Skewed Joint

A series of welds were run in which the travel path of the electrode was skewed with respect to the joint centerline. With this condition, it

would be expected that the arc signals would initially indicate good centering of the electrode in the joint, and that the signals would indicate a gradual deterioration of proper centering as the weld progressed.

Weld number 14, third pass (Data File ONR143 AS) was one of the welds chosen to demonstrate this skewed condition. This weld pass (number 3) was made with the joint skewed with respect to the line traversed by the electrode by approximately 2.5 mm over the 600 mm length of the weld. The nominal current was 550 amperes, the nominal voltage was 31 volts, the CTWD was 12.7 mm, the wire speed was 3937 mm/min, the travel speed was 279 mm/min, the peak-to-peak oscillation width was 11.25 mm, and the oscillation frequency was 1.25 Hz.

Figure 20 shows the current, voltage, cross-seam position, and wire speed broken down on a cycle by cycle basis. The trace labelled #1 is the voltage, the trace labelled #2 is the current, the trace labelled #3 is the cross-seam position, and the trace labelled #4 is the wire speed. It can be seen that at each extreme of the cross-seam oscillation excursion, the voltage decreases and the current increases. We will see later that the instantaneous power decreases at each extreme of the cross-seam oscillation excursion as well. Since the instantaneous power is equal to the product of the instantaneous voltage and the instantaneous current, we would conclude from this observation that the voltage decreases proportionately more than the current increases, otherwise the instantaneous power would remain constant or show an increase at the peaks of oscillation excursion. (Both theoretical modeling of the process dynamics and more

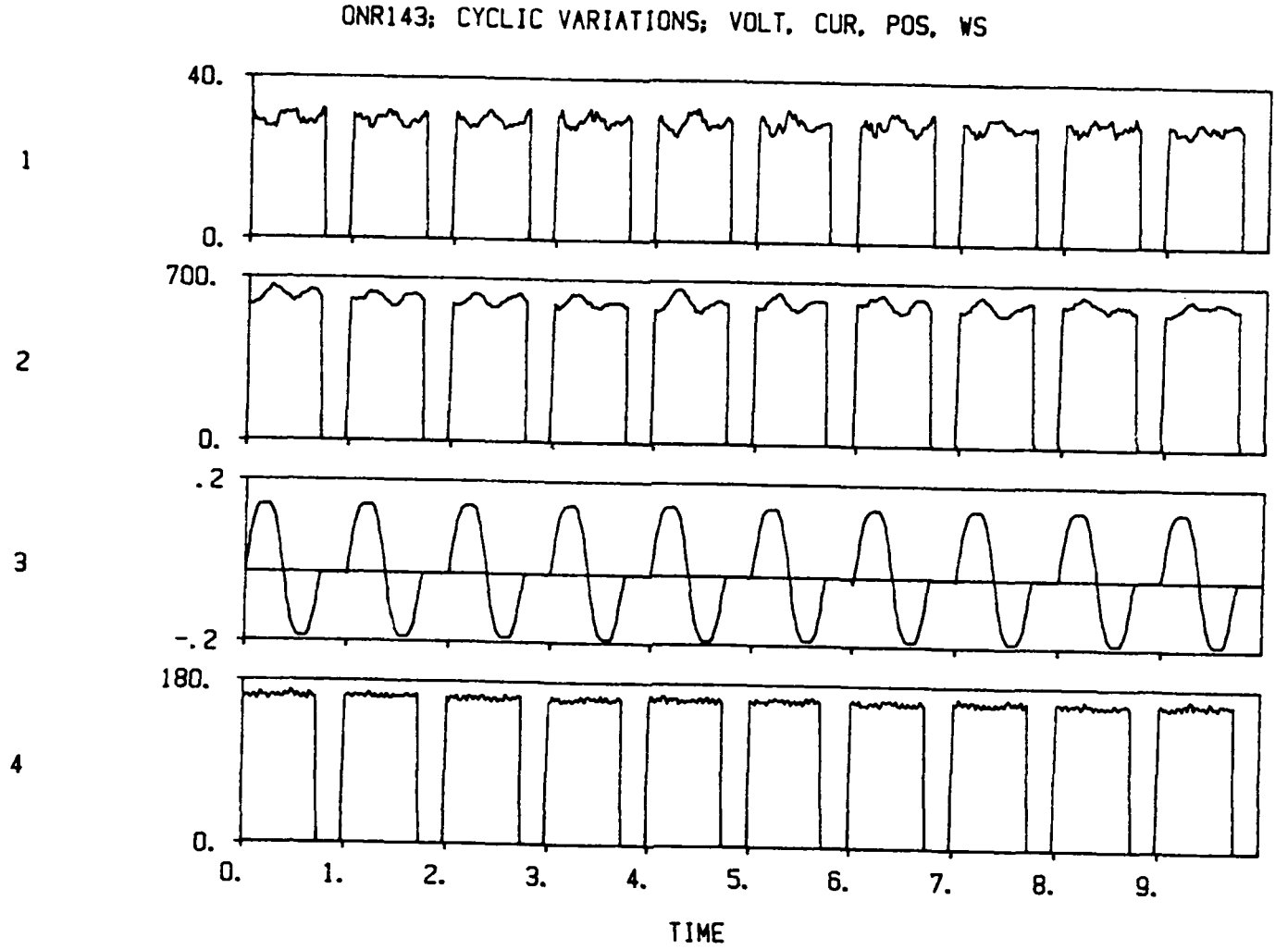

Fig. 20. Cycle by cycle variations of voltage (1),current (2), position (3), and wire speed (4) for first ten cycles of skewed joint test.

extensive experimentation will be required in the Phase II research program before any general conclusions relative to these observations can be reached).

The objective of decomposing the various recorded waveforms on a cycle-by-cycle basis was to permit cycle-by-cycle analysis and modeling of an adaptive processing system. Figure 21 shows the first 10 cycles of the cross-seam position as a function of time. The results show, as expected, a steady transistion from one peak excursion to the other. For this particular test, the peak cross-seam excursion is 3.75 mm. The cross-seam position curves shown in Figure 21 serve as a useful base of comparison for the corresponding electrical signal variations.

The cycle-by-cycle variations in current are shown in Figures 22-26. The two extreme points of the cross-seam oscillation correspond to the left and right sides of these figures. Each figure contains 10 cross-seam oscillation cycles.

The first ten cycles are plotted in Figure 22. As can be seen, there is a slight bias toward the right-hand side of the plot, i.e., the current peaks are somewhat greater on the right side. This observation is confirmed in the plots produced in the section Pattern Recognition and Control Algorithms. It is shown there that over the portion of the weld where data was gathered, there is indeed a slight offset to the left at the start of the data collection period. The percentage increase in current at each side is approximately 10% of the current at the center of oscillation. This is a

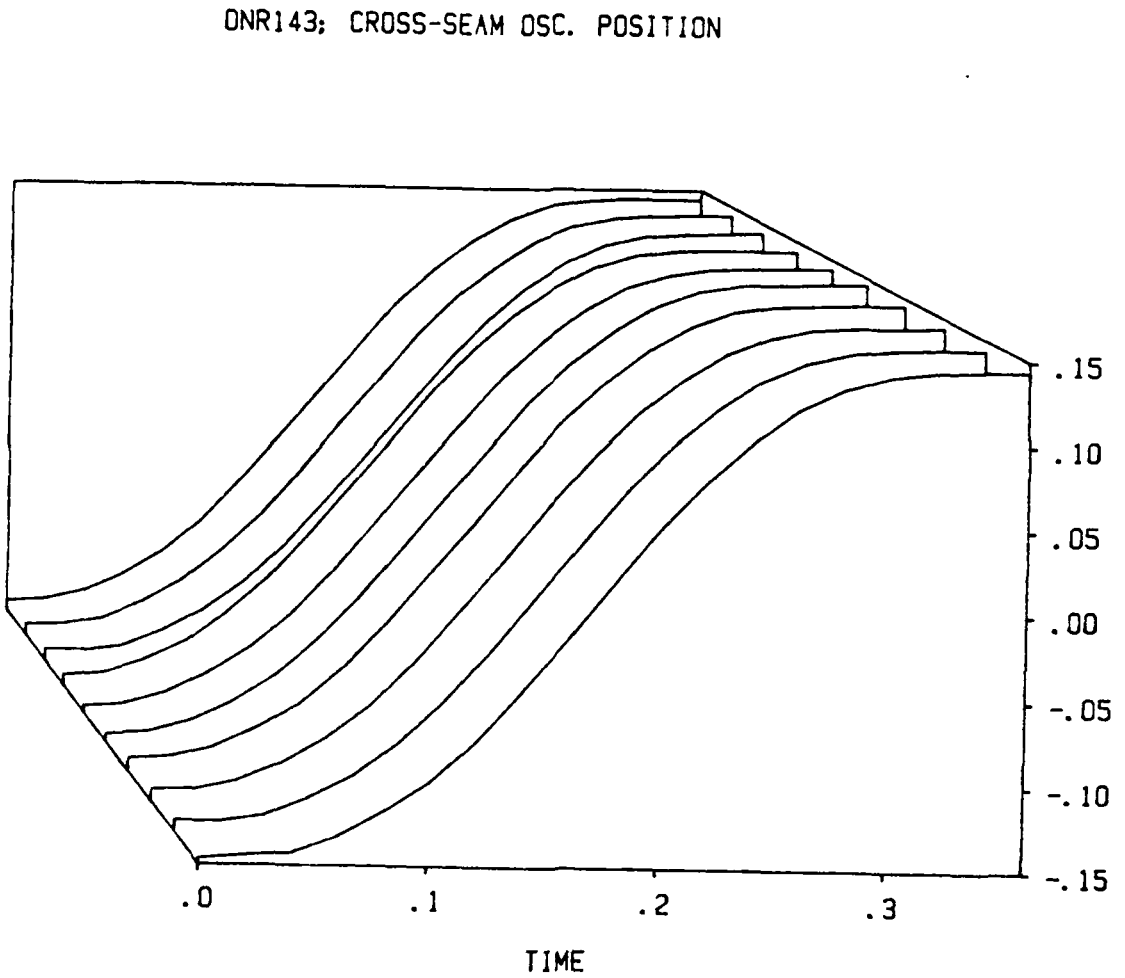

Fig. 21. Cycle by cycle variations of cross-seam position for first ten cycles of skewed joint test.

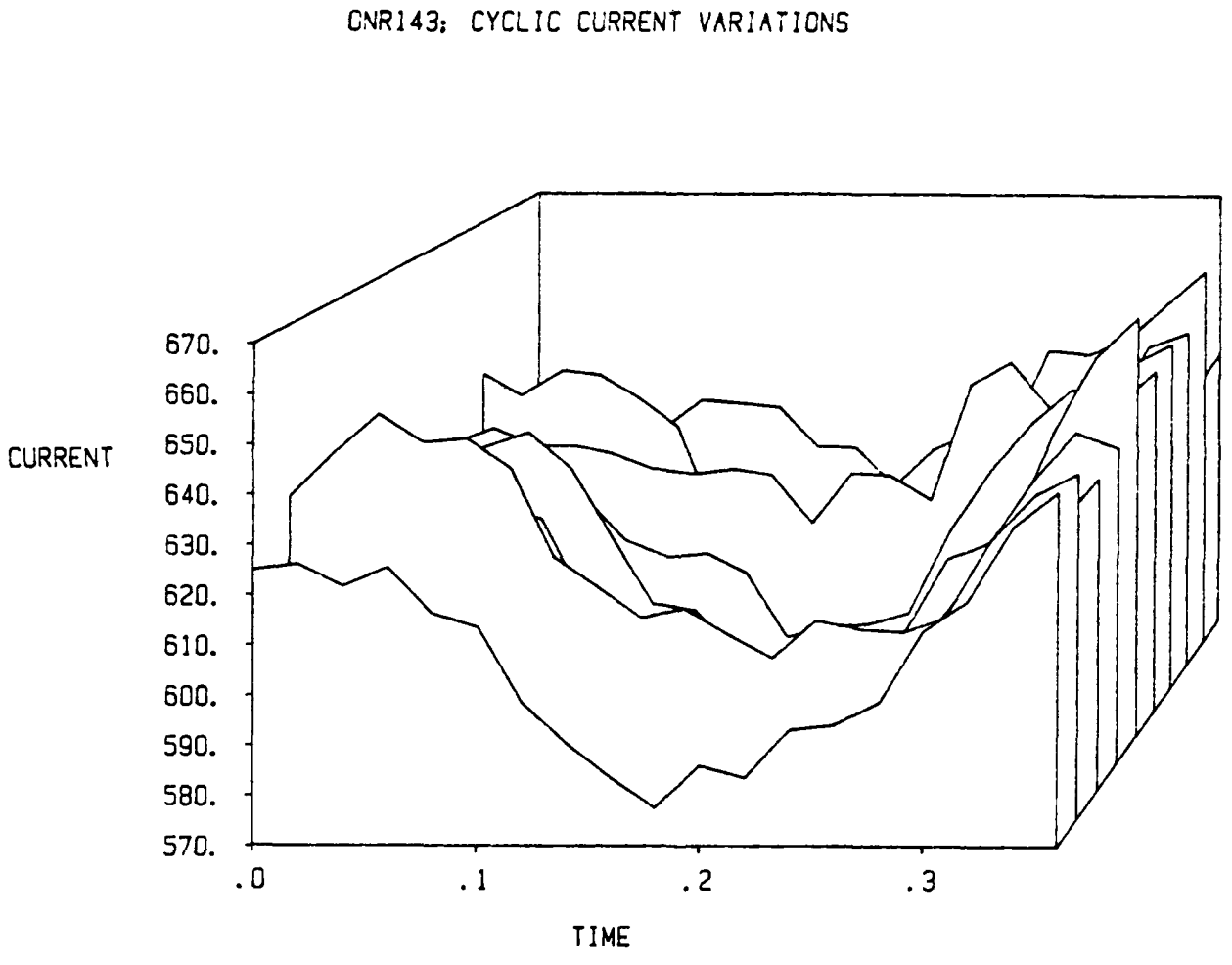

Fig. 22. Cycle by cycle variations of current for first ten cycles of skewed joint test.

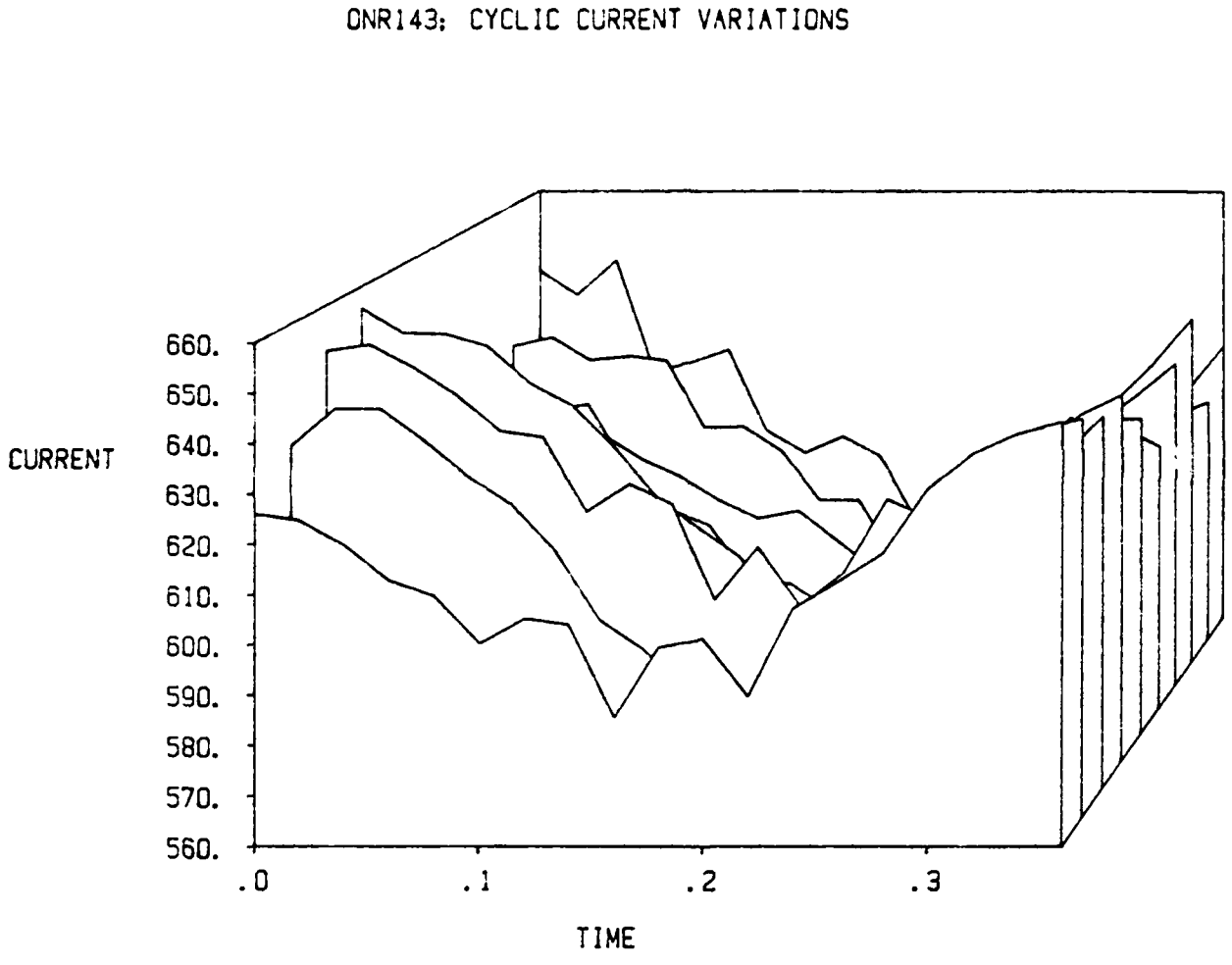

Fig. 23. Cycle by cycle variations of current for cycle number 11-20 of skewed joint test.

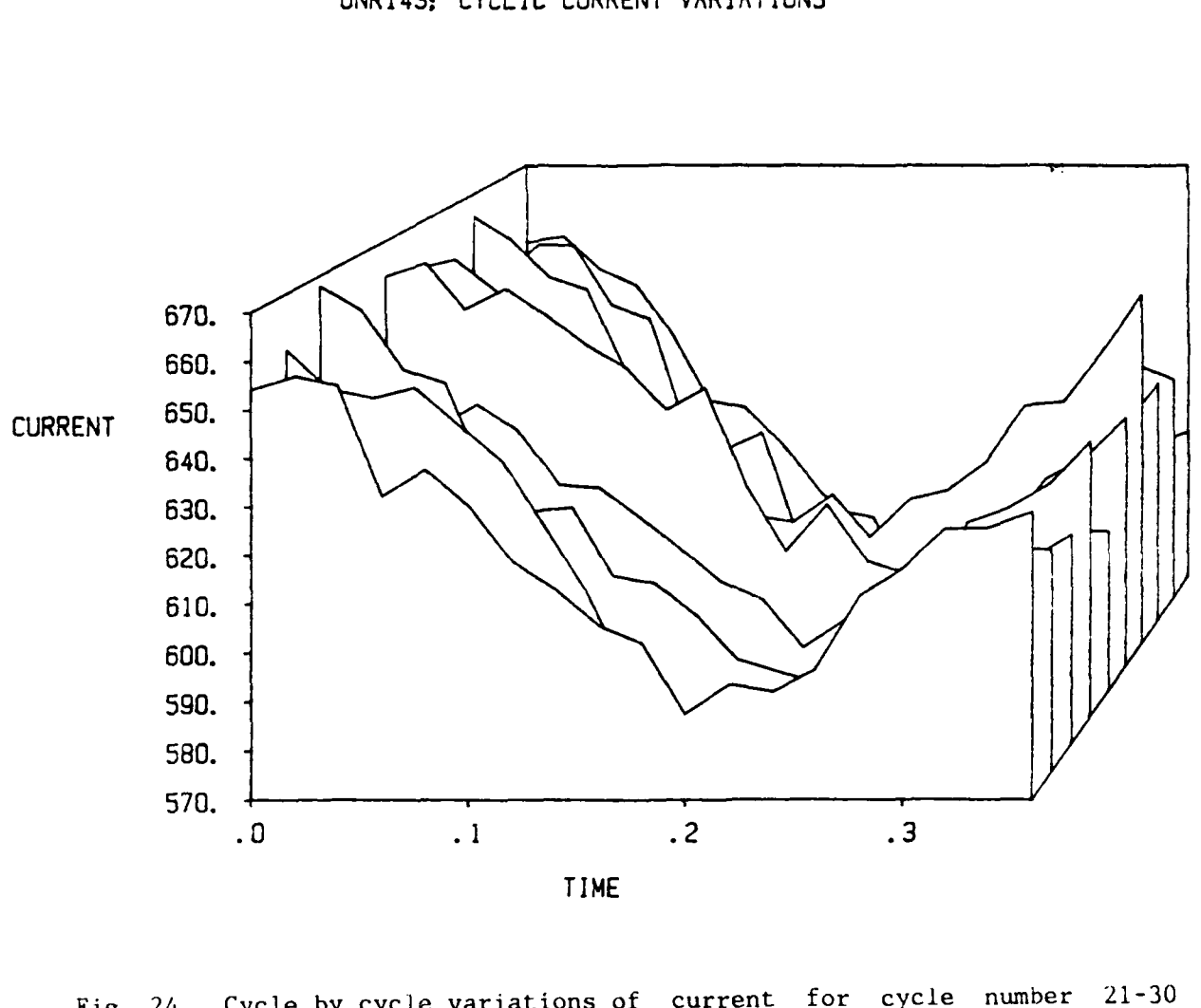

Fig. 24. Cycle by cycle variations of current for cycle number 21-30 of skewed joint test.

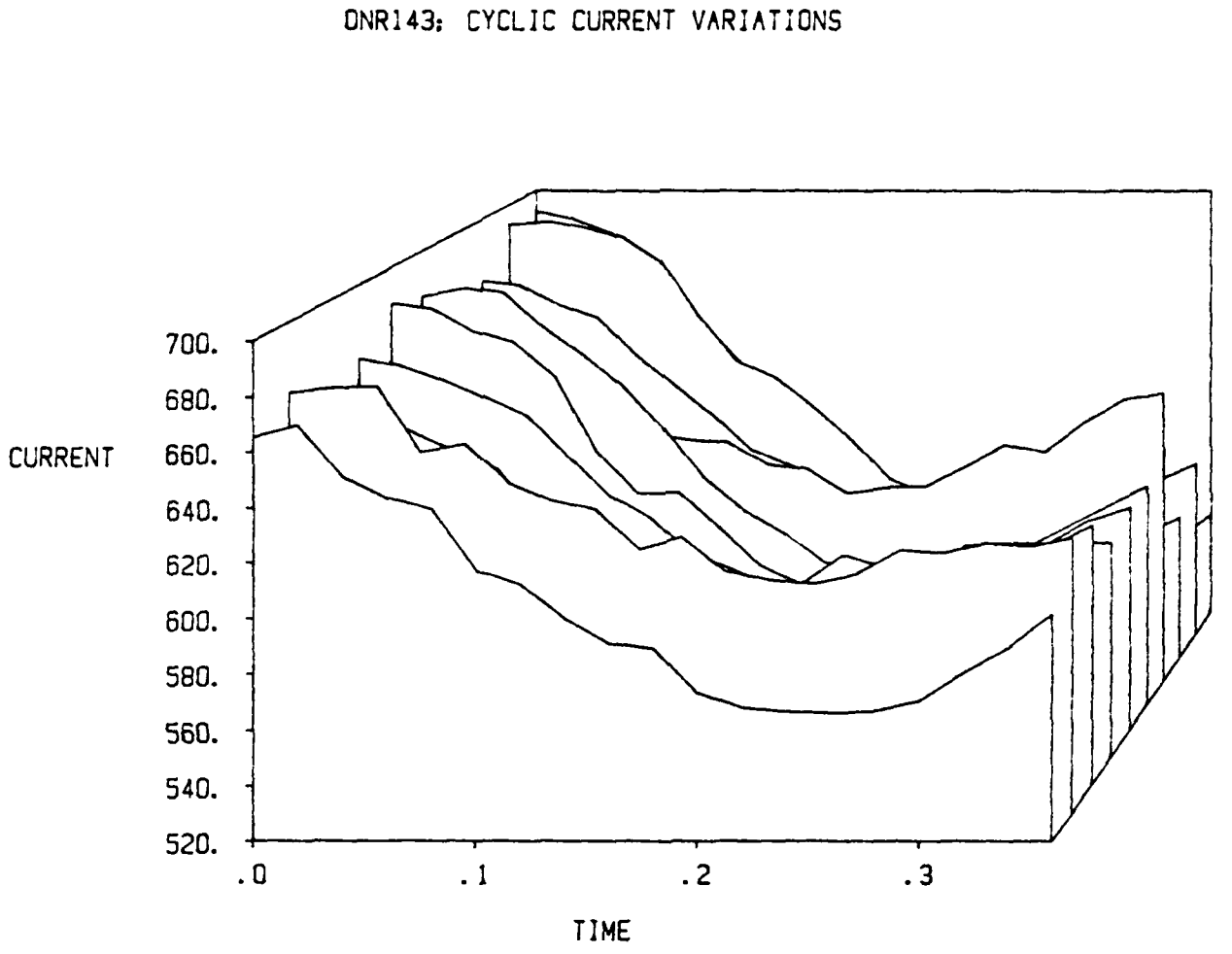

Fig. 25. Cycle by cycle variations of current for cycle number 31-40 of skewed joint test.

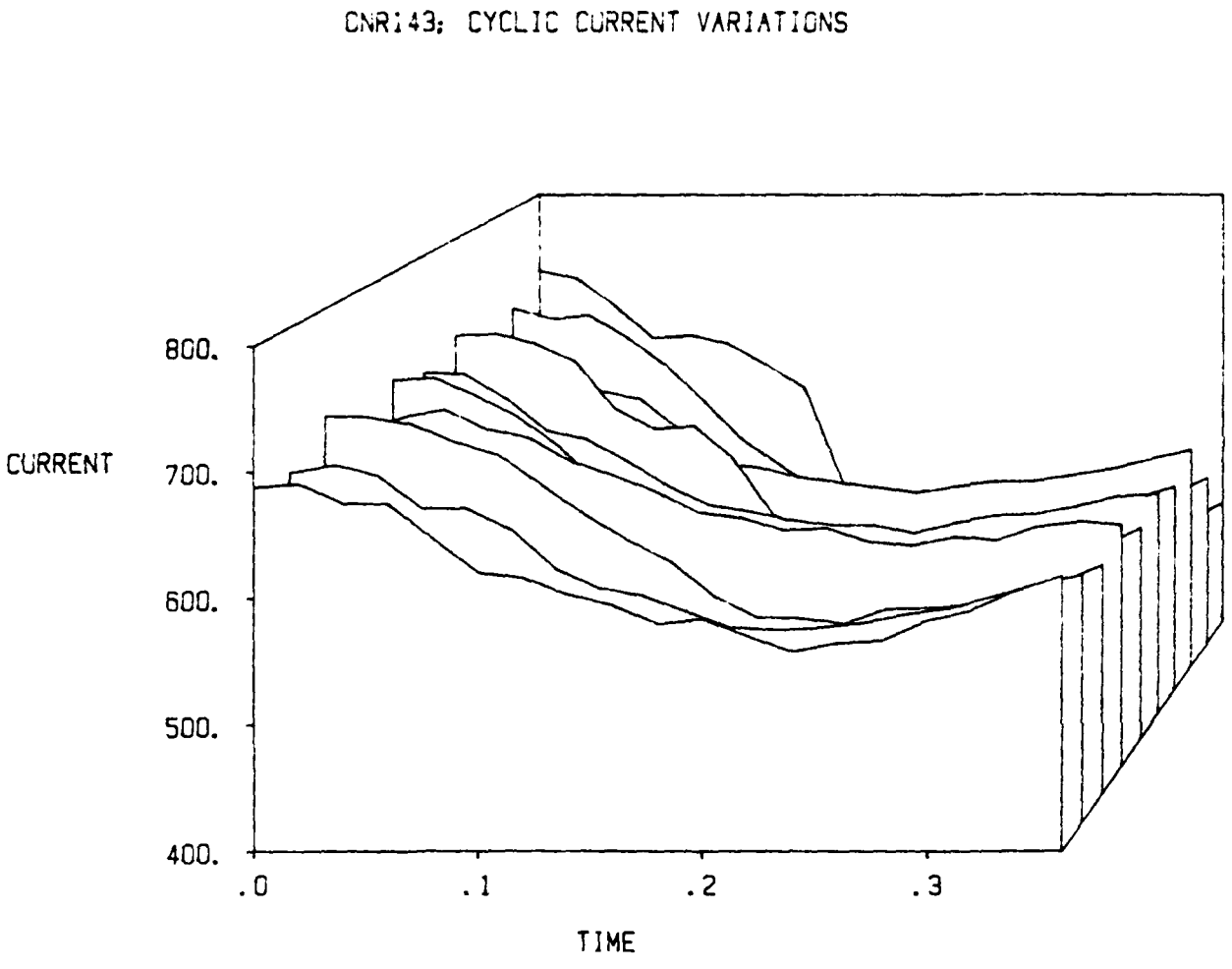

Fig. 26. Cycle by cycle variations of current for cycle number 41-50 of skewed joint test.

very robust signal for control purposes, particularly in light of the relatively small oscillation excursion. Metallographic sections of the weld are presented and discussed in the section Pattern Recognition and Control Algorithms. As discussed there, the oscillation excursion is not excessive from the standpoint of weld quality.

The next forty cycles of cross-seam oscillation are plotted in Figures 23-26. Each figure contains ten cycles. Cycles 11 through 20 are plotted in Figure 23. Over this part of the weld, the electrode is very nearly centered in the joint. Figures 24, 25, and 26 show the current gradually becoming biased toward the left-hand side of the weld. This corresponds to the skew between the electrode travel and the joint centerline. This apparent trend in the current variation is confirmed by the analysis algorithms discussed in the section Pattern Recognition and Control Algorithms.

To investigate the possibility of using power or impedance as the signal indicative of CTWD changes (and hence, joint profile relative to the electrode location), the instantaneous power and instantaneous impedance were computed and broken down on a cycle-by-cycle basis in the same manner as the current. The results of doing this for the first ten cycles of cross-seam oscillation are shown in Figure 27. As can be seen, both the power and the impedance decrease at the left and right extremes of the cross-seam oscillation. As previously stated, the decrease in power indicates that the proportionate decrease in voltage is greater than the increase in current. If the proportionate change in voltage equalled that

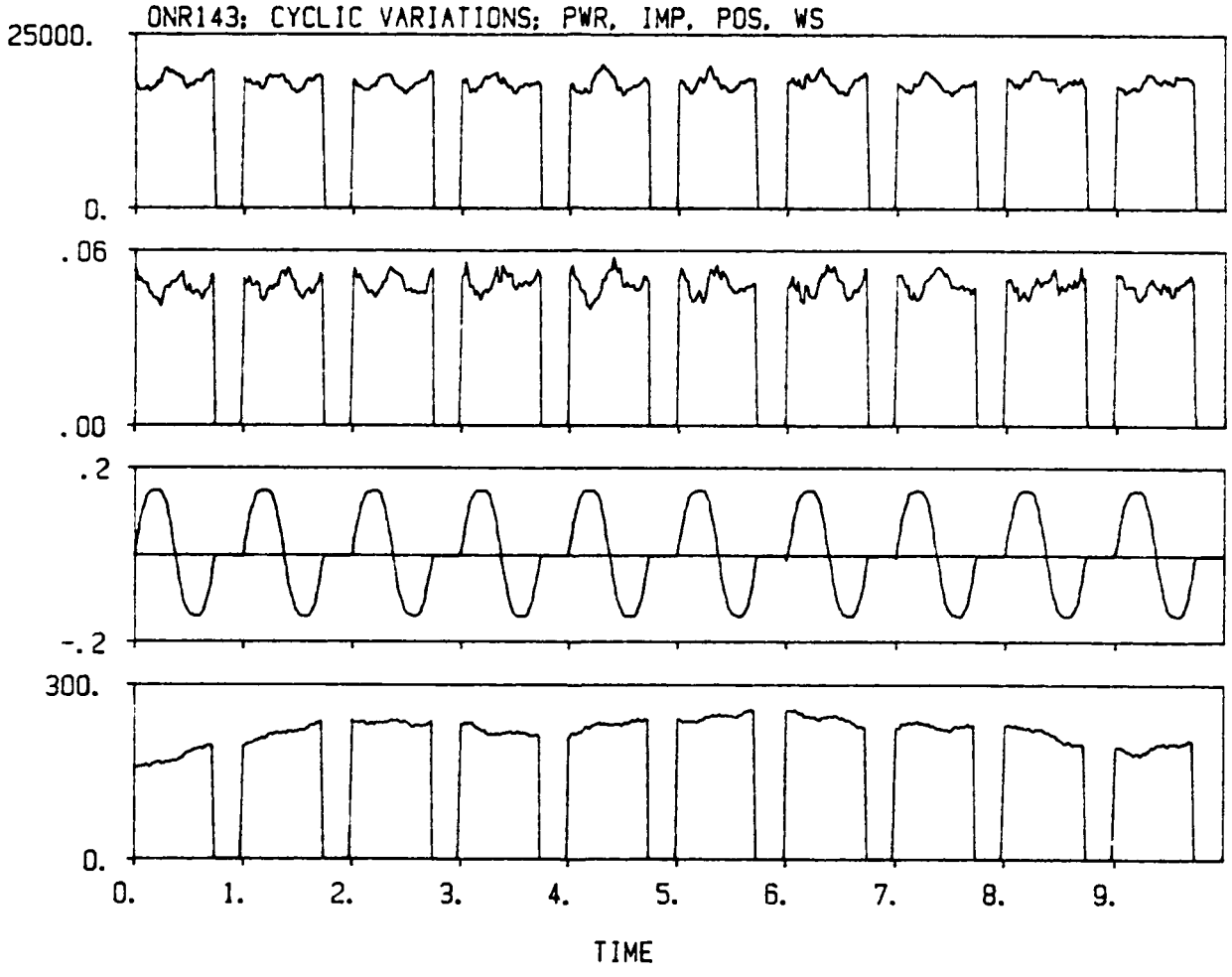

Fig. 27. Cycle by cycle variations of power (1), impedance (2), cross-seam position (3), and wire feed variation (4) for first ten cycles of skewed joint test.

of the voltage, then there would be no change in the power. If the proportionate change in voltage were less than that of the current, then the power would increase. Further investigation will be required in the Phase II research to determine whether these latter two conditions can be expected in practice.

While the instantaneous power waveform may not, on the basis of these observations, provide a consistent variation for all conditions, the impedance function, on the other hand, should be consistent. This is because the instantaneous impedance is the ratio of the instantaneous voltage to the instantaneous current. At the sidewall, the voltage decreases and the current increases. Both of these variations, tend to make the impedance decrease. On the basis of these theoretical observations, the impedance would hence stand out as a logical choice over power and current as well, as the best control signal. The analysis algorithms discussed in the section Pattern Recognition and Control Algorithms do not fully support this observation, however. Further investigation is called for in the Phase II research program.

The last ten cycles of the instantaneous power variation are plotted in Figure 28. The skew to the left at this end of the weld is clearly shown by the greater power on the left than on the right side of the plots.

The instantaneous impedance for cycles 11 through 20 are shown in Figure 29. The impedance minimum is roughly the same on both sides

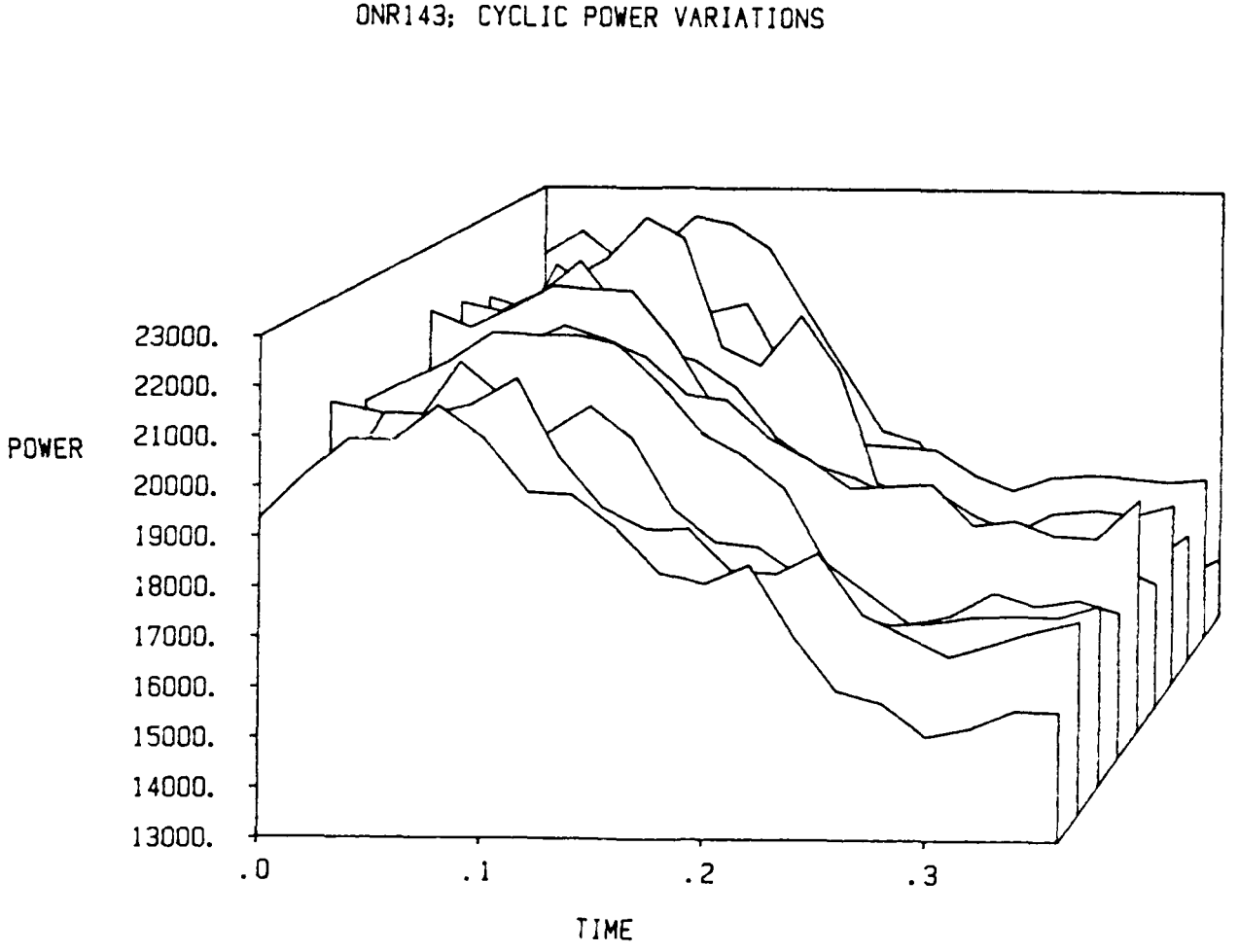

Fig. 28. Cycle by cycle variations of instantaneous power for cycle number 41-50 of skewed joint test.

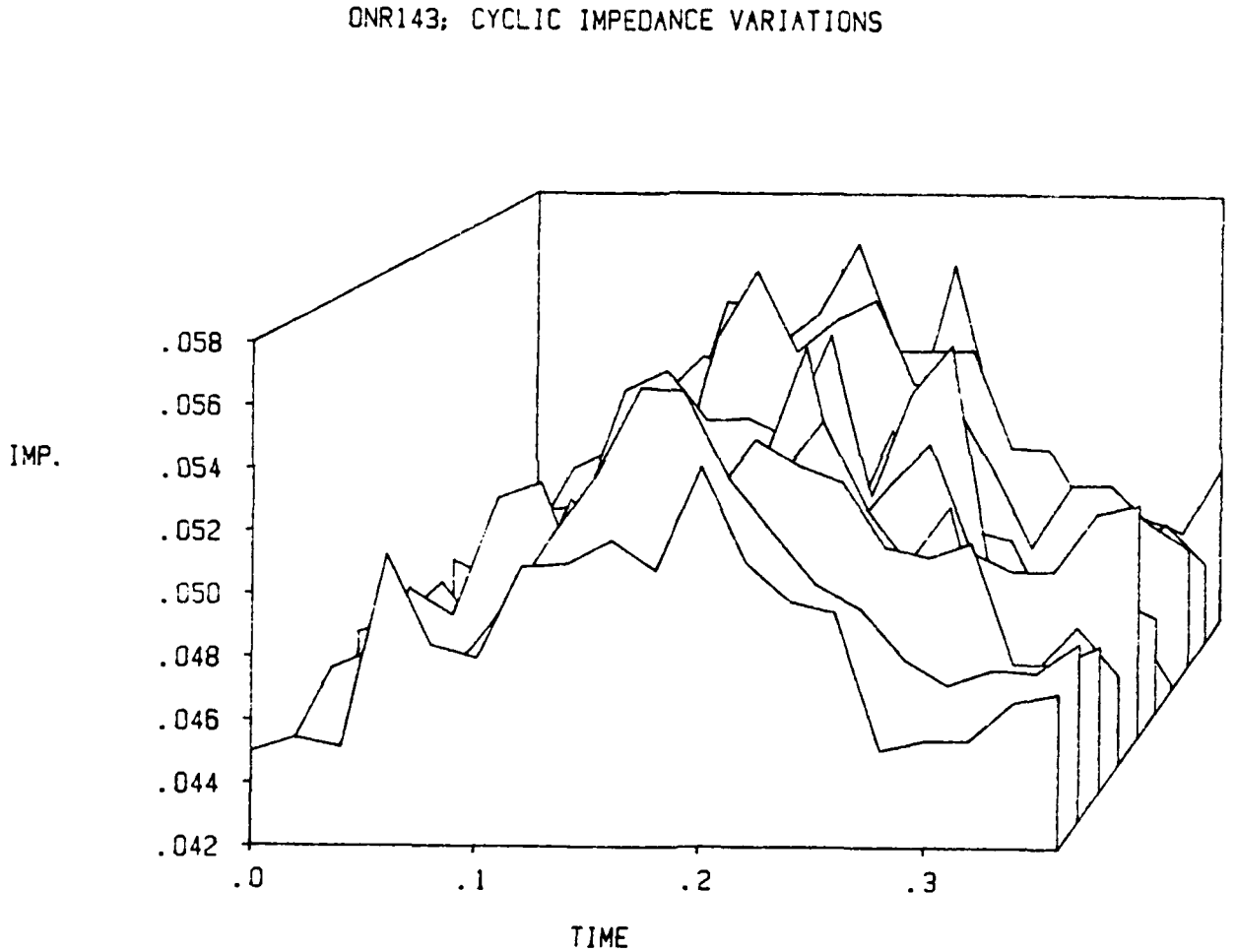

Fig. 29. Cycle by cycle variations of instantaneous impedance for cycle number 11-20 of skewed joint test.

indicating proper centering, which is consistent with observations based on the current variations. Since the impedance function decreases for both a decrease in voltage and an increase in current, it tends to be more sensitive than the other waveforms. From the standpoint of signal robustness, this is a desirable feature. However, it also tends to make the impedance more susceptible to random variations in the voltage or current signals. This more "noisy" character of the impedance function can be seen by comparing Figures 28 and 29. Because of the greater apparent noise of the impedance waveform, different smoothing algorithms may be required to fully exploit its potential capabilities. This investigation will be carried out in the Phase II research program.

To further substantiate the effect of the small skew between the joint centerline and the path of the electrode, power spectra were computed and plotted for current, power, and impedance waveforms over three different regions of the weld. The power spectra were computed using the Fast Fourier Transform (FFT) with 128 points corresponding to data time spans of 2.3 seconds. The specific regions chosen for computing the power spectra were t = 0 to 2.3 seconds, t = 19 to 21. 3 seconds, and t = 36 to 38.3 seconds. Based on knowledge that the joint skew was such that the electrode was centered near the beginning of the weld and progressively deviated from the joint center as the weld was made, it was concluded that these conditions should be reflected in the power spectra functions.

At the beginning of the weld, the power spectra should show a pronounced peak at twice the cross-seam oscillation frequency. This is due to symmetrical peaks in the current signal and symmetrical minimal in the voltage signal at either extreme of the oscillation excursion, and hence a current variation at twice the frequency of the cross-seam oscillation frequency. Near the center of the weld, the electrode has become progressively biased toward one side, and hence, the peaks in the current signal and the minimal in the voltage signal at each extreme of the oscillation excursion should no longer be symmetrical. As a result, the power spectra in this region of the weld would be expected to exhibit not only a strong peak at twice the oscillation frequency, but to exhibit a strong peak at the fundamental frequency of oscillation as well. Finally, at the end of the weld, the skew is sufficient to make the current and voltage variations essentially one-sided, in which case the power spectra should exhibit a strong peak at the fundamental frequency of oscillation and only a relatively small component at twice the oscillation frequency.

The power spectra of the current waveform, computed for the three regions of the weld, are shown in Figures 30-32. As predicted, the power spectrum for the region [0-2.3 seconds], shows a pronounced and dominant peak at twice the fundamental frequency of the cross-seam oscillation. The power spectrum for the region [19-21.3 seconds] shows, as expected, a large peak at both the fundamental frequency of the cross-seam oscillation as well as at twice the cross-seam oscillation frequency. Finally, the

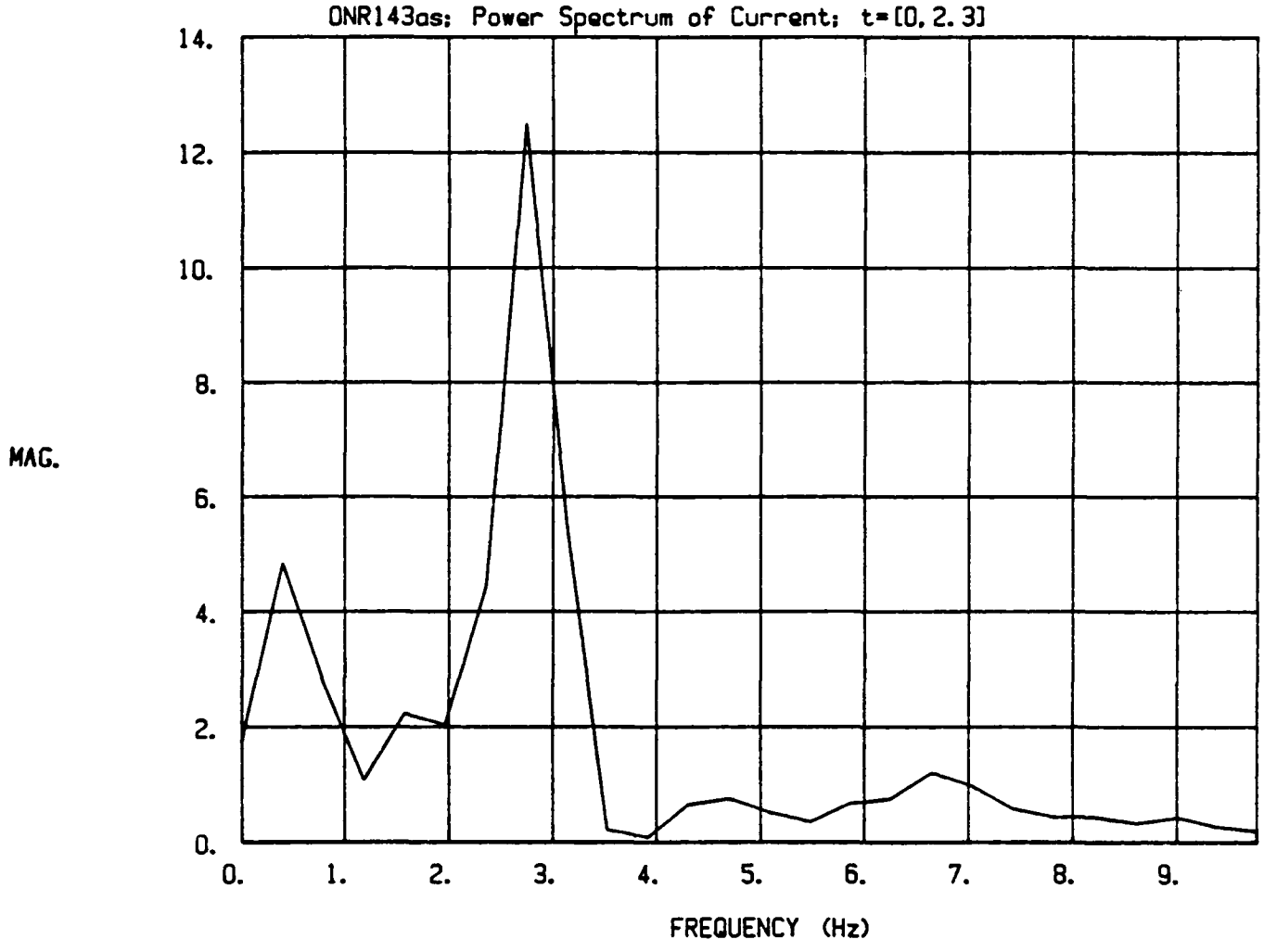

Fig. 30. Power spectrum of current waveform taken from first third of skewed joint test.

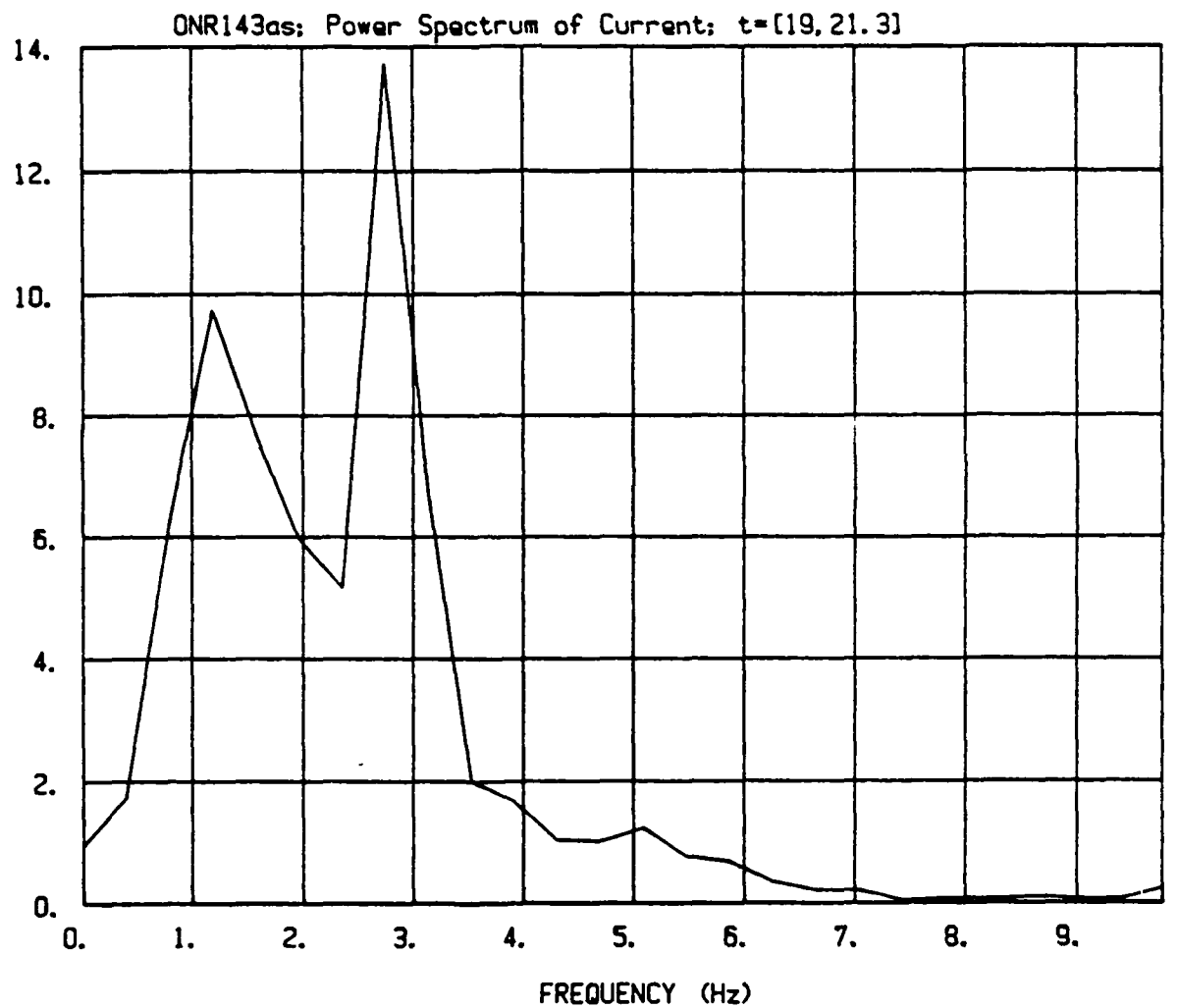

Fig. 31. Power spectrum of current waveform taken from middle third of skewed joint test.

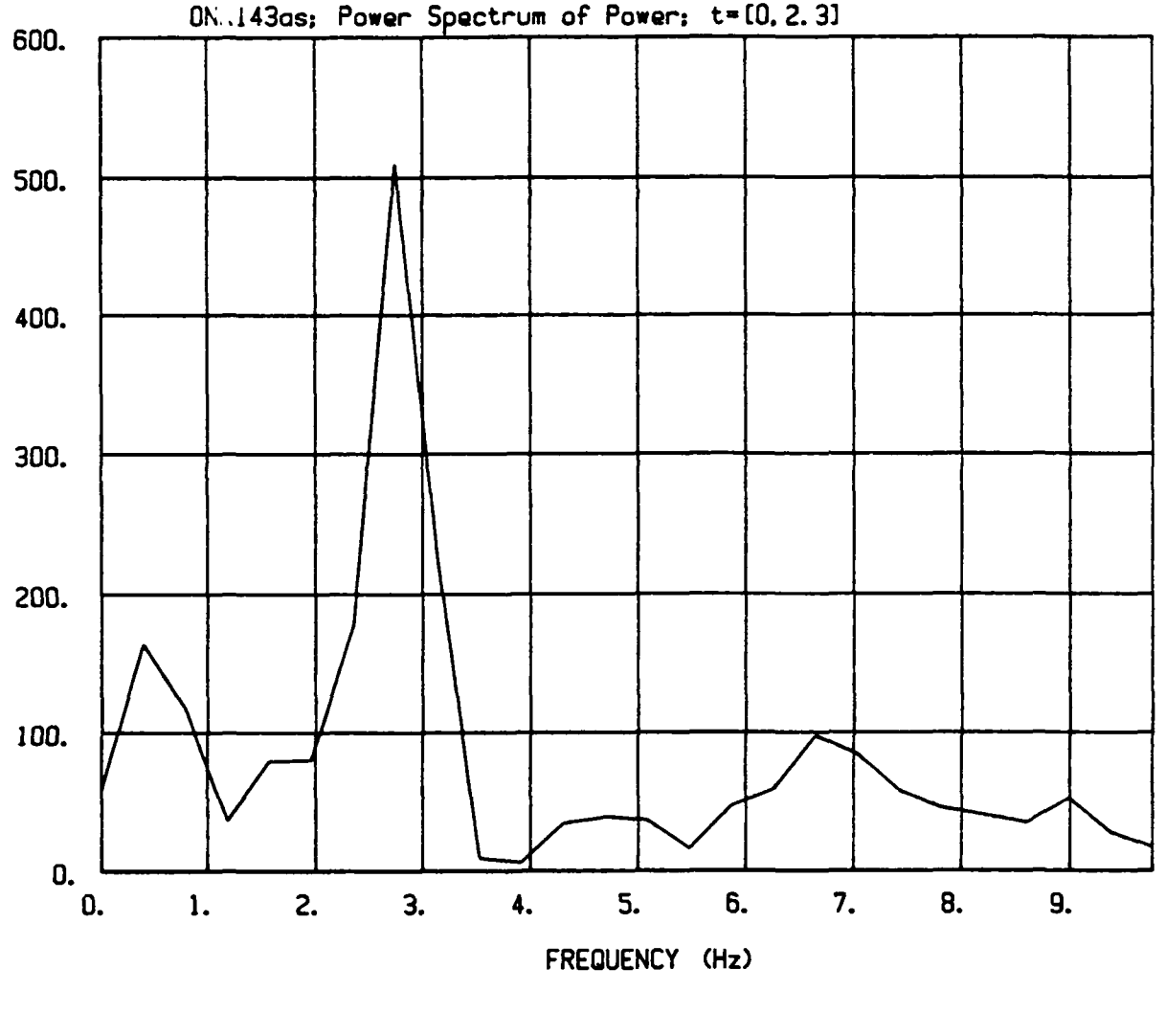

Fig. 32. Power spectrum of current waveform taken from last third of skewed joint test.

power spectrum for the region [36-38.3 seconds] shows a large peak at the fundamental frequency of the cross-seam oscillation and only a minor peak at twice the fundamental frequency.

Power spectra of the instantaneous power waveforms and the instantaneous impedance waveforms, computed over the same three regions of the weld show exactly the same results as conveyed by the plots of power spectra for the current waveform. The power spectra of the instantaneous power waveforms are plotted in Figures 33-35, and the power spectra of the instantaneous impedance waveforms are plotted in Figures 36-38.

The rather remarkable conclusion that can be drawn from this test and the signal analysis presented, is that even for a total centering offset of less than half the wire diameter the signals are very robust and very accurately predict the precise positioning of the electrode. It is emphasized that the small condition of centering offset tested in this experiment would normally be considered well within normal acceptable tolerances for producing sound welds. This is further substantiated by the metallographic sections taken from the three sections of the weld, as discussed later in the section, Pattern Recognition and Control Algorithms, and as shown there in Figures 83-85.

Analysis of Welding With Bias to One Sidewall

To further demonstrate the sensitivity of the through-the-arc sensing

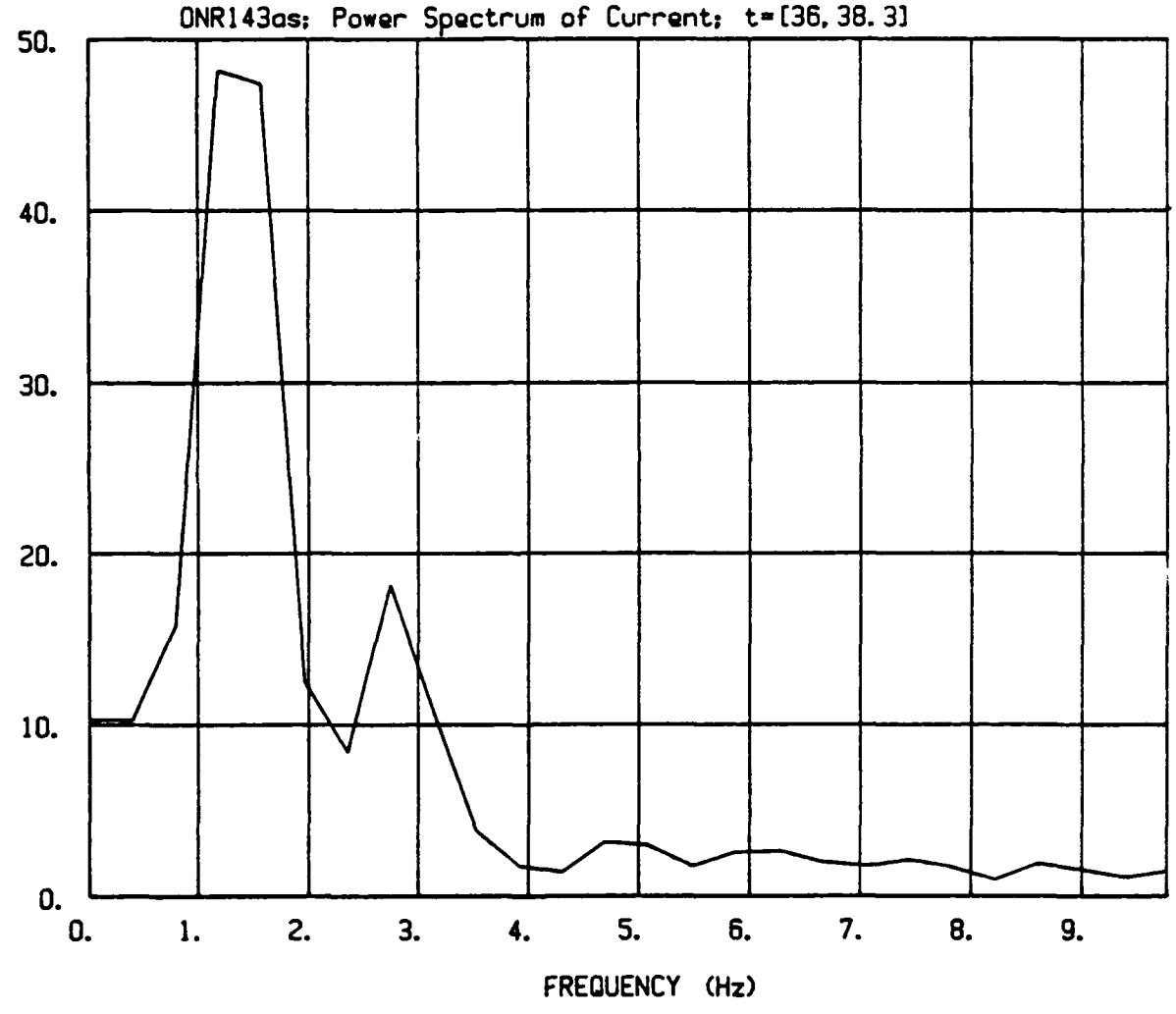

Fig. 33. Power spectrum of instantaneous power waveform taken from first third of skewed joint test.

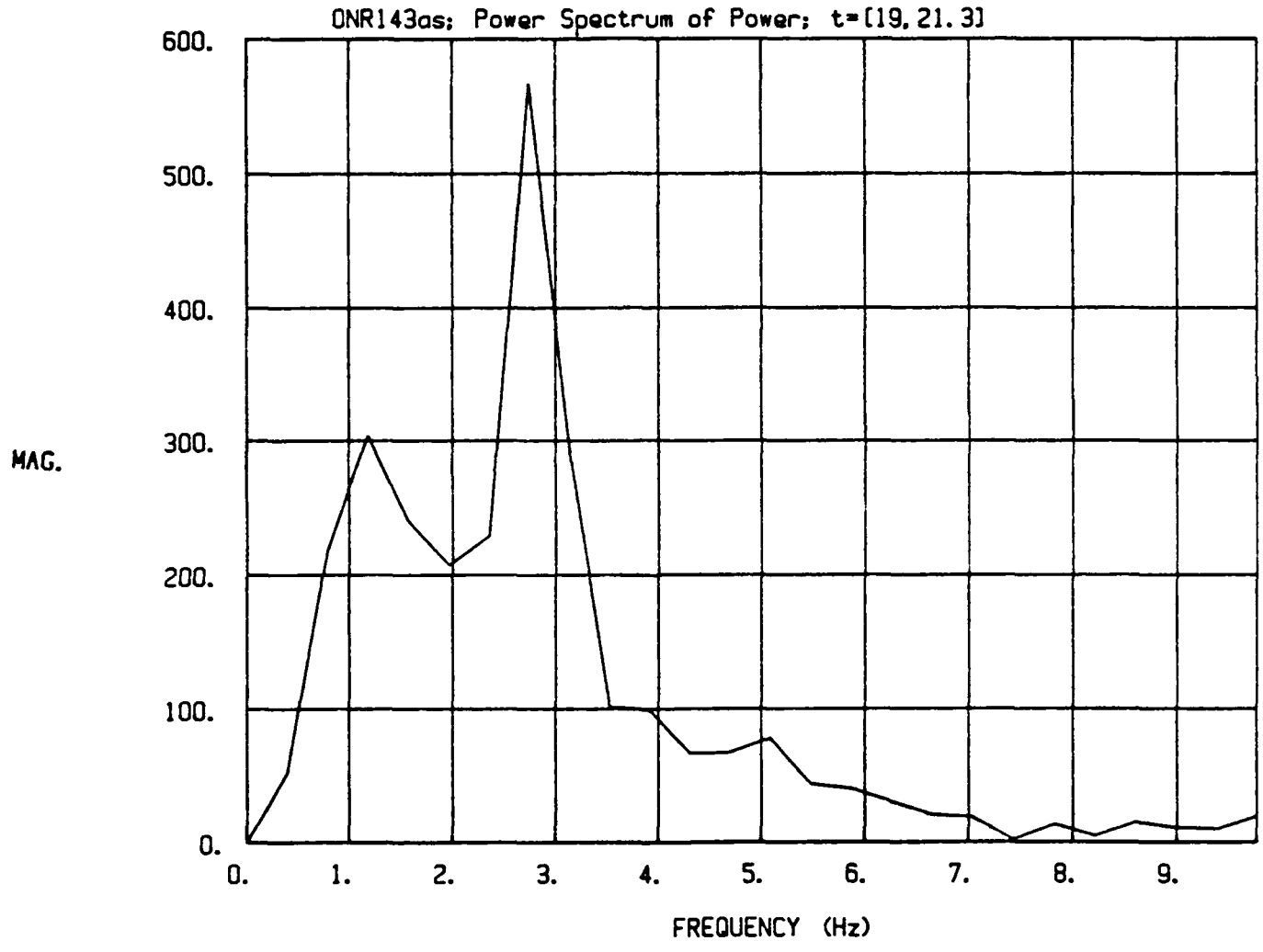

Fig. 34. Power spectrum of instantaneous power waveform taken from middle third of skewed joint test.

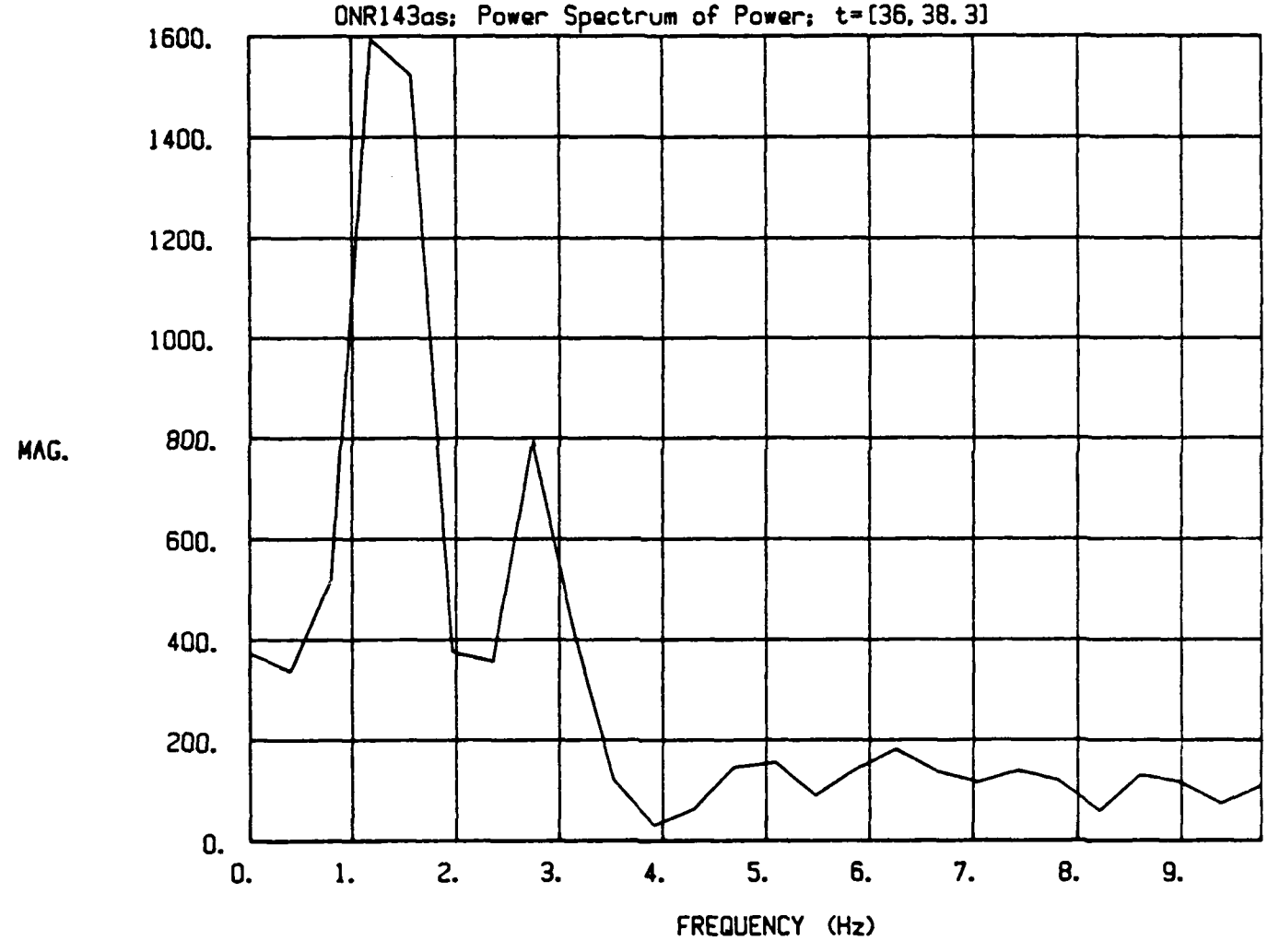

Fig. 35. Power spectrum of instantaneous power waveform taken from last third of skewed joint test.

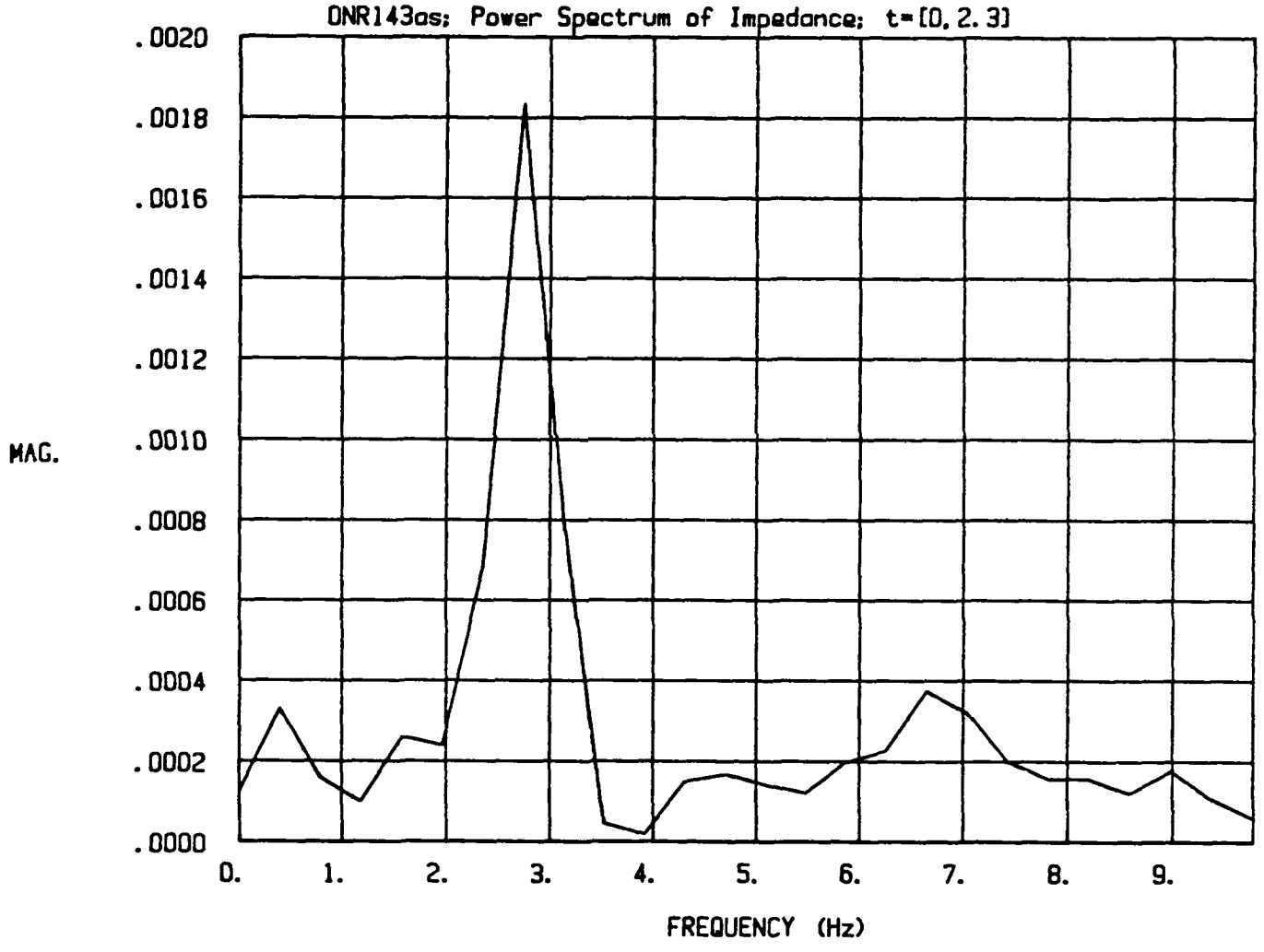

Fig. 36. Power spectrum of instantaneous impedance waveform taken from first third of skewed joint test.

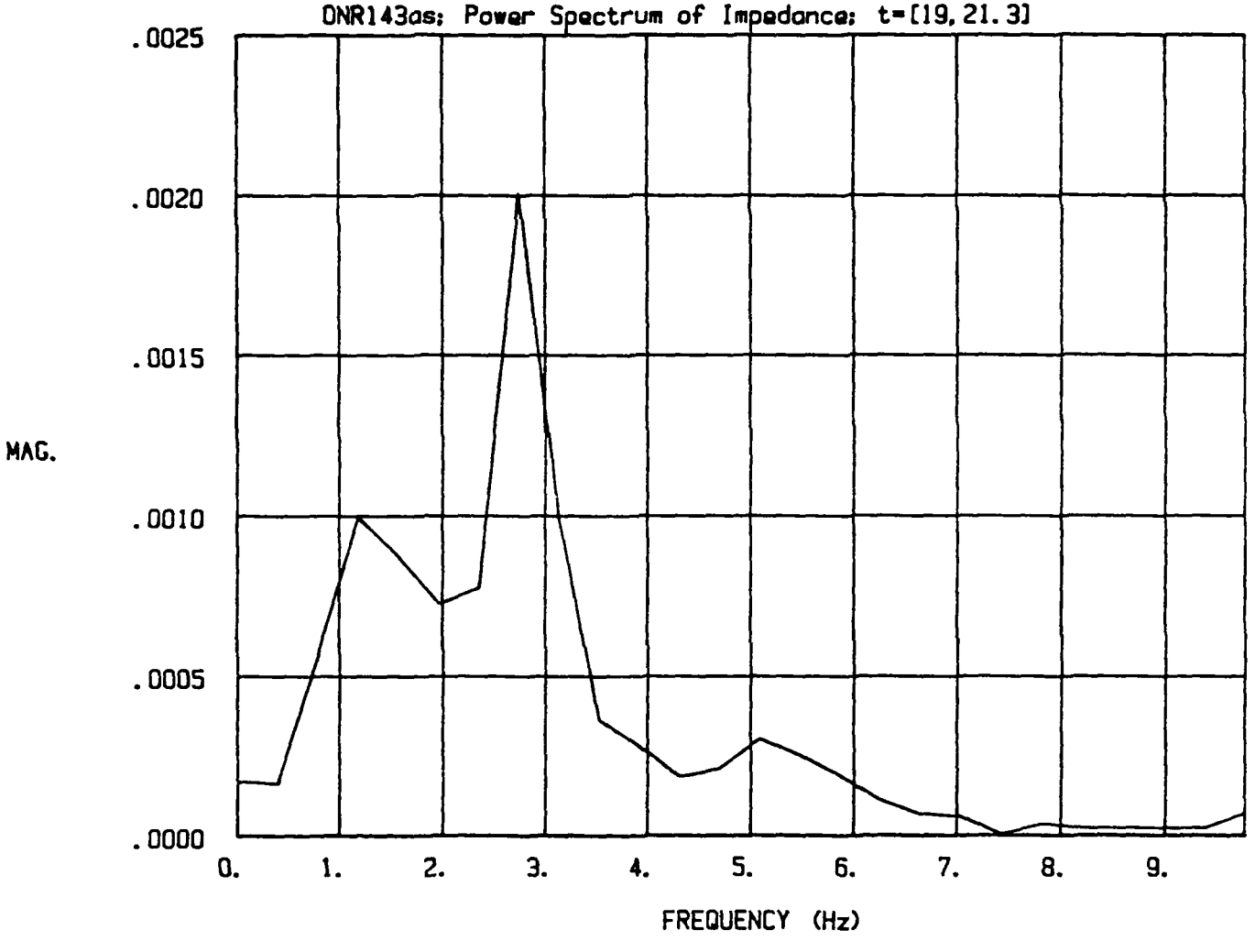

Fig. 37. Power spectrum of instantaneous power waveform taken from middle third of skewed joint test.

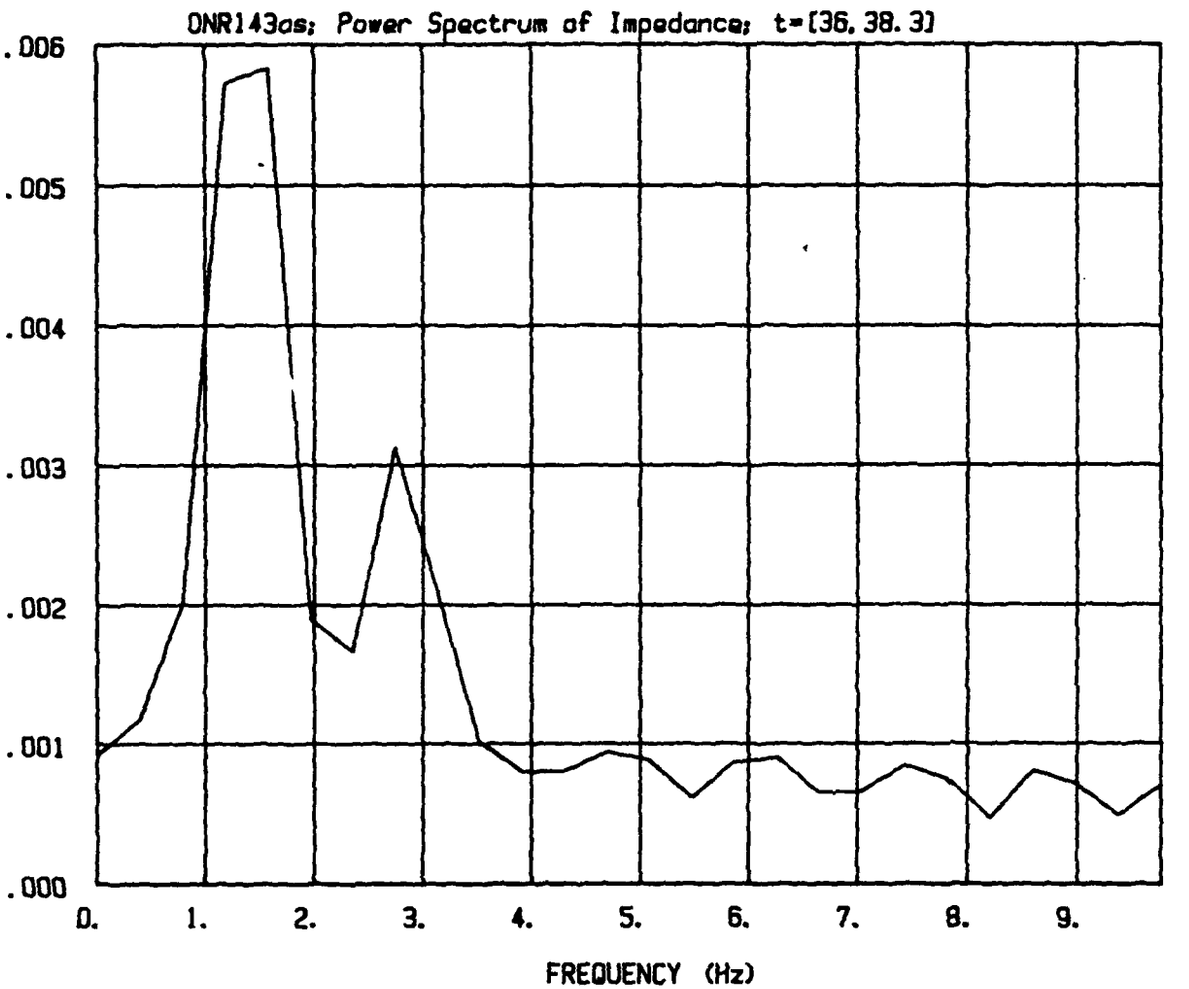

Fig. 38. Power spectrum of instantaneous power waveform taken from last third of skewed joint test.

methodology and its applicability to the SAW process, test welds were made with the electrode deliberately biased slightly toward one sidewall. This information was considered valuable and needed for side-by-side beads (stringer beads) in both conventional joints and Narrow Gap joints.

The weld that will be used in this report as an example of these tests is weld number 2, pass one (Data File ONR021AS). This was a root pass made with fixed oscillation width and fixed oscillation rate. The weld was made on a joint having a 45-degree included angle and a 5.25 mm root gap. The nominal current was 550 amperes, the nominal voltage was 31 volts, the CTWD was 25.4 mm, the wire feed speed was 3937 mm/min, the travel speed was 406 mm/min, the oscillation width was 3.3 mm peak-to-peak and the oscillation frequency was 2 Hz.

Waveforms of voltage (1), current (2), and position (3) are plotted in Figure 39. As can be seen by inspection of either the voltage or the current waveforms, they show a pronounced variation at one side of the oscillation cycle but little or no variation at the other side of the oscillation. Hence, it would be expected that the power spectra of the electrical signal waveforms would show a pronounced peak at the fundamental frequency of the cross-seam oscillation.

The power spectrum of the position signal is plotted in Figure 40. As can be seen, the predominant peak is at 2 Hz, the fundamental frequency of the cross-seam oscillation. Since the cross-seam oscillation waveform

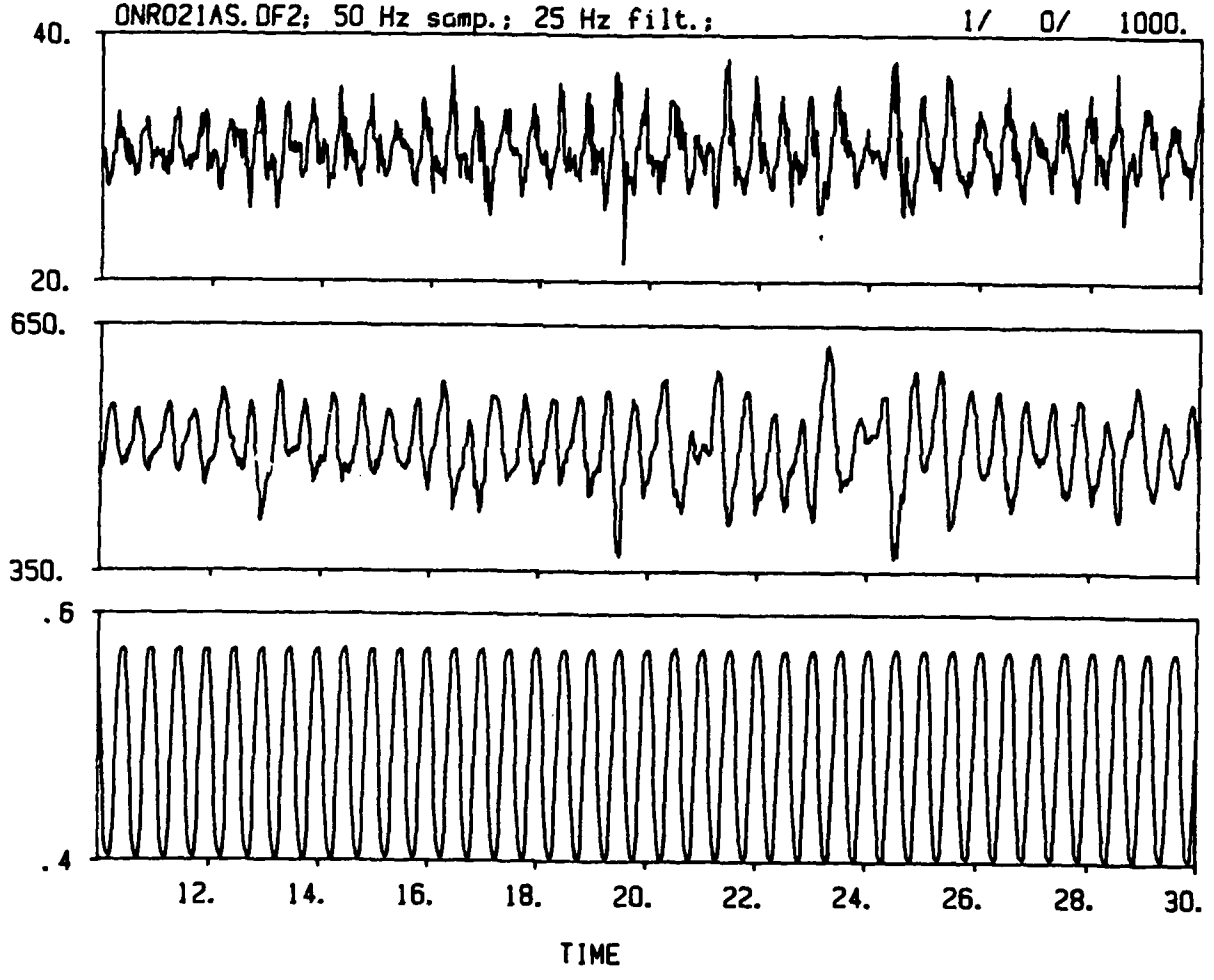

Fig. 39. Waveforms of voltage (1), current (2), and position (3) of weld with bias to one sidewall.

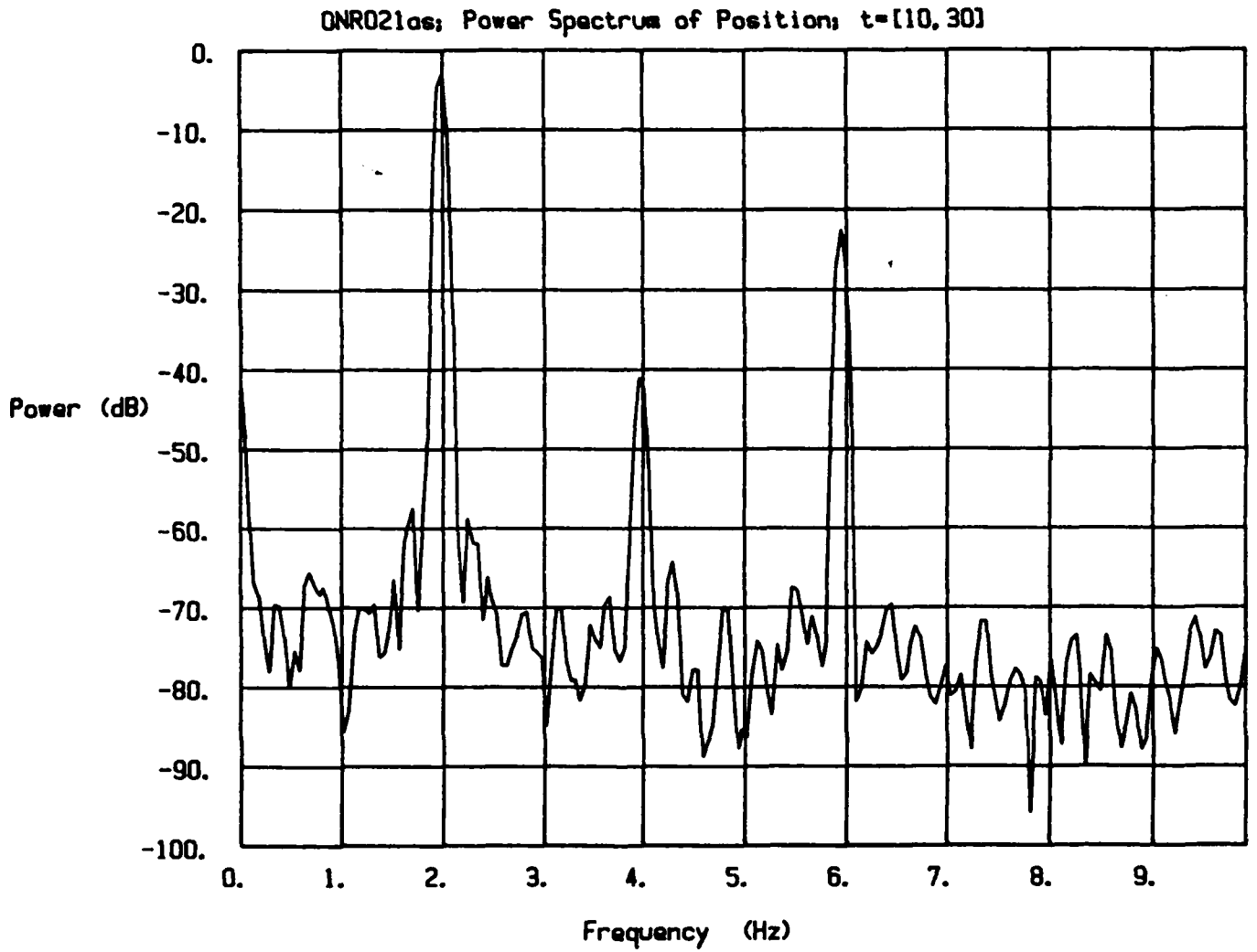

Fig. 40. Power spectrum of cross-seam position signal for weld with bias to one sidewall.

is not sinusoidal, but instead, more triangular in shape, the power spectrum also shows peaks at the harmonic frequencies of 4 and 6 Hz as well. We observe, however, that the peak at 4 Hz is approximately 35 dB less than the fundamental peak at 2 Hz. On a linear scale, it would, hence, barely be visible.

The power spectra of the current waveform, the voltage waveform, the instantaneous power waveform, and the instantaneous impedance waveform are shown in Figures 41 through 44 respectively. As can be seen, each of these waveforms shows a distinct peak at the fundamental frequency of 2 Hz. The curves also show a peak of significantly lesser amplitude at twice the fundamental frequency, i.e., at 4 Hz. This signal component would be expected to be present, even if the position waveform were purely sinusoidal and showed only one peak at the fundamental frequency of 2 Hz. The reason is that, while the electrode is biased toward one side, there is still some variation that can be expected in the voltage and current waveforms on the other side as well. Even though these variation are small and not detachable in the raw waveforms, they show up in the power spectra plots. Another argument that might be offered to explain the peaks in the waveforms at 4 Hz is that they are in response to the 4 Hz component of the cross-seam position signal. This is discounted, however, because the 4 Hz component of the cross-seam position signal is approximately 35 dB less than the fundamental component, which corresponds to only a 0.4 mm peak-to-peak cross-seam excursion. Furthermore, if this argument were valid, then there should be a peak in the waveforms at 6 Hz as well, corresponding to the

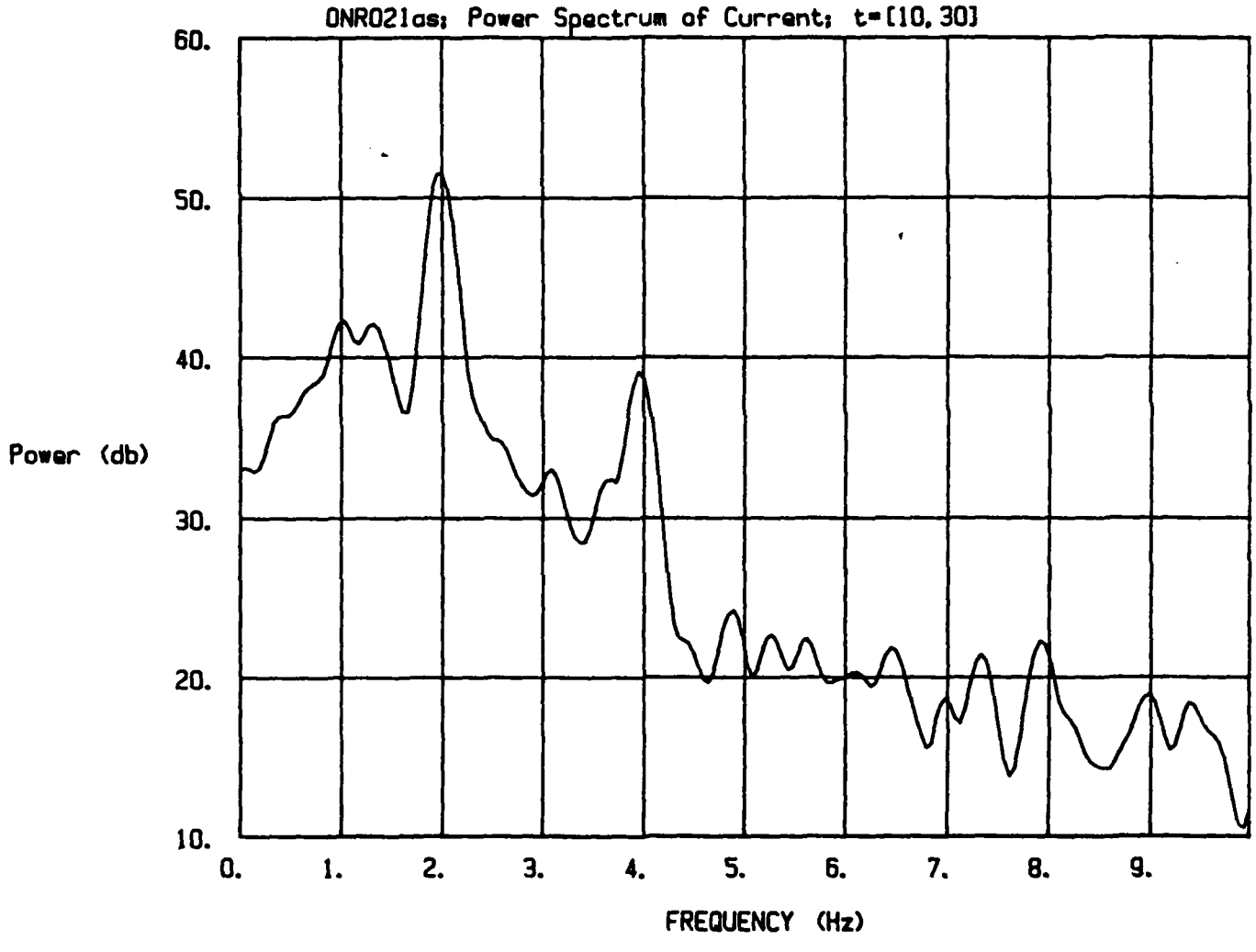

Fig. 41. Power spectrum of current waveform for weld with bias to one sidewall.

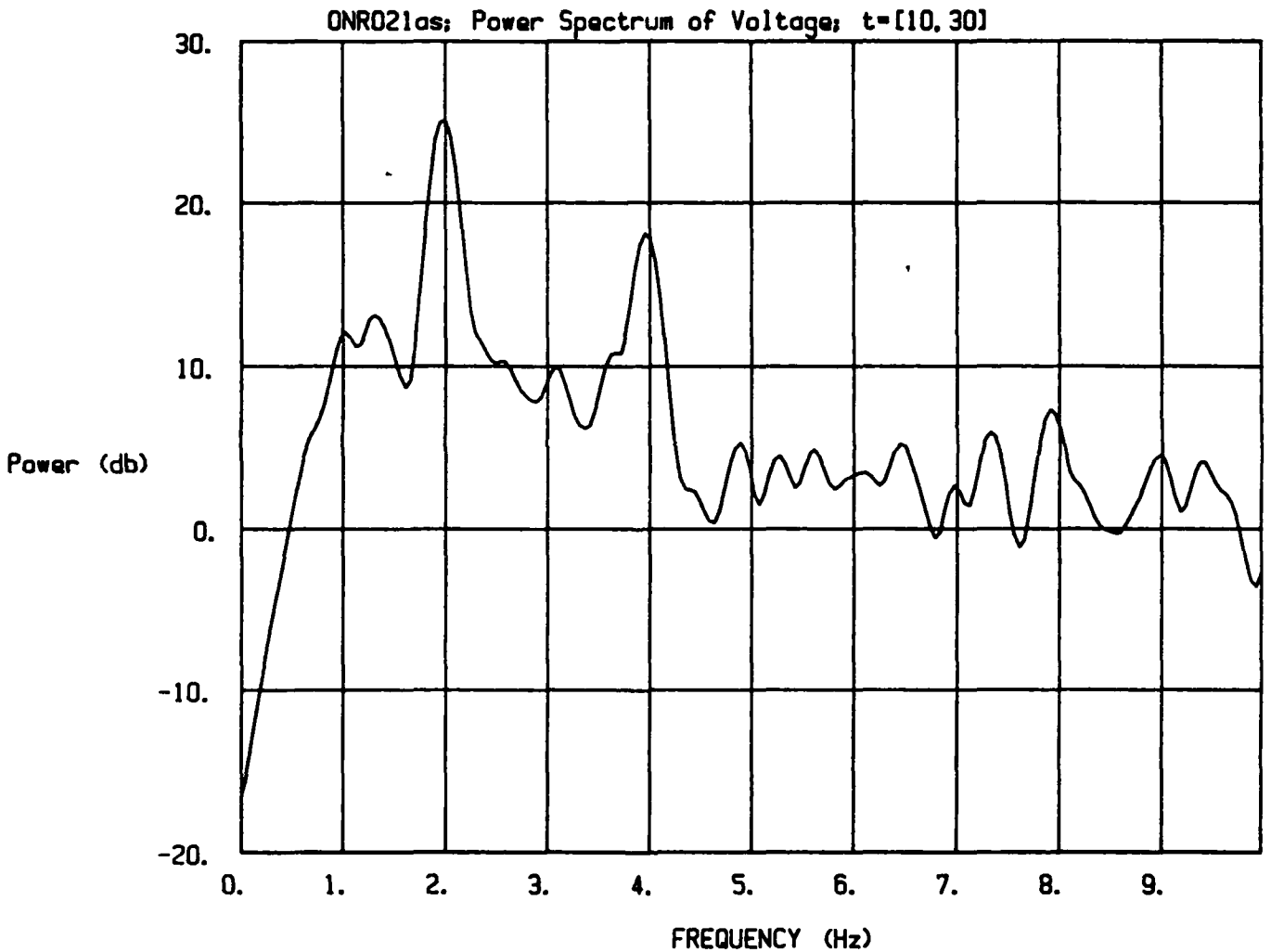

Fig. 42. Power spectrum of voltage waveform for weld with bias to one sidewall.

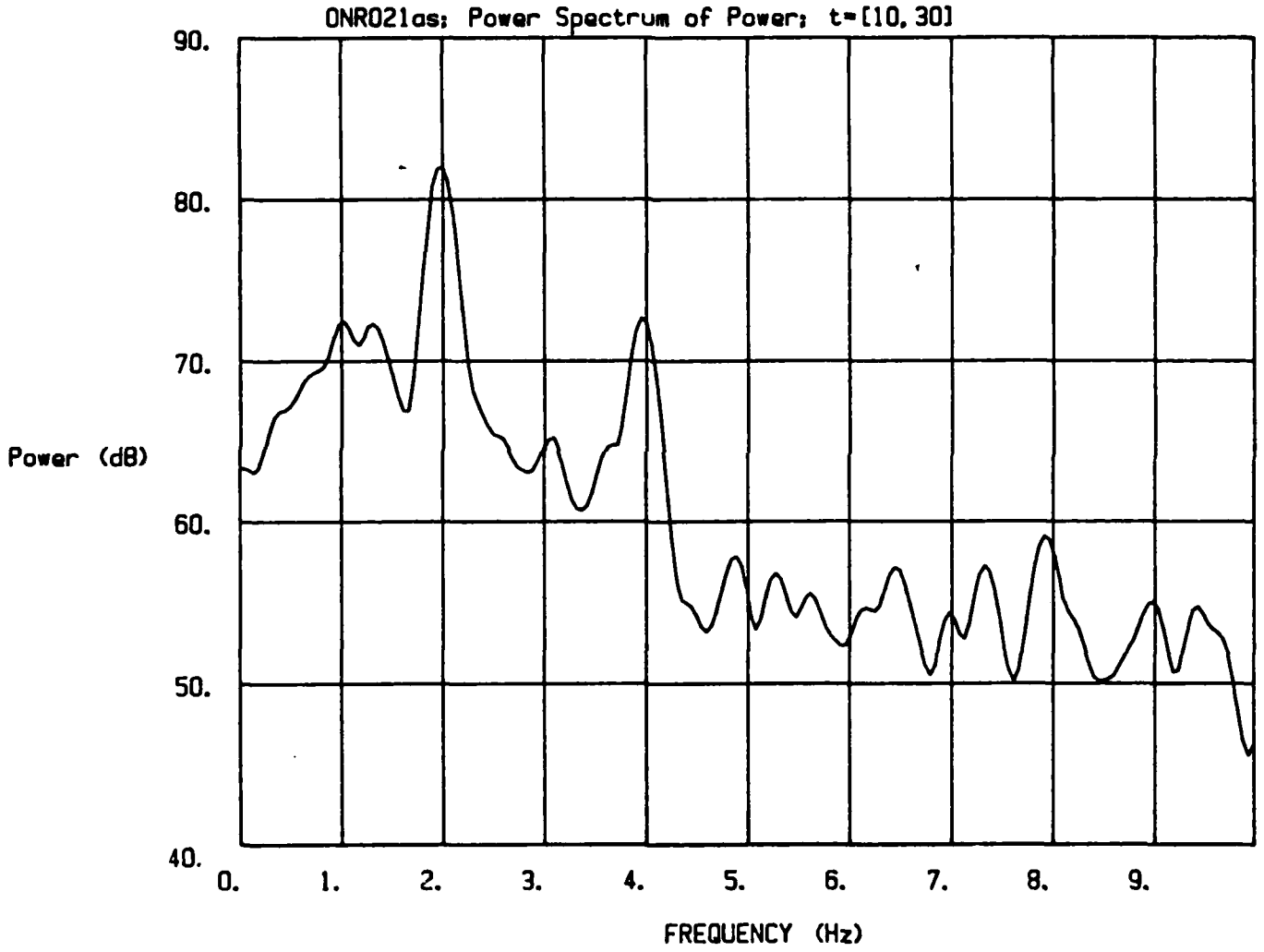

Fig. 43. Power spectrum of instantaneous power waveform for weld with bias to one sidewall.

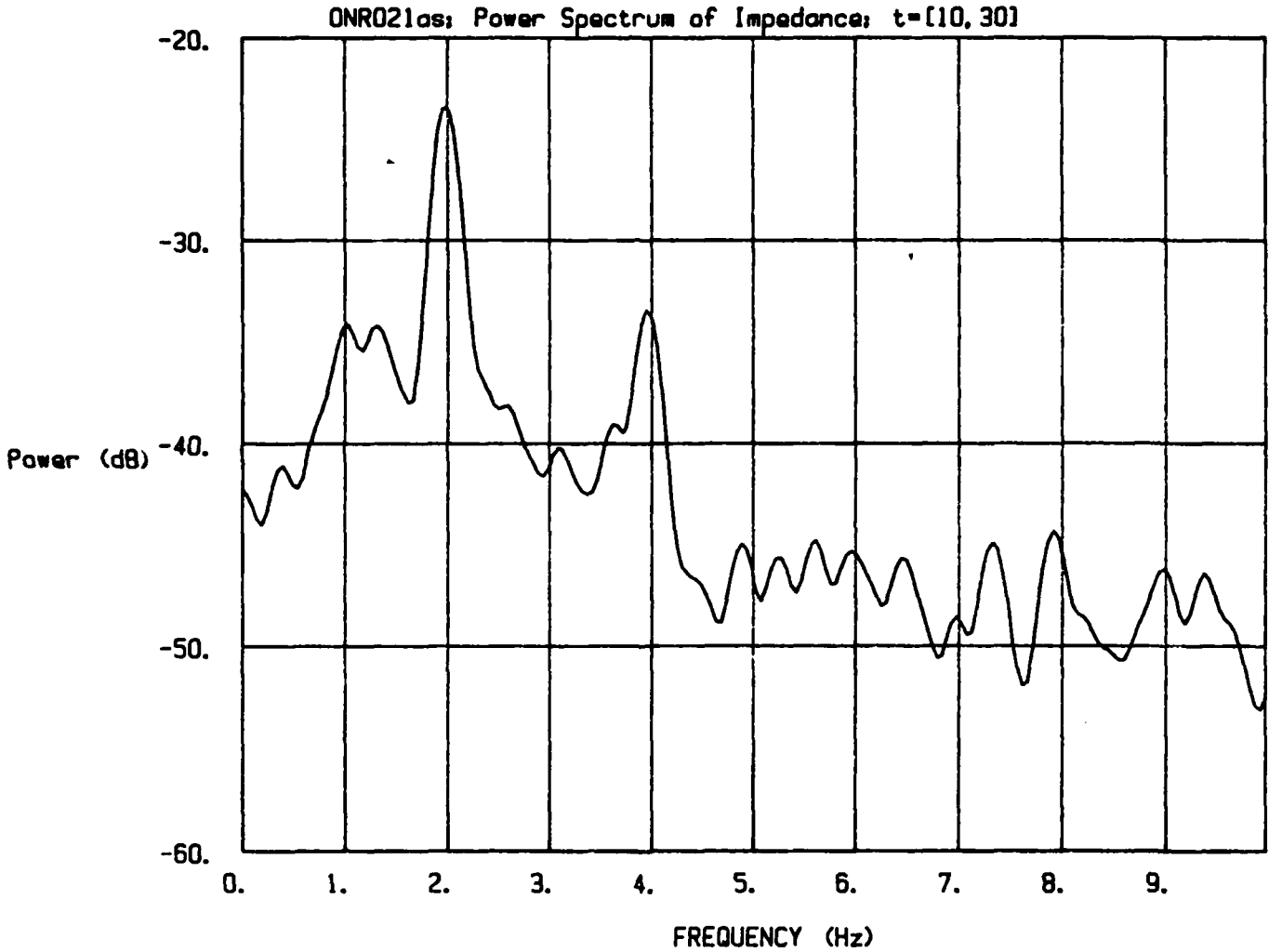

Fig. 44. Power spectrum of instantaneous impedance waveform for weld with bias to one sidewall.

6-Hz peak in the position spectrum, and there isn't any peak present.

The metallographic section shown in Figure 45 confirms the above observations, and, once again, points out the exceptional sensitivity of the through-the-arc methodology as applied to the SAW process. As can be seen, good sidewall fusion and good penetration are present even though there was a slight bias to one side of the joint. The position bias was too small to be evident in the weld result, yet the signal analysis clearly showed the presence of the small bias.

Fffect of Lateral Oscillation

A number of weld tests were run to determine the amount of oscillation needed for reliable signal processing considerations and to determine the effect, if any, on the quality of the weld. Since lateral oscillation has rarely, if ever, been used with conventional SAW welding, these tests were considered of fundamental importance.

As an example of these tests, weld number 16, pass 4 (Data File ONR164AS) will be discussed in this section. On this weld pass (pass number 4), the oscillation width was varied in three steps, with data taken for approximately 50 mm at each width setting. The width setting at the beginning of the weld was 8 mm peak-to-peak; during the next segment of the weld it was increased to 10 mm peak-to-peak; and during the last segment the oscillation width was set at 12.5 mm.

Figure 45. Photomacrograph of weld number 2.

The wire speed was 3937 mm/min, the travel speed was 229 mm/min, the nominal current was 550 amperes, the nominal voltage was 31 volts, the CTWD was 19.0 mm, and the oscillation dwell times at both the left and right sides were 0.2 seconds.

Figure 46 shows the power spectrum of the position signal taken during the first segment of the test with an oscillation width of 8 mm peak-to-peak. The oscillation frequency can be seen to be approximately 1.1 Hz. The power spectra of current, voltage, instantaneous power, and instantaneous impedance, computed from the same data segment are shown in Figures 47 through 50 respectively. As can be seen from these plots, there is about as much energy at the fundamental oscillation frequency of 1.1 Hz as at twice this frequency, i.e., 2.2 Hz. This suggests that the oscillation width is not quite adequate to achieve robust signals for reliable analysis and control.

Figure 51 shows the power spectrum of the position signal taken during the second segment of the test with an oscillation width of 10 mm peak-to-peak. The oscillation frequency can be seen to now be approximately 1 Hz. The frequency is lowered by increasing the oscillation width because the oscillator mechanism sets the oscillation rate rather than frequency. The power spectra of current, voltage, instantaneous power, and instantaneous impedance, computed from the same data segment are shown in Figures 52 through 55 respectively. As can be seen, the dominant peak in the power

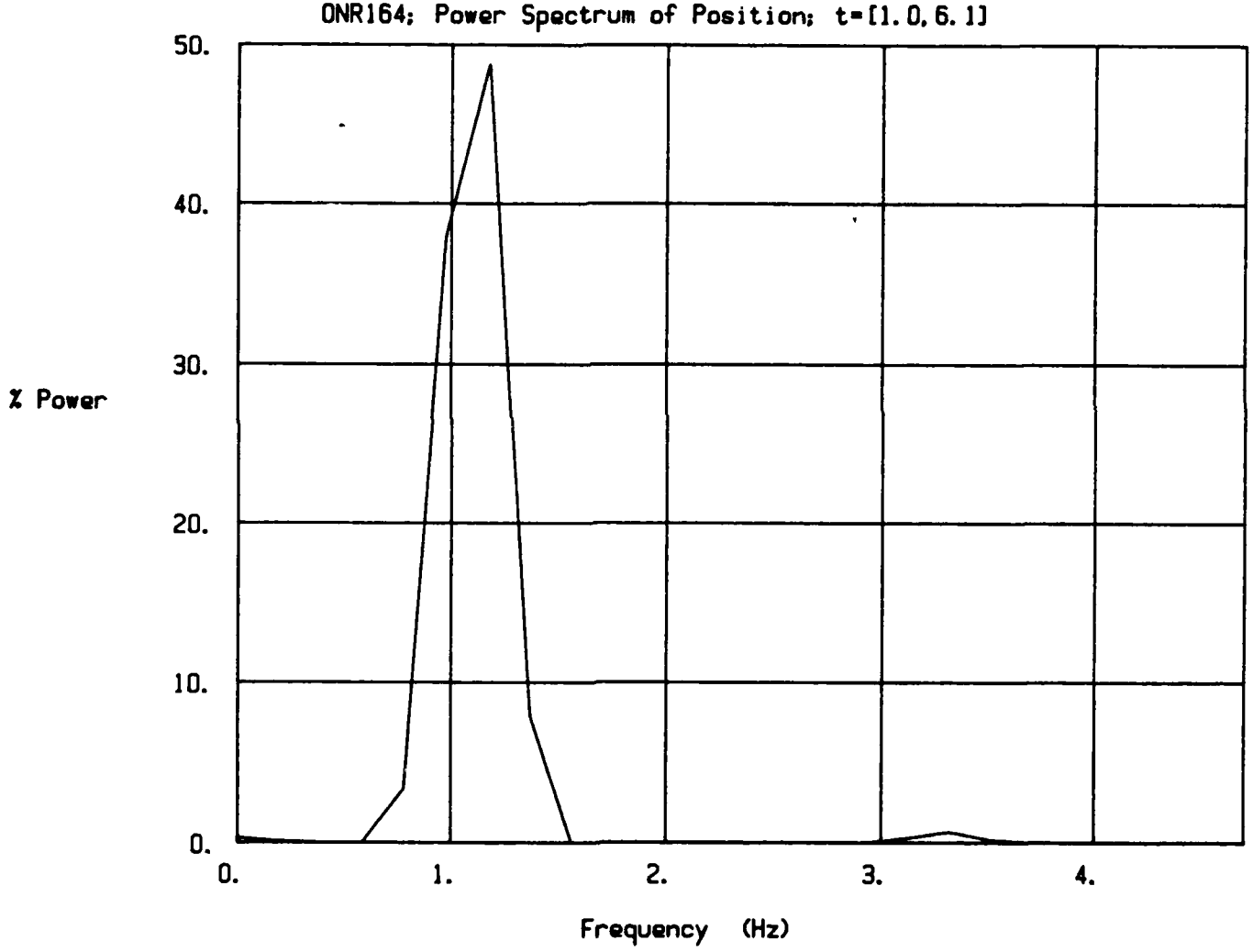

Fig. 46. Power spectrum of cross-seam position signal taken from data acquired during first third of weld, for weld with varying oscillation width.

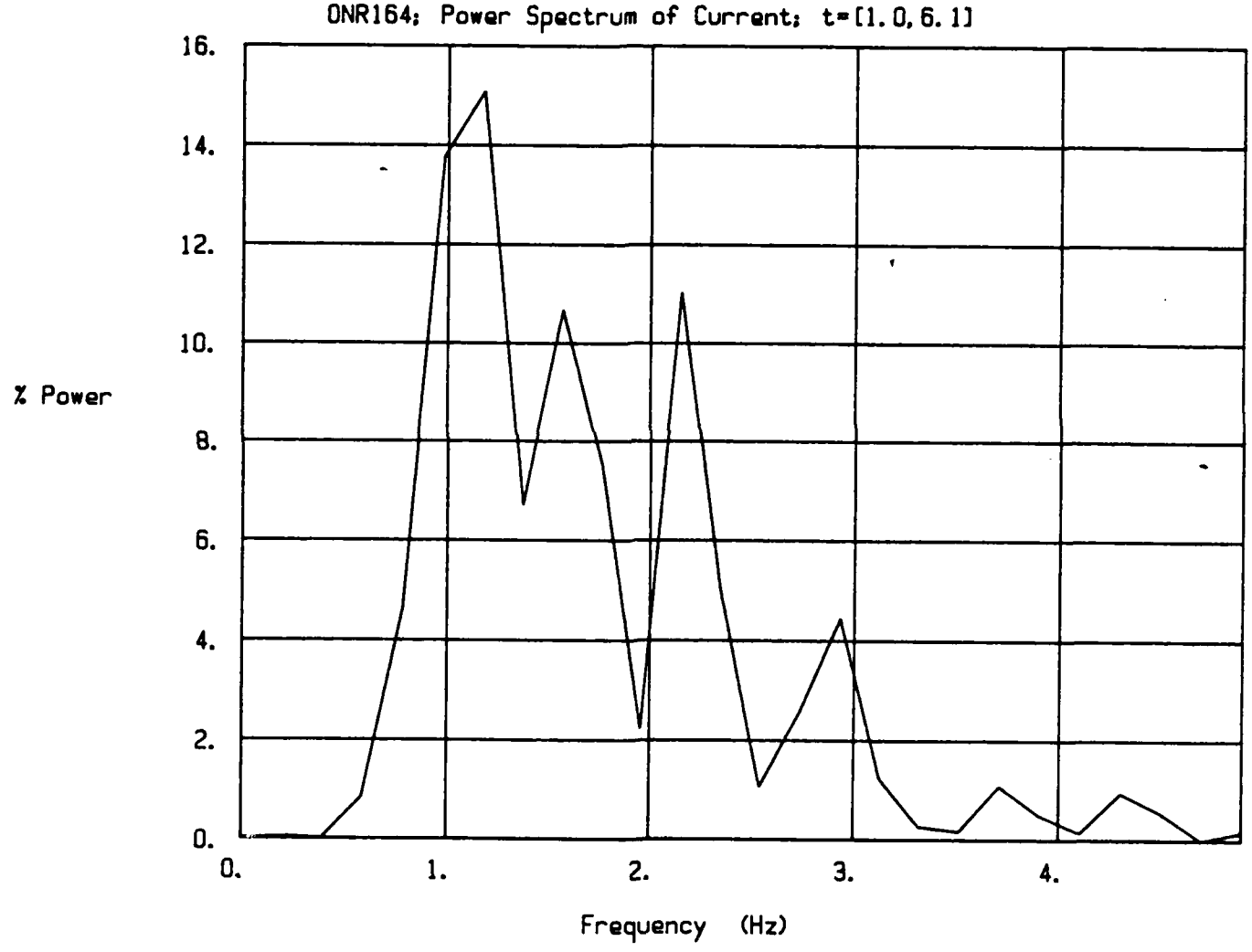

Fig. 47. Power spectrum of current waveform taken from data acquired during first third of weld, for weld with varying oscillation width.

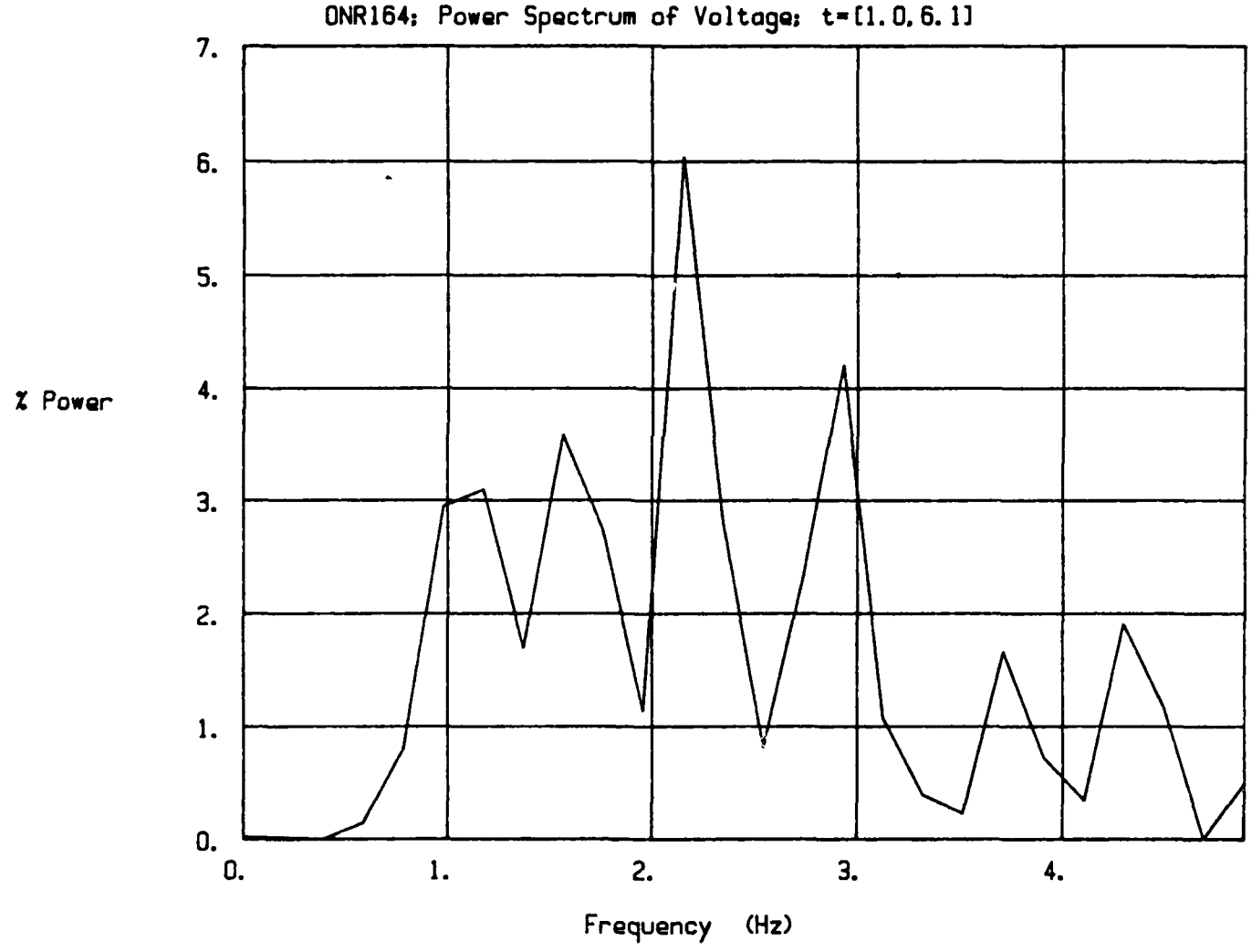

Fig. 48. Power spectrum of voltage waveform taken from data acquired during first third of weld, for weld with varying oscillation width.

AD-A166 328 SUBMERGED ARC WELDING CONTROL VIA ARC SENSING(U) 2/2
CRC-EVANS AUTOMATIC WELDING HOUSTON TX
M D RANDALL ET AL. 31 JAN 86 CRCAW-0001AC
UNCLASSIFIED N00014-85-C-0750 F/G 13/8 NL

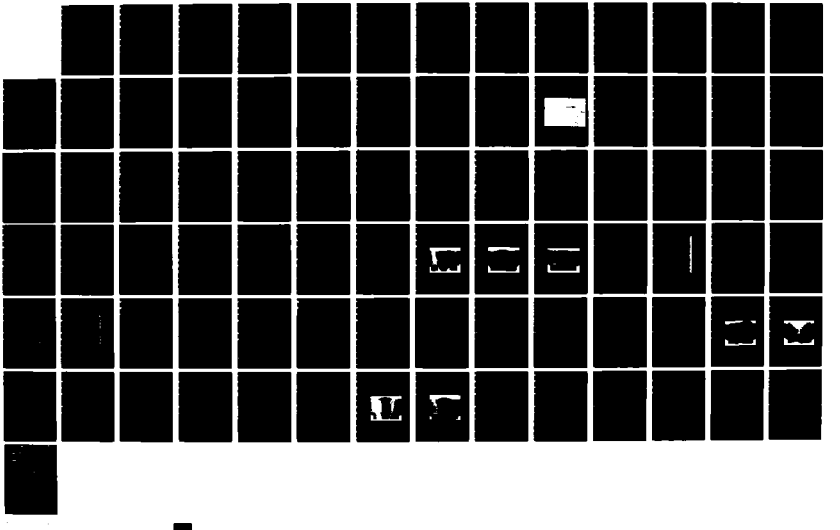

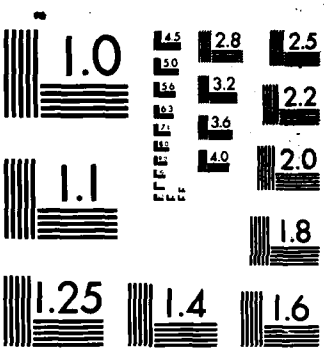

MICROCOPY RESOLUTION TEST CHART
NATIONAL BUREAU OF STANDARDS-1963-A

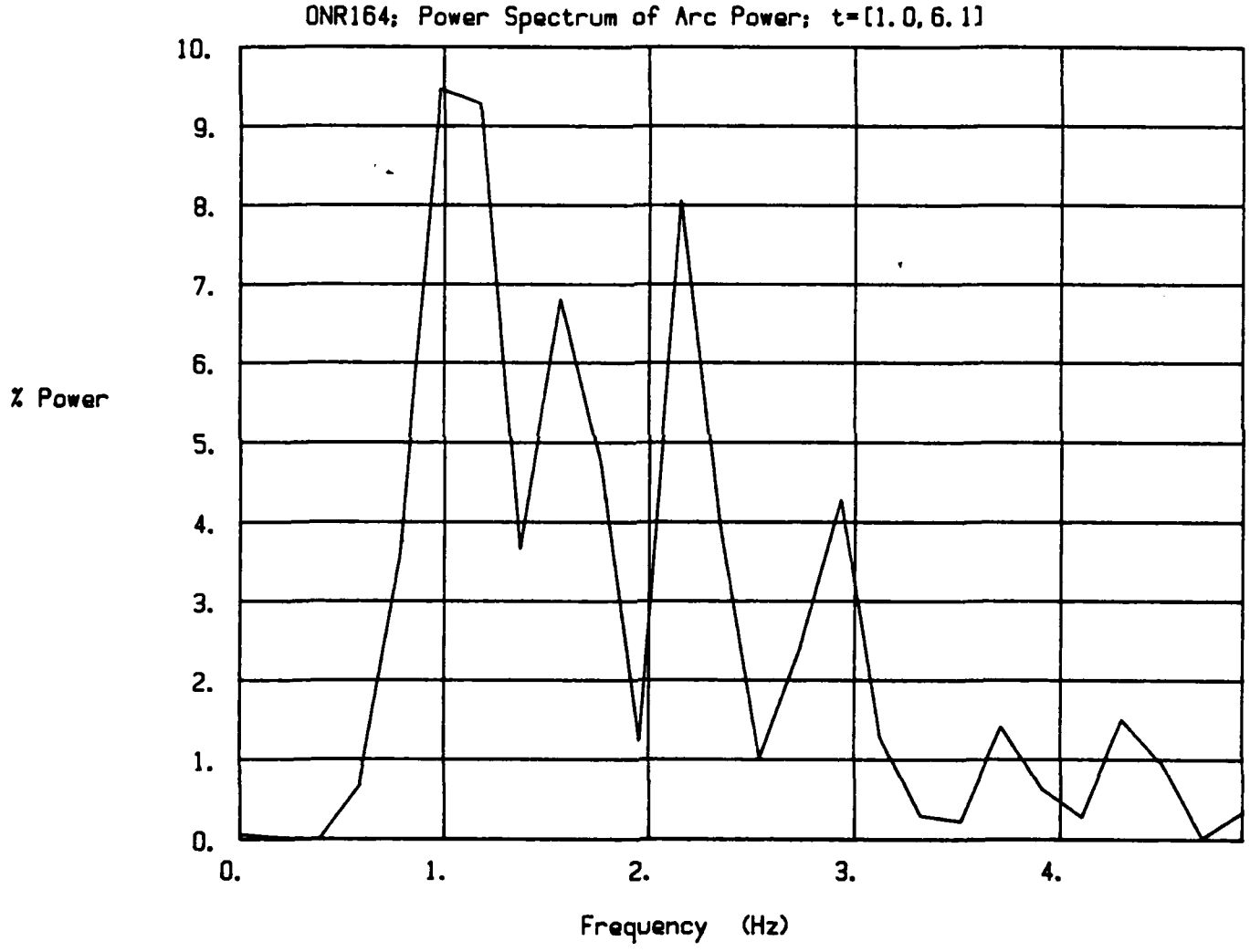

Fig. 49. Power spectrum of instantaneous power waveform taken from data acquired during first third of weld, for weld with varying oscillation width.

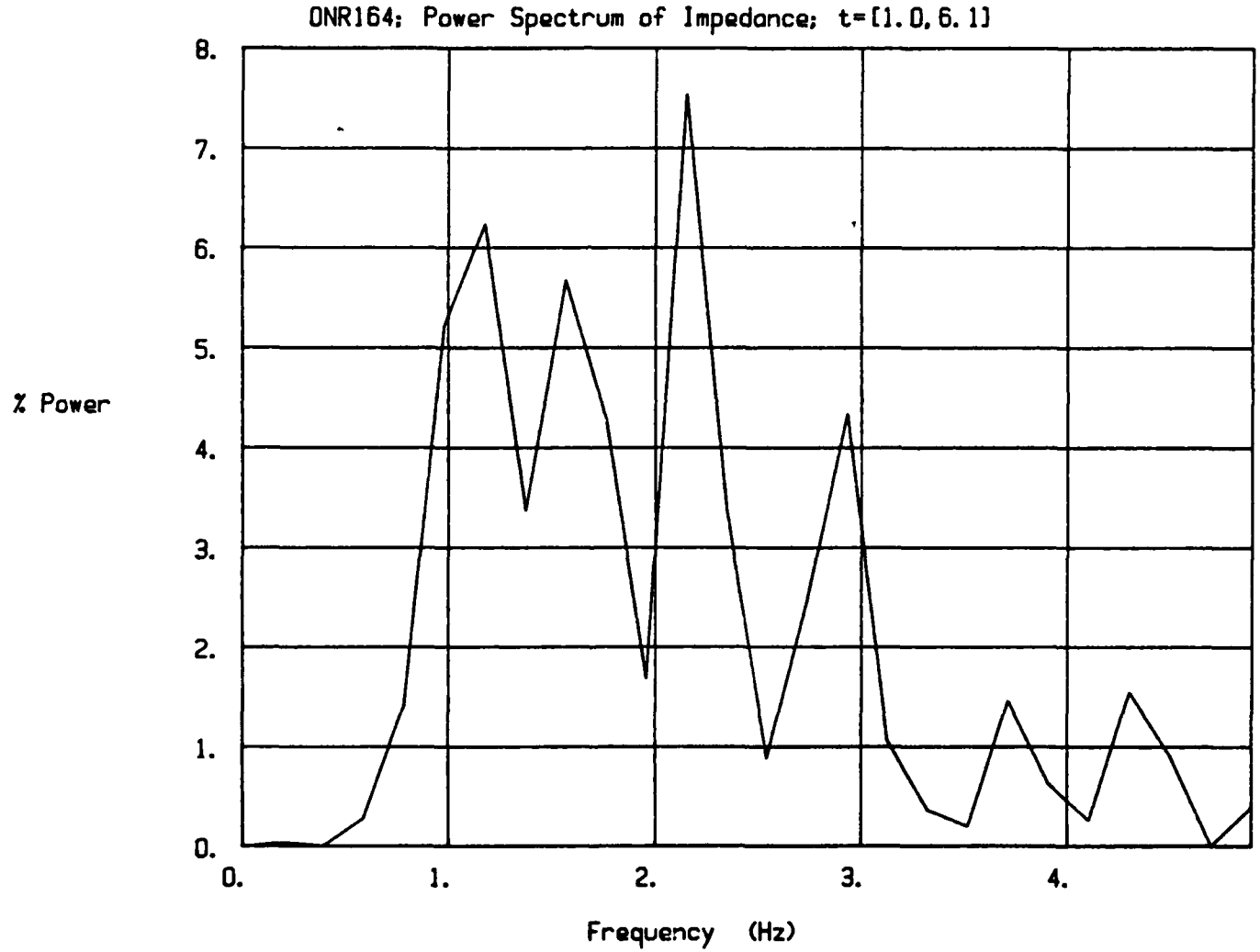

Fig. 50. Power spectrum of instantaneous impedance waveform taken from data acquired during first third of weld, for weld with varying oscillation width.

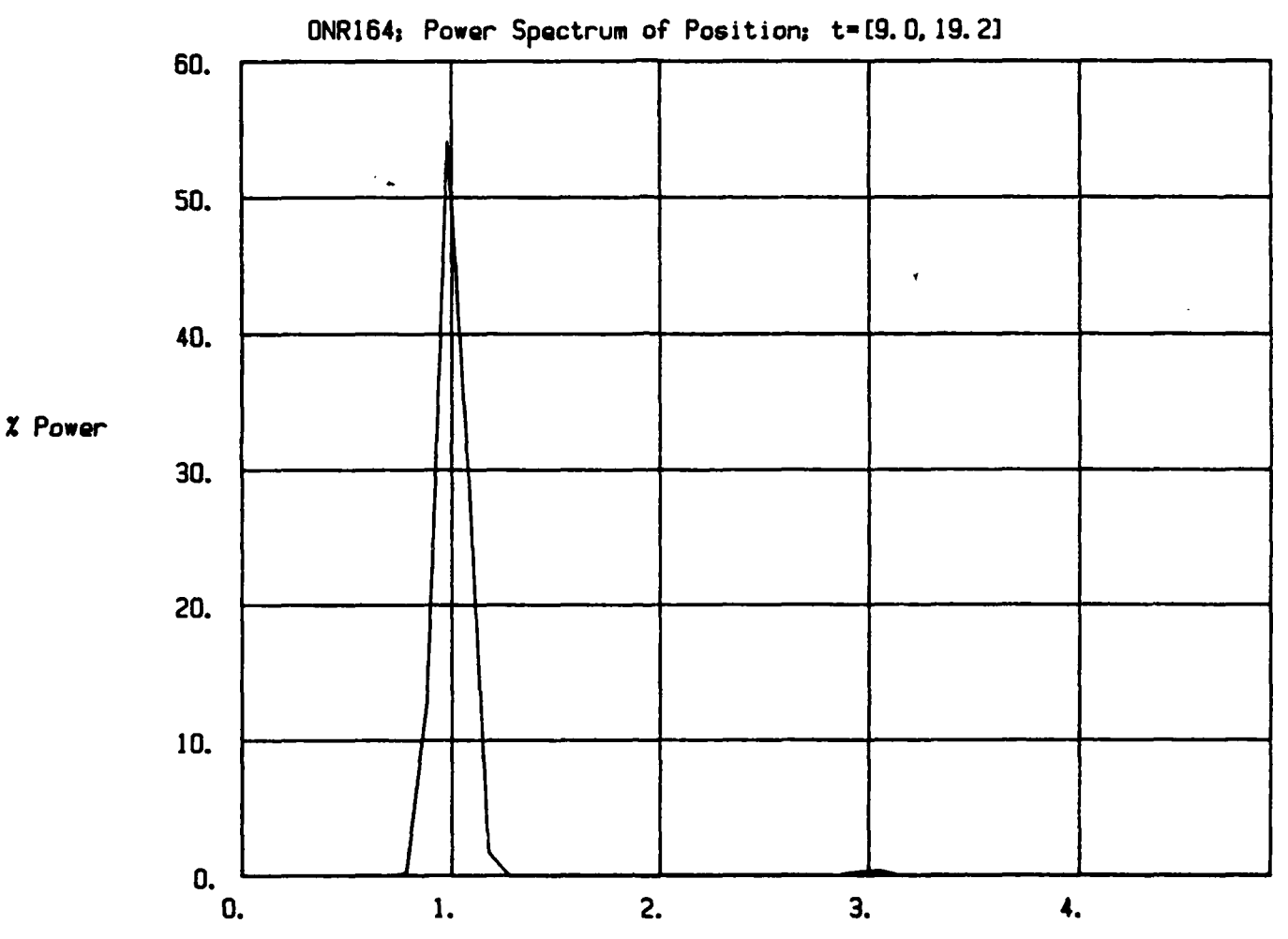

Fig. 51. Power spectrum of cross-seam position signal taken from data acquired during middle third of weld, for weld with varying oscillation width.

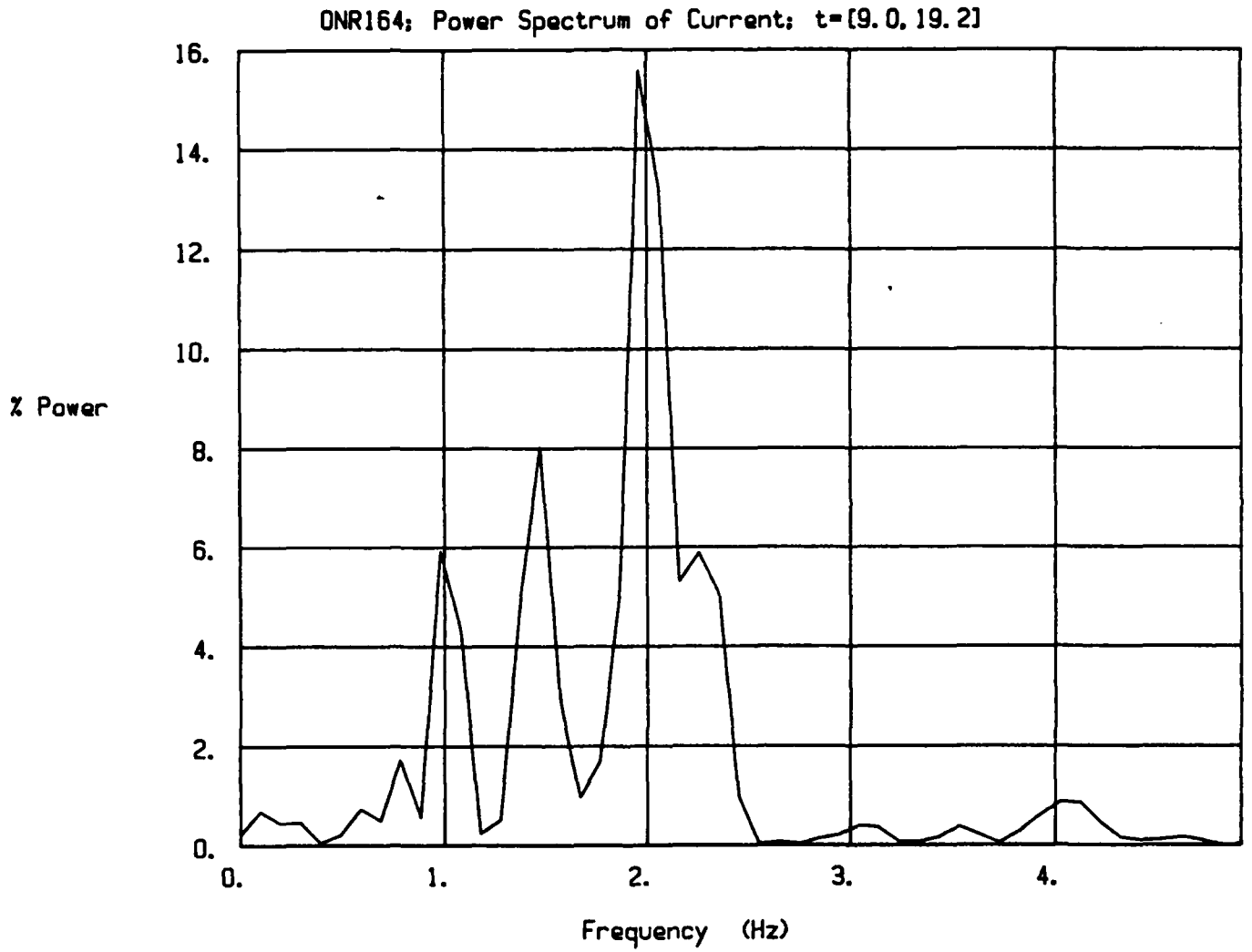

Fig. 52. Power spectrum of current waveform taken from data acquired during middle third of weld, for weld with varying oscillation width.

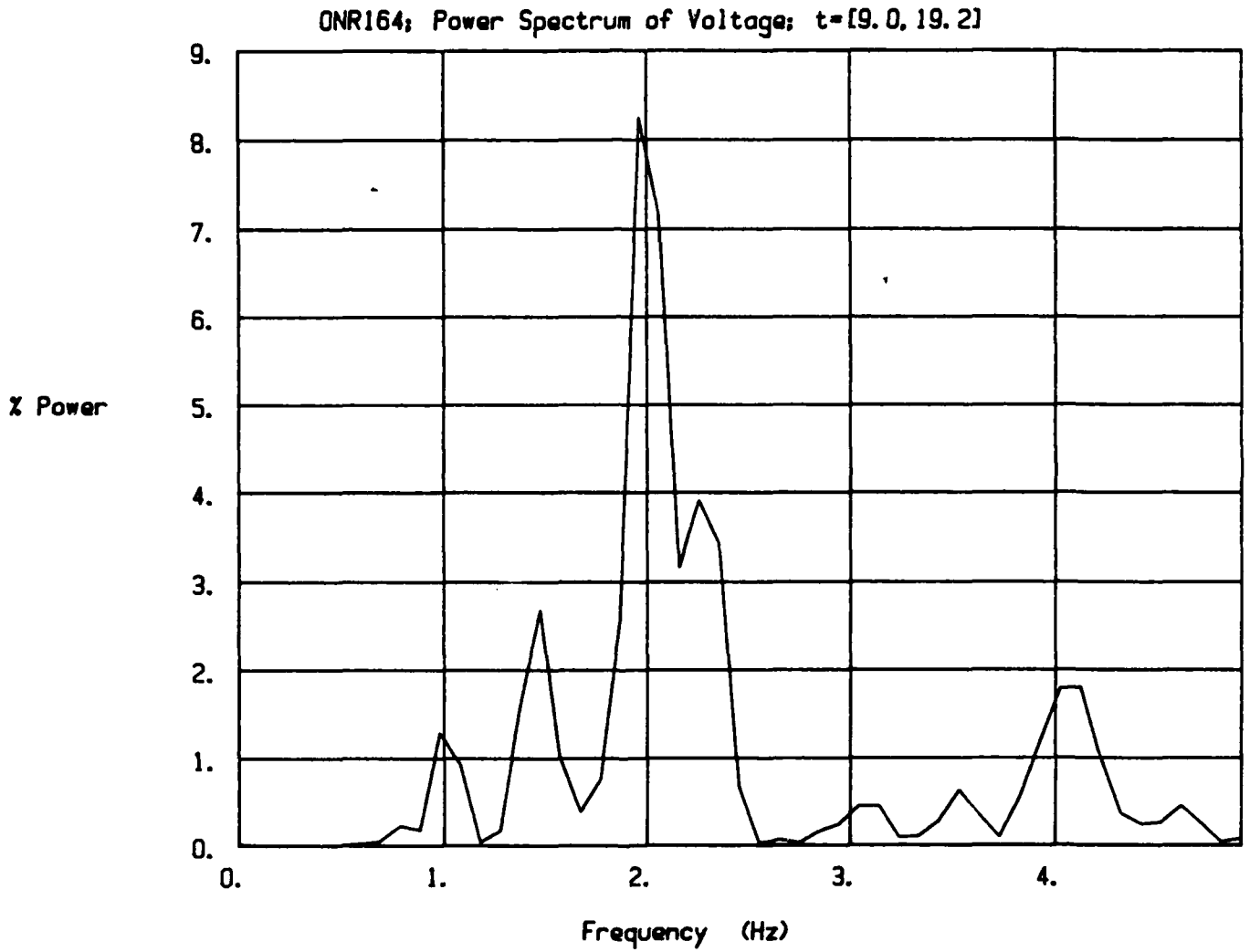

Fig. 53. Power spectrum of voltage waveform taken from data acquired during middle third of weld, for weld with varying oscillation width.

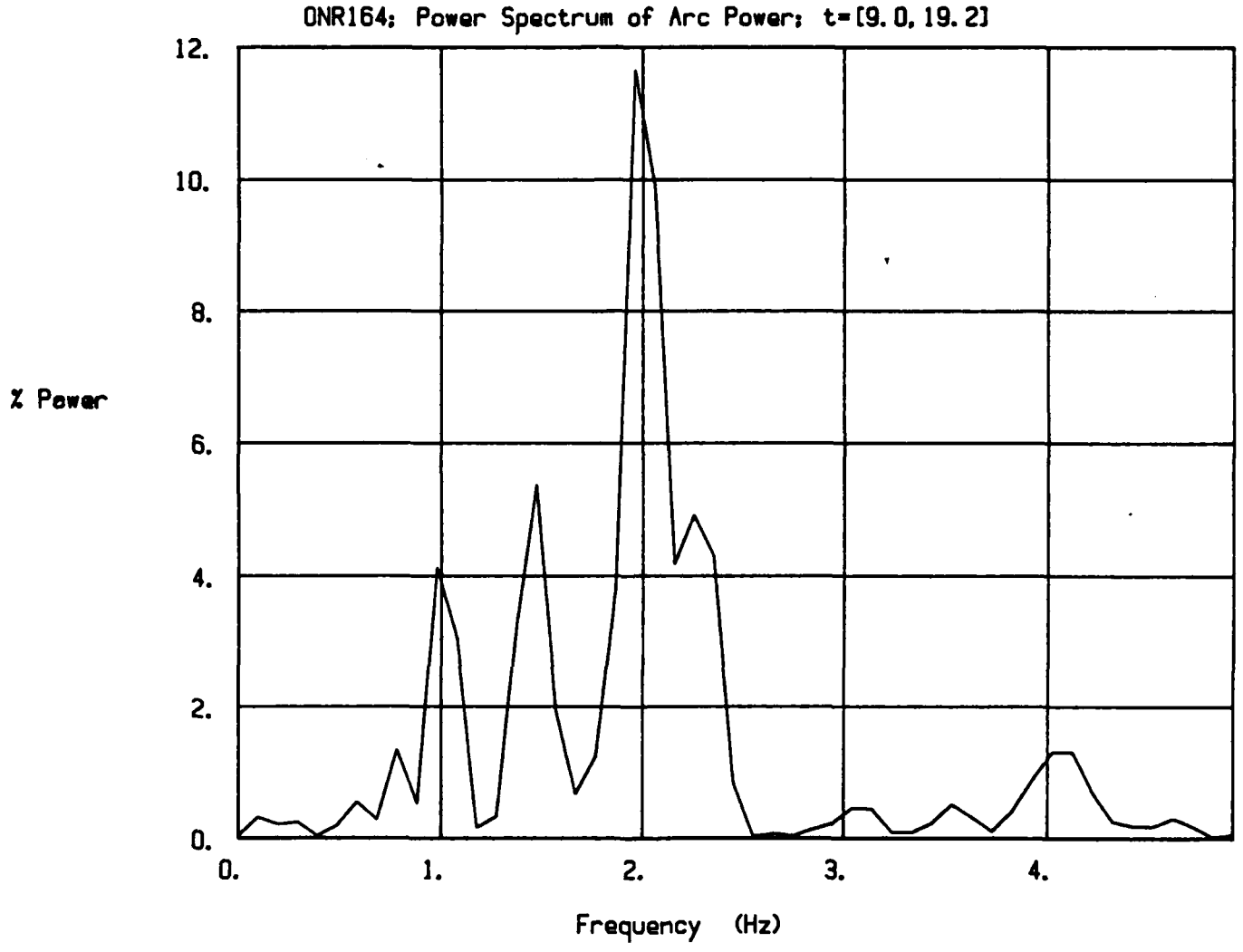

Fig. 54. Power spectrum of instantaneous power waveform taken from data acquired during middle third of weld, for weld with varying oscillation width.

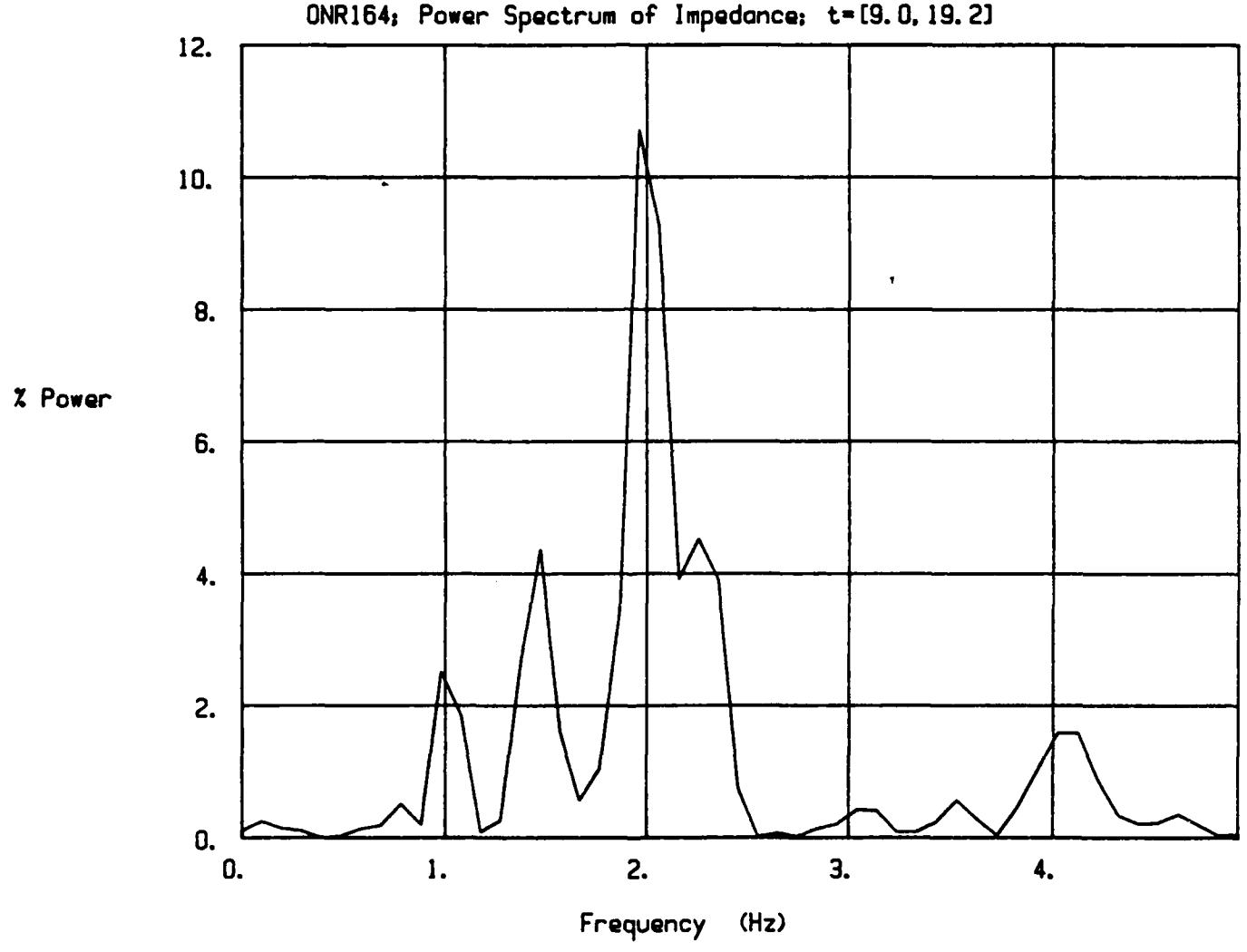

Fig. 55. Power spectrum of instantaneous impedance waveform taken from data acquired during middle third of weld, for weld with varying oscillation width.

spectra curves now occurs at twice the cross-seam oscillation frequency, i.e, 2 Hz. This indicates that this setting of the oscillation width is adequate to obtain reliable signals for analysis and control purposes. A post weld visual inspection of the surface of the bead showed that for both segments 1 and 2, the sidewall fusion was good and the general bead shape was good.

While the second segment proved to be adequate to obtain robust signals, the third segment was run at even a greater oscillation width to see if there were any improvement (or deterioration) in the voltage and current signals and if there were any deterioration in the weld bead appearance. Figure 56 shows the power spectrum of the position signal taken during the final segment of the test. The oscillation width is now 12.5 mm, and the oscillation frequency can be seen to be approximately 0.85 Hz. The power spectra of current, voltage, instantaneous power, and instantaneous impedance, computed from the same data segment are shown in Figures 57 through 60 respectively. As can be seen, the dominant peak in the power spectra curves still occurs at twice the cross-seam oscillation frequency, i.e., 1.7 Hz. There is not any noticeable improvement in the signal content, however; the second oscillation width setting, i.e., 10 mm, providing just as good signals. A visual inspection of the bead after the weld was made showed some small amount of scalloping in this segment of the weld, indicating a slightly excessive oscillation width.

The conclusion to be reached from this test, as well as others made with a similar objective, is that the amount of lateral cross-seam

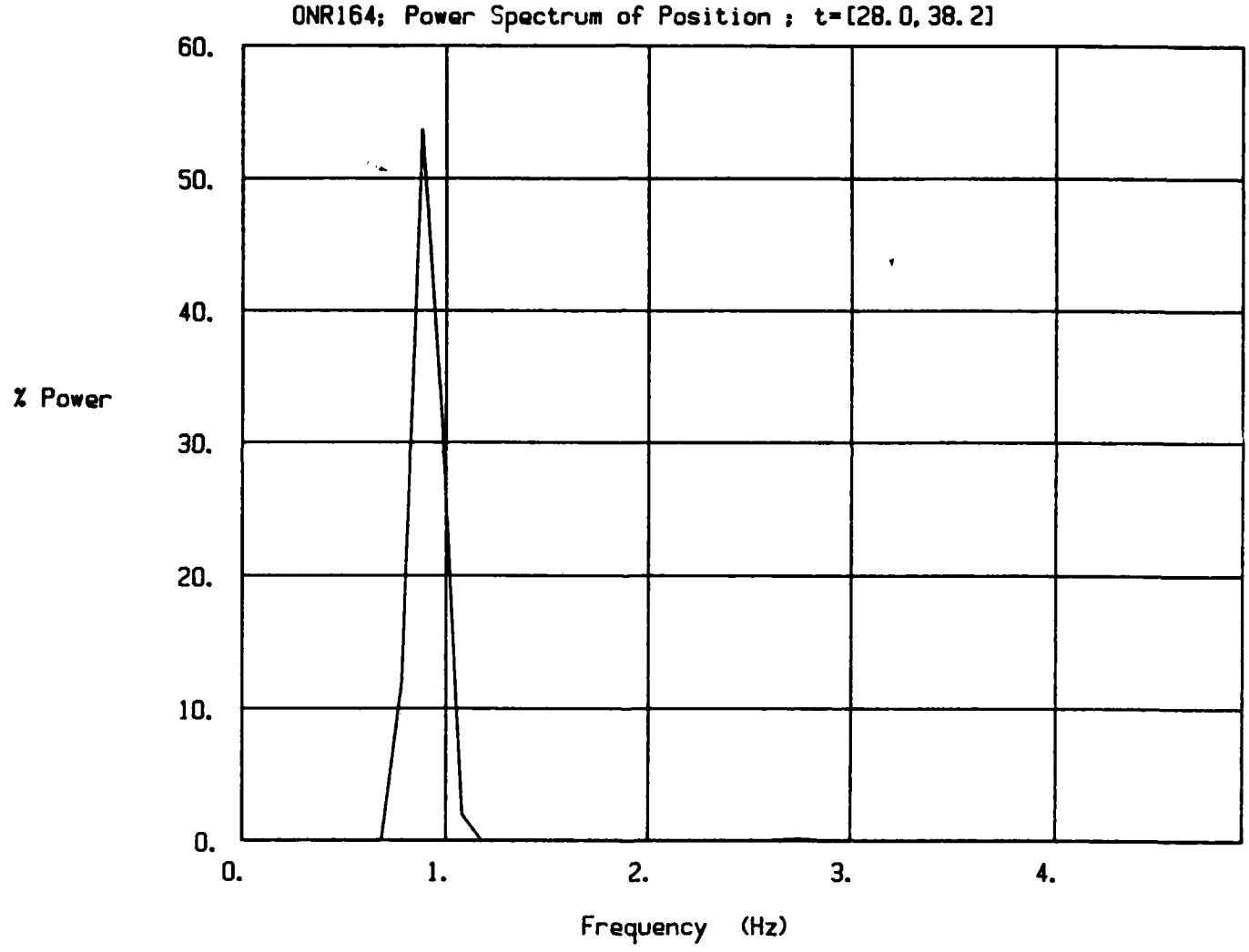

Fig. 56. Power spectrum of cross-seam position signal taken from data acquired during last third of weld, for weld with varying oscillation width.

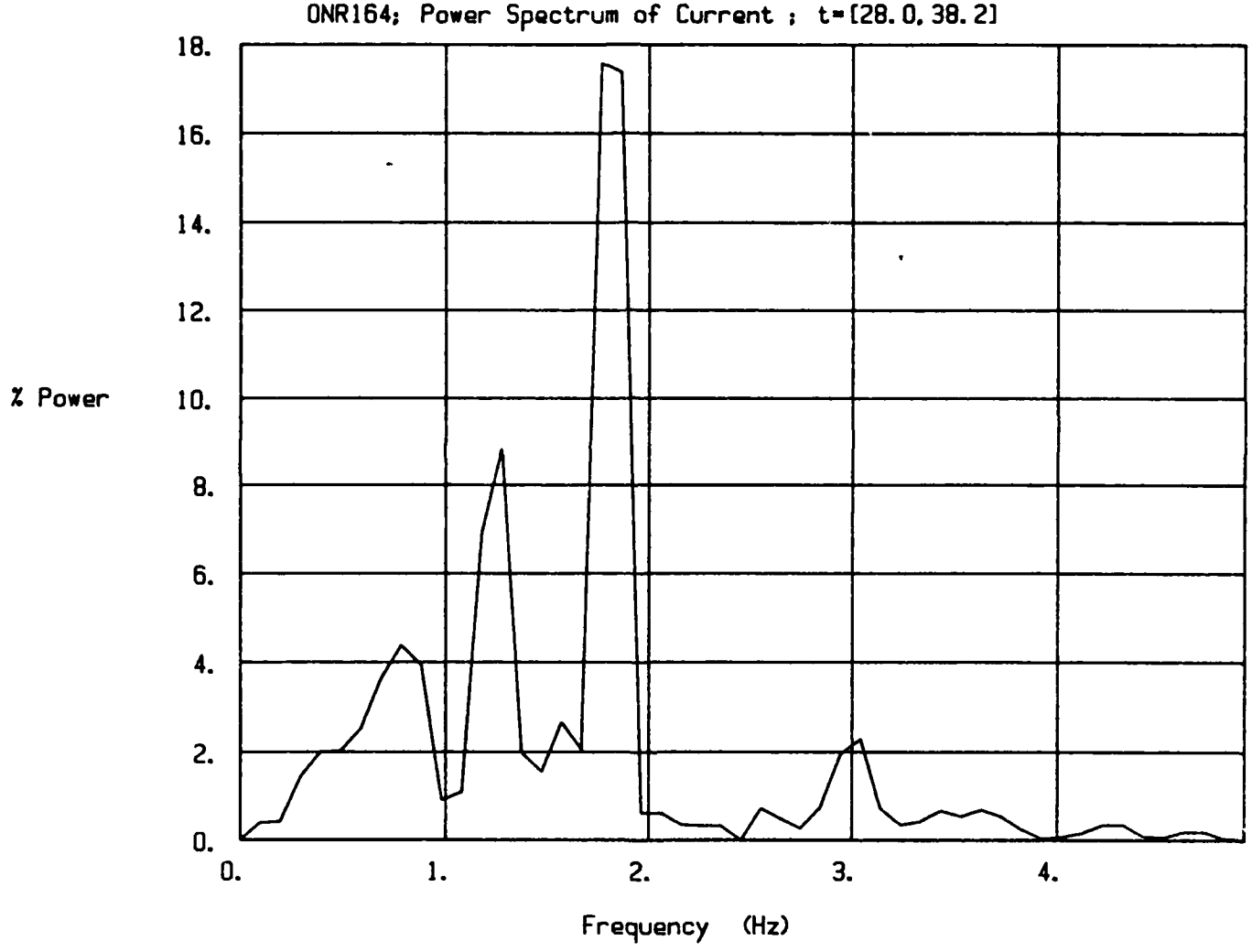

Fig. 57. Power spectrum of current waveform taken from data acquired during last third of weld, for weld with varying oscillation width.

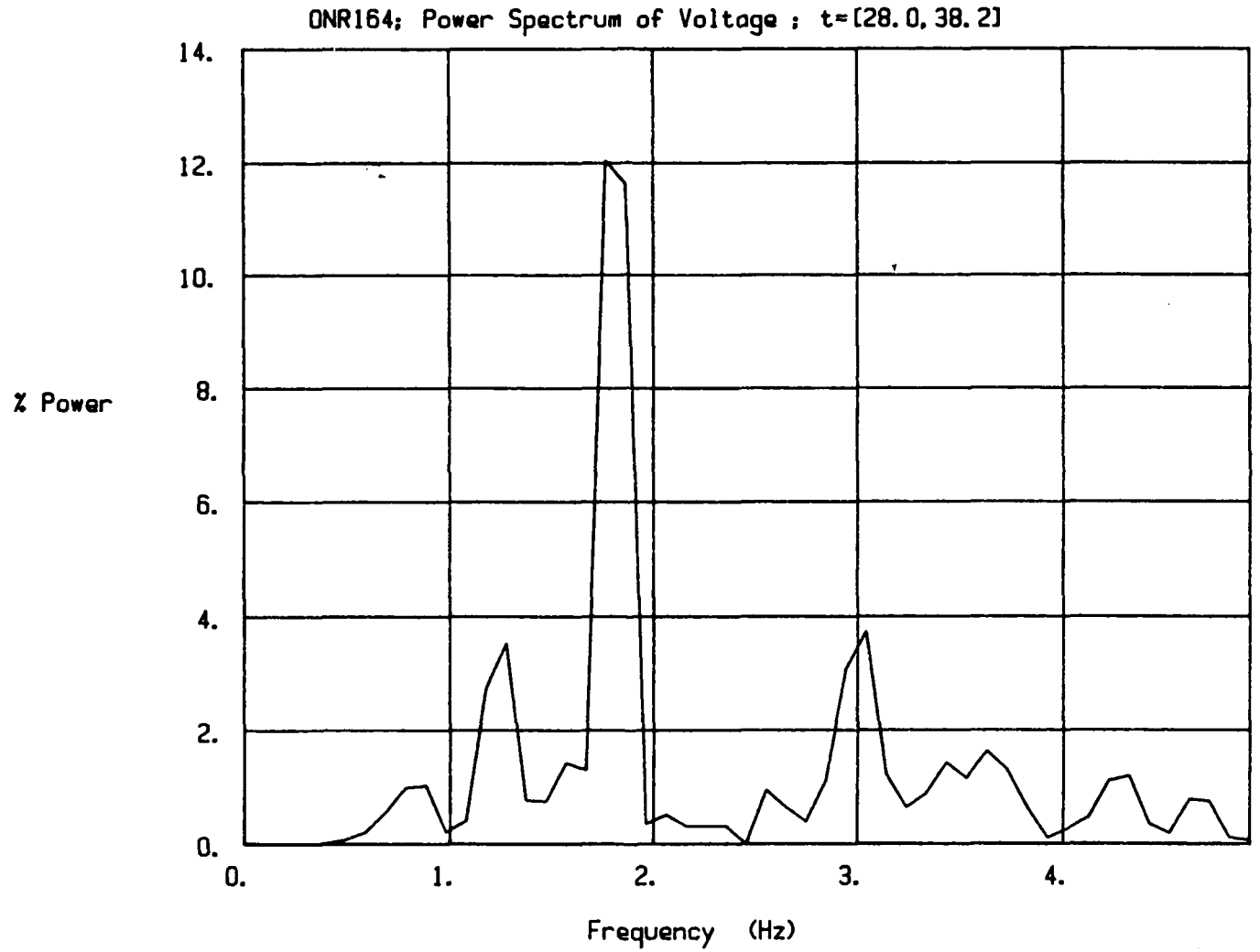

Fig. 58. Power spectrum of voltage waveform taken from data acquired during middle third of weld, for weld with varying oscillation width.

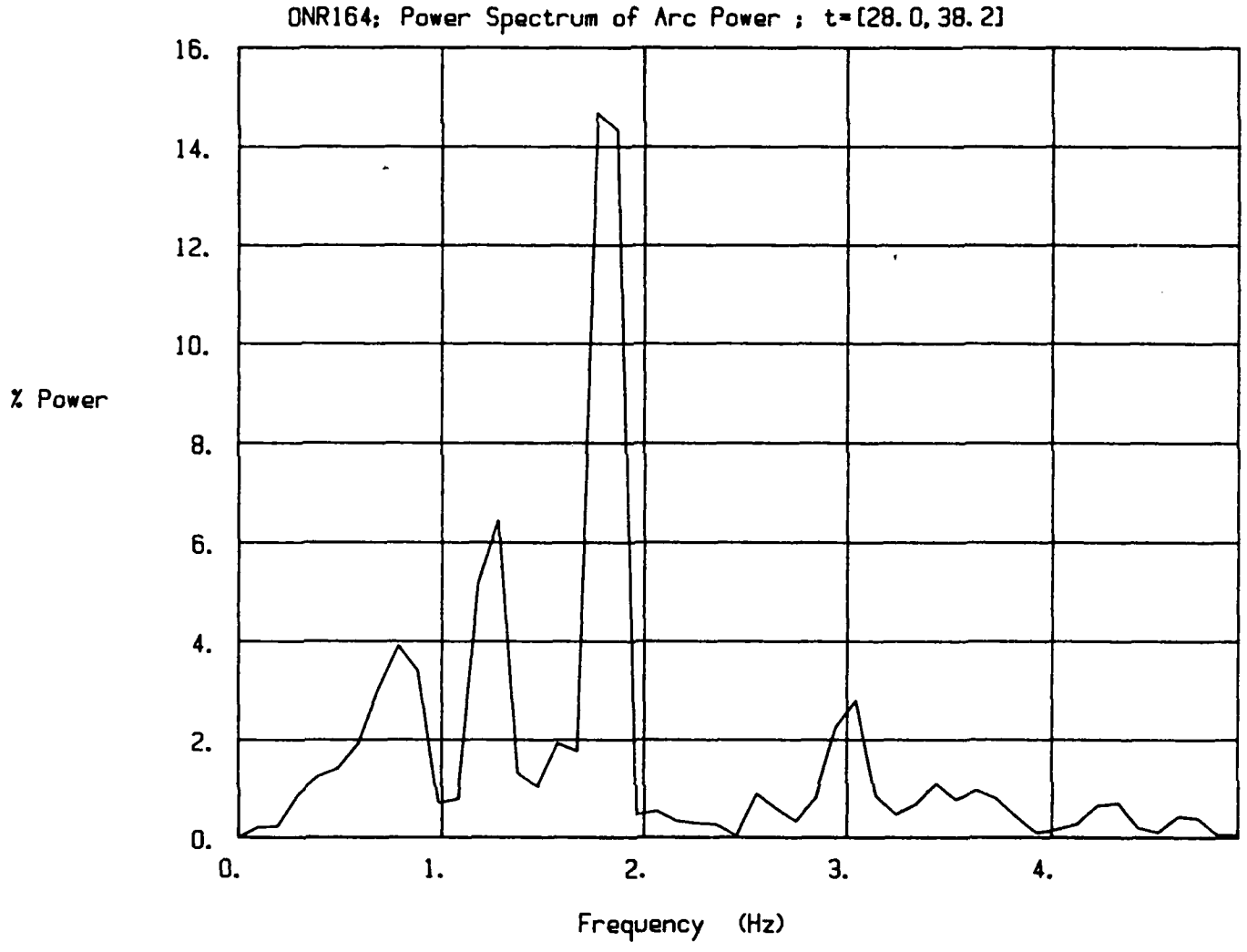

Fig. 59. Power spectrum of instantaneous power waveform taken from data acquired during last third of weld, for weld with varying oscillation width.

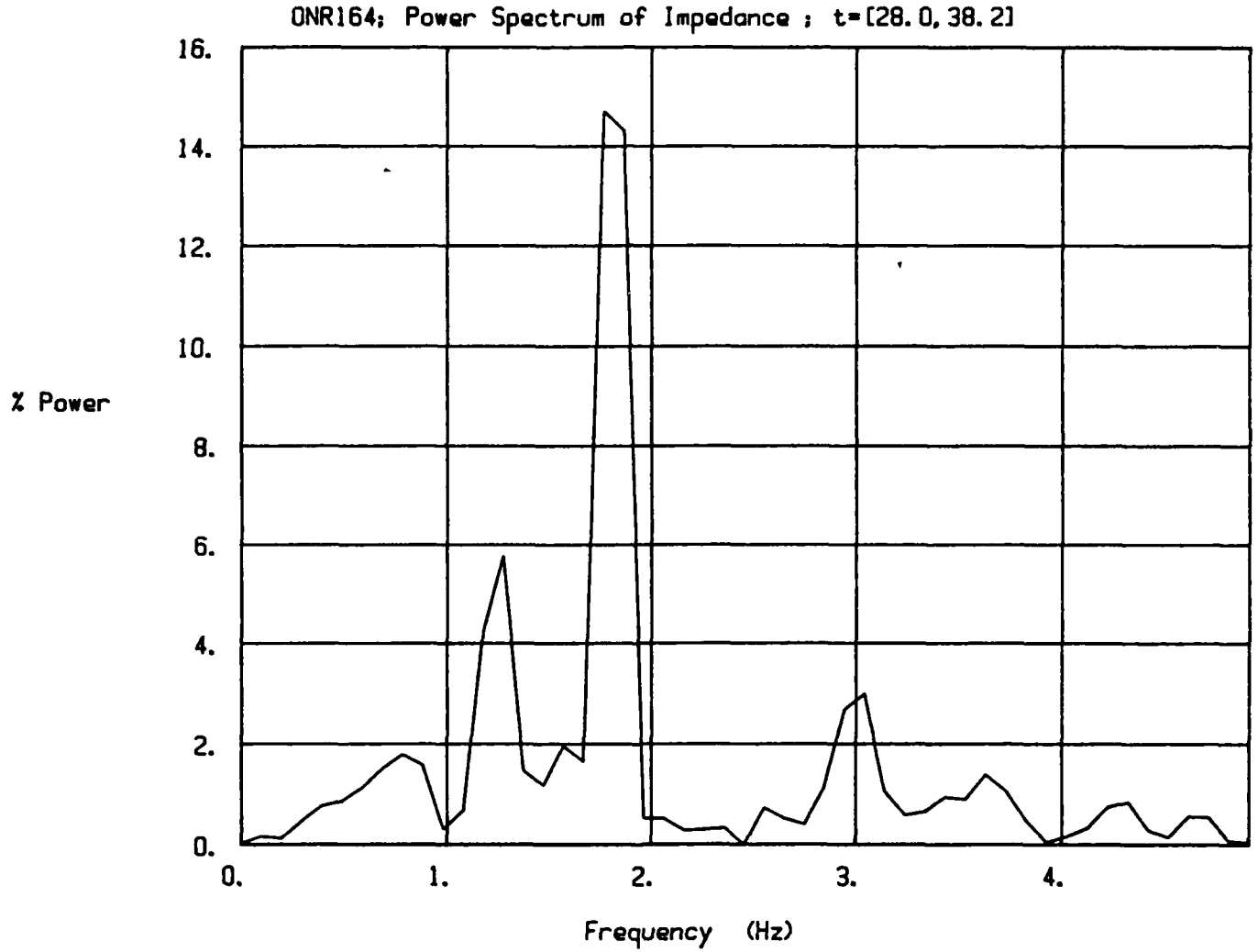

Fig. 60. Power spectrum of instantaneous impedance waveform taken from data acquired during last third of weld, for weld with varying oscillation width.

oscillation needed to obtain robust current and voltage variations for control purposes results in good weld bead quality as well. Metallographic sections shown elsewhere in this report show this also. More extensive testing in the Phase II research program will be required to thoroughly investigate the advantages of cross-seam oscillation from the standpoint of weld soundness. It is well known that cross-seam oscillation is frequently used with other welding processes, and that metallurgical advantages are realized. It is anticipated that the Phase II research will show advantages of cross-seam oscillation with the SAW process as well. In any case, however, the preliminary results obtained in this Phase I limited research effort show that the necessary amount of oscillation needed for good through-the-arc signal analysis and control is not detrimental to the weld soundness, and indeed appears to offer improvements in the bead shape and sidewall fusion.

Pattern Recognition and Control Algorithms

The objective of this part of the Phase I research program was to investigate control algorithms that could be used to make reliable corrections in the torch position, lateral oscillation, and process parameters as a function of the processed signals obtained from the voltage and current waveforms. Generally, it was found that the signal changes experienced with the SAW tests (conducted thus far) were of equal or greater magnitude than those obtained with the GMAW or FCAW processes. Therefore, all of the algorithms that have been used with the GMAW or FCAW processes are potentially useful in controlling

the SAW process as well.

In this section a number of these algorithms are described and discussed for weld tests conducted in which the weld joint was skewed with respect to the longitudinal travel of the electrode. In these tests, no corrections were made to the electode centering. Therefore, the expected result from the algorithms is a signal that calls for a steadily increasing lateral correction as the weld proceeds from one end of the test workpiece to the other.

Algorithms Based on Peak Current Measurements

Perhaps the simplest algorithms are those based on the peak values of the current waveform at either extreme of oscillation and the value of the current at the center of the oscillation. These three values of current, measured per half-cycle of lateral oscillation, may be used to control the electrode position relative to the joint in several different ways. For simple centering purposes, the peak value on the left extreme of the oscillation excursion may be compared to the peak value on the right extreme of the oscillation excursion, and the difference of these two signals used to determine the direction and the amount of lateral correction called for on the next oscillation cycle. To illustrate this simple algorithm, the peak current, measured on the left excursion, is plotted in Figure 61 versus the oscillation cycle number for the weld sample 14, pass 3.

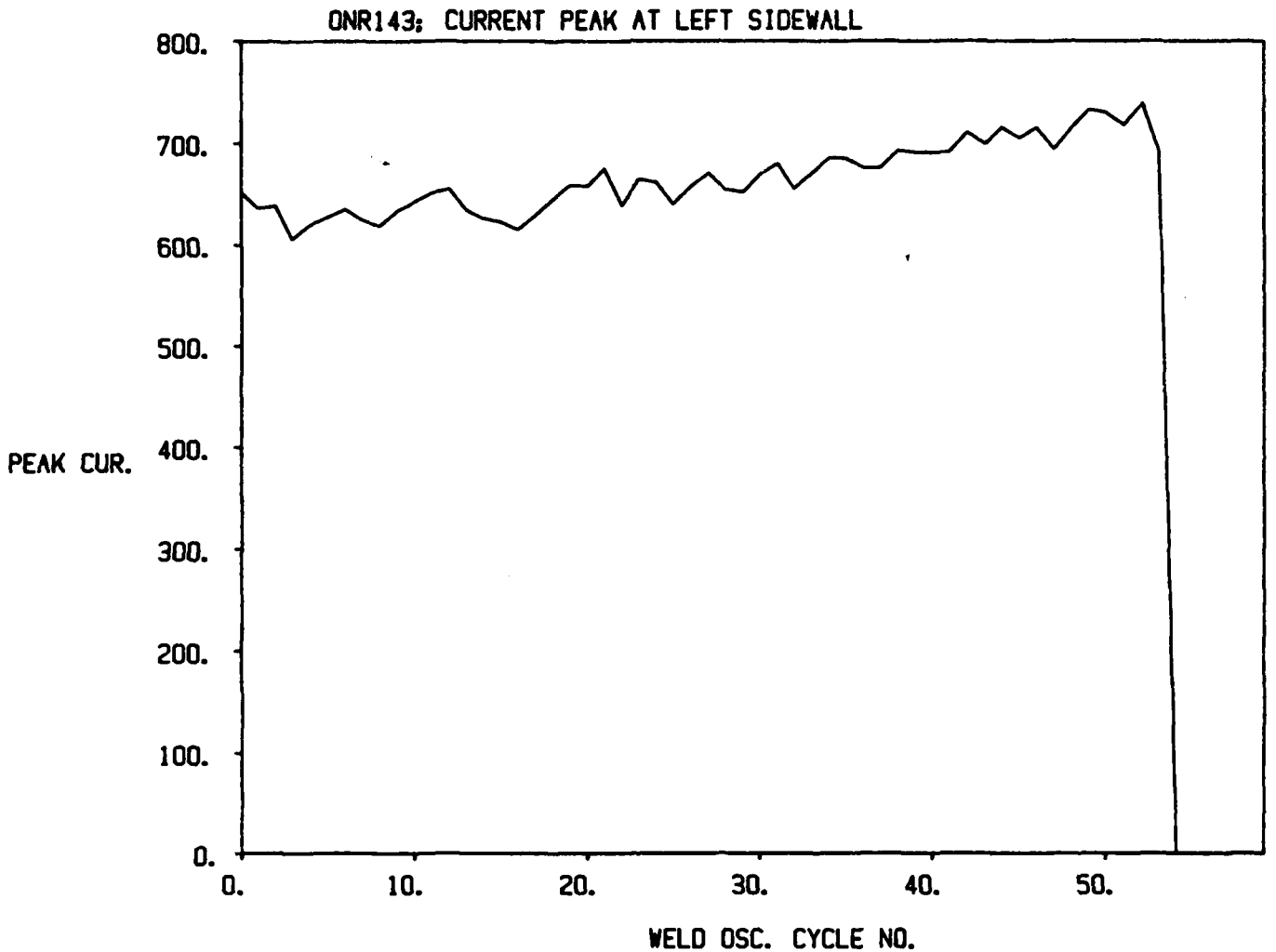

Fig. 61. Peak current measurement per cycle at left sidewall for skewed joint test.

The weld sample number 14, pass 3 (Data File ONR143AS) was made with the joint skewed with respect to the line traversed by the electrode by approximately 2.5 mm over the 600 mm length of the weld. The nominal current was 550 amperes, the nominal voltage was 31 volts, the contact tip to work distance (CTWD) was 12.7 mm, the wire speed was 3937 mm/min, the travel speed was 279 mm/ min, the peak-to-peak oscillation width was 11.25 mm, and the oscillation frequency was 1.25 Hz.

The peak current, measured on the right excursion, is plotted in Figure 62, and the current measured at the center of oscillation is plotted in Figure 63. Finally, the current difference between the left-and right-hand sides is plotted in Figure 64. In each of these figures, i.e., 61-64, the data is plotted as though it is continuous. In reality, only one data point per cycle of oscillation is taken for each of the figures. The data points are shown connected simply for convenience in using the plotting routine.

The difference plot, shown in Figure 64, clearly shows the effect of the plate being skewed relative to the line of travel of the electrode. The horizontal line at 0. represents the centerline of the joint; the slanting line represents the path of the electrode. The plot shown in Figure 64 represents only 40 seconds of the approximate 131 seconds required to make the complete weld of 600 mm length. Hence, the skew between the joint and the electrode's line of travel, for the 40 seconds of data shown, is approximately 0.75 mm. The effect of the skew can be seen

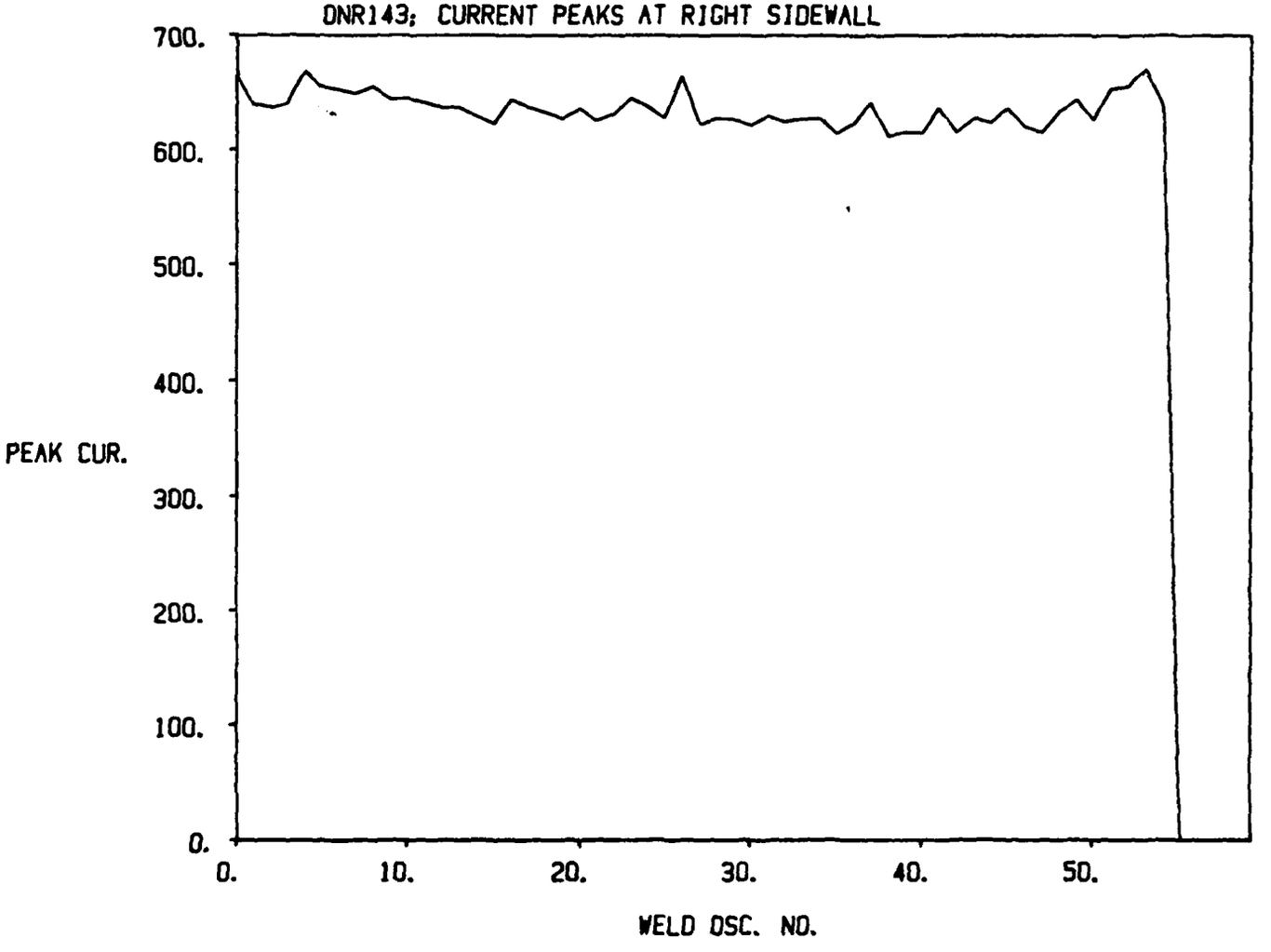

Fig. 62. Peak current measurements per cycle at right sidewall for skewed joint test.

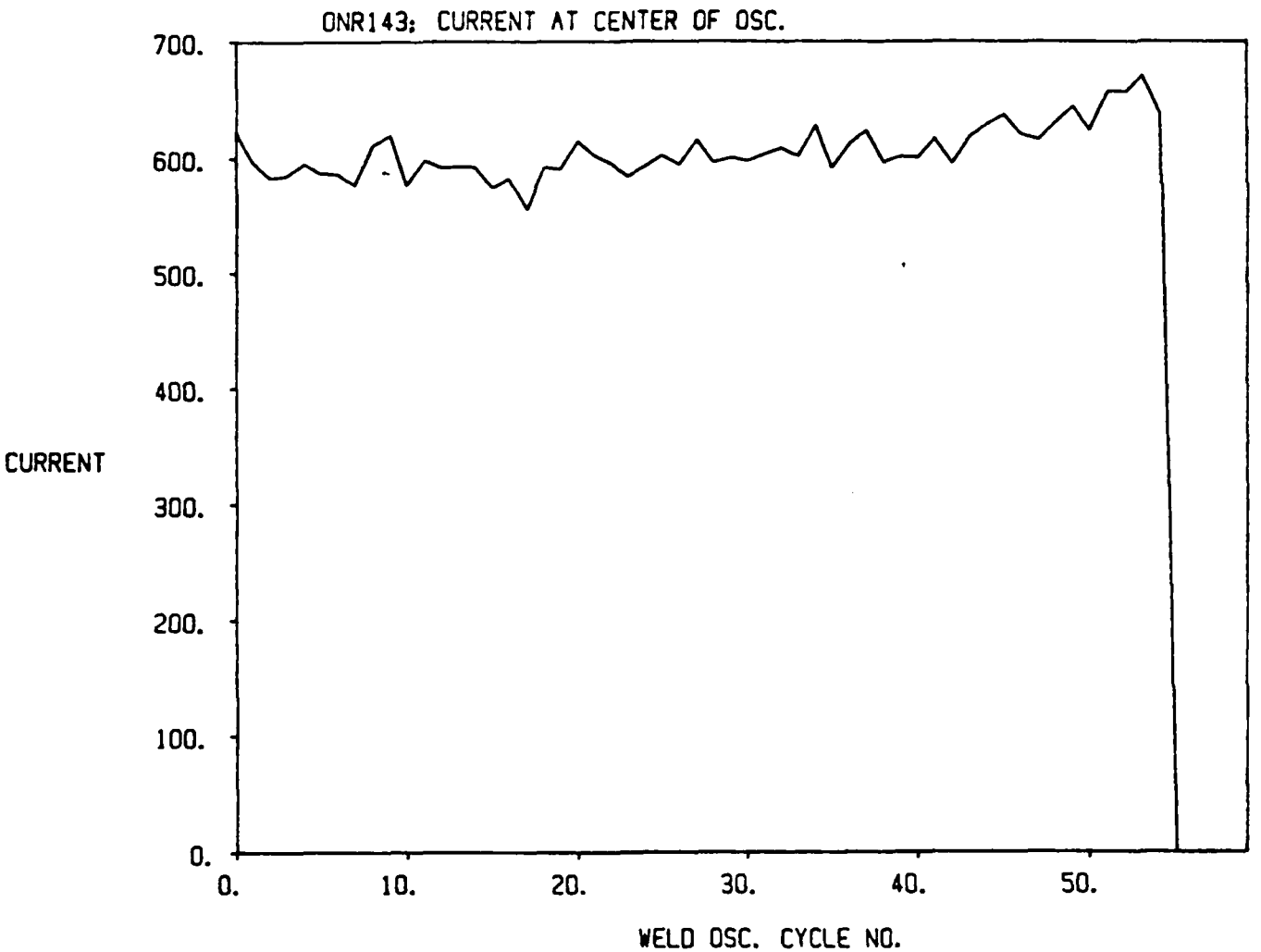

Fig. 63. Current measurements per cycle at center of oscillation cycle for skewed joint test.

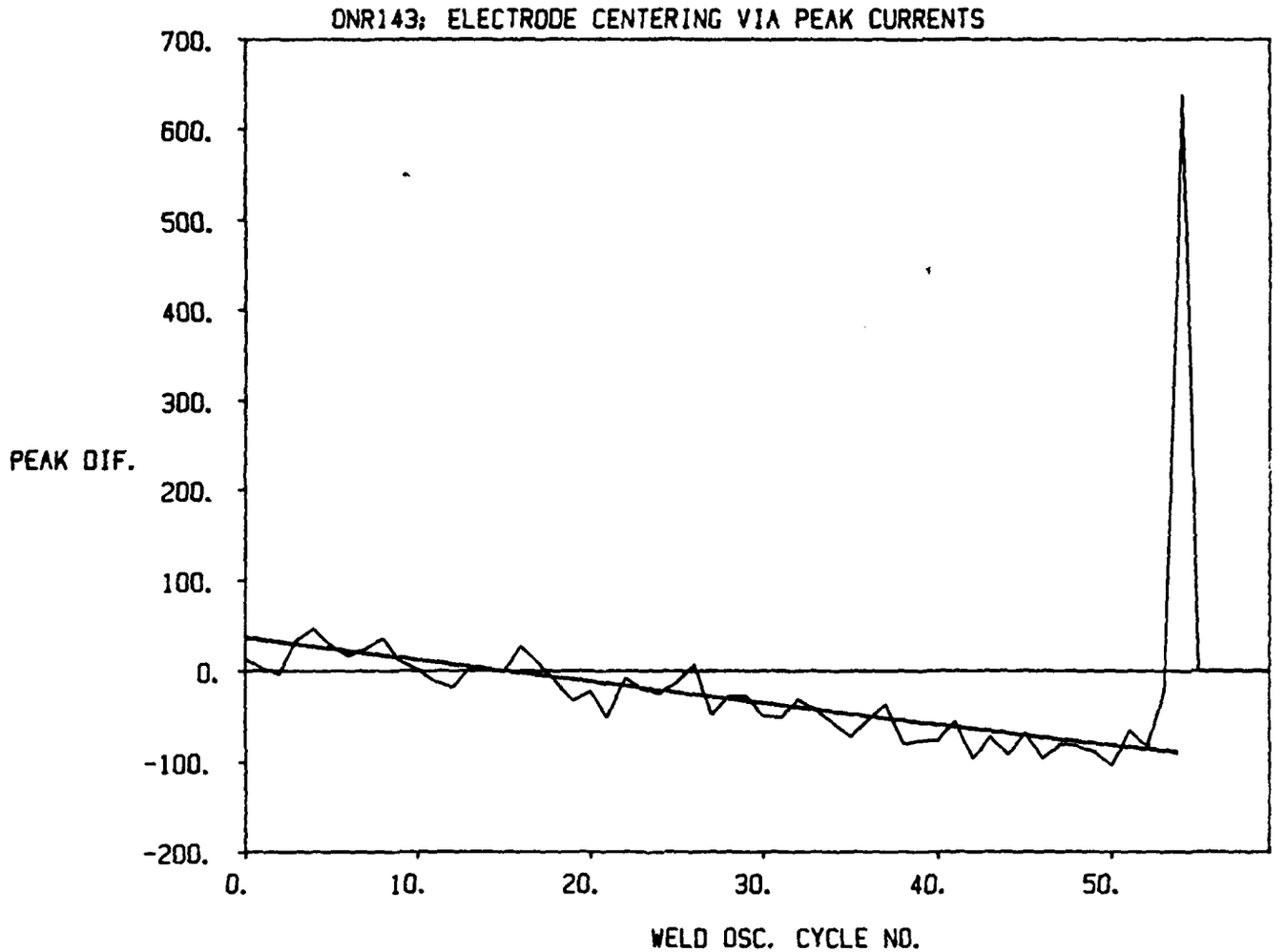

Fig. 64. Peak current difference between left and right sidewalls for skewed joint test.

in the photograph of the completed weld, shown in Figure 65.

The current difference signal, shown in Figure 64, represents the command signal that would be fed to the centering control system to progressively make the lateral corrections as the weld proceeds. This algorithm may be compared with the other algorithms for electrode centering by comparing them on the basis of the amount of random excursions about the skewed line, the less the variation, the better the performance of the algorithm.

The data that is plotted in Figures 61-64 was obtained from the filtered and decimated data (corresponding to a 50 Hz sampling rate). (The filtering and decimation process used to reduce the number of samples from 1000 per second to 50 per second is described in detail in the section, Data Acquisition and Signal Preprcessing Considerations.) Hence, as compared to the original data, considerable smoothing has taken place and effectively represents a smoothing of 1000/50 or 20 data points obtained at the original sampling rate. Further smoothing could be implemented to reduce the variance of the peak current estimates.

The algorithm described above and depicted in Figures 61-64 is but one of several algorithms that could be implemented based on the same peak current measurements. The sample taken at the center of the oscillation excursion may be compared against a fixed reference to obtain an

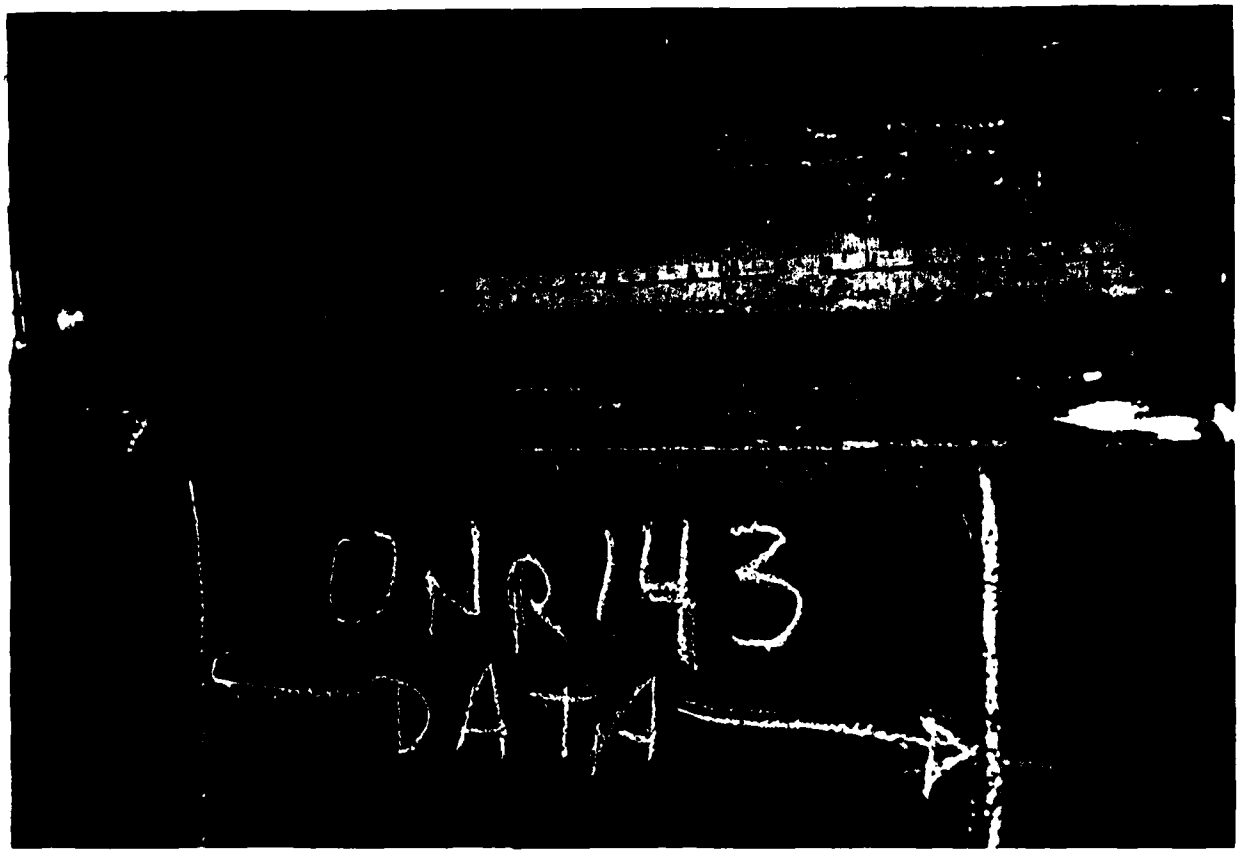

Figure 65. Photograph of weld number 14.

error signal for the CTWD positioning. This error signal may be used to drive a servo in the proper direction to maintain the CTWD constant.

For adaptive width control, the peak currents, measured at the extremes of oscillation excursion, may be compared against a constant value corresponding to desired sidewall fusion. If the measured peak current is less than the reference, then the oscillation width is increased; if the measured peak current is more than the reference, then the oscillation width is decreased.

A slight modification of the peak current measurement approach may be used to implement centering and width control on an instantaneous cycle by cycle basis. With this approach, the oscillation mechanism is directed to move the electrode toward a sidewall at a desired selectable rate until the current reaches a preset value corresponding to a desired condition of sidewall fusion. The direction of lateral oscillation is then reversed, and the process is repeated on the opposite side. By so doing the automatic adjustment of electrode centering and width control is simultaneously achieved. To avoid driving the electrode into the sidewall, under conditions of noisy current measurements, position windows may be placed on the amount of increase or decrease in oscillation width permitted from one cycle to the next.

Algorithms Based on Integration of Current Waveform Over Full Half Cycle

To obtain more noise-free data, the current waveform may be averaged over a full half cycle of lateral oscillation. The averaged current on the

left may be compared to the averaged current on the right to obtain a centering correction signal. The result of doing this for weld sample 14, pass 3, is shown in Figure 66. A comparison of this result with that obtained with the peak current comparison method (Figure 64) shows the two methods to be roughly equivalent for this specific test. Both methods provide robust information that could be used to reliably maintain the electrode centered in the joint.

The algorithm described above may be modified to reduce computational burden and to permit simultaneous width and centering control on an instantaneous cycle by cycle basis. The computational burden may be reduced by using the integral of the current waveform rather than the average of the waveform. A comparison of the integrals of current during each half cycle should provide the same information as a comparison of the average values, provided the oscillation rate and width remain fixed during any cycle of the lateral oscillation.

A more desirable method of using the integral of the welding current is to compare the instantaneous integral of the waveform with a pre-established reference value and reverse the direction of the oscillation travel when the two are equal. This may then be repeated on the other side. As previously described for the peak current method, this approach automatically corrects for width and electrode centering variations. The sensitivity of this method may be further improved by subtracting the current measured at the center of oscillation from the measured current

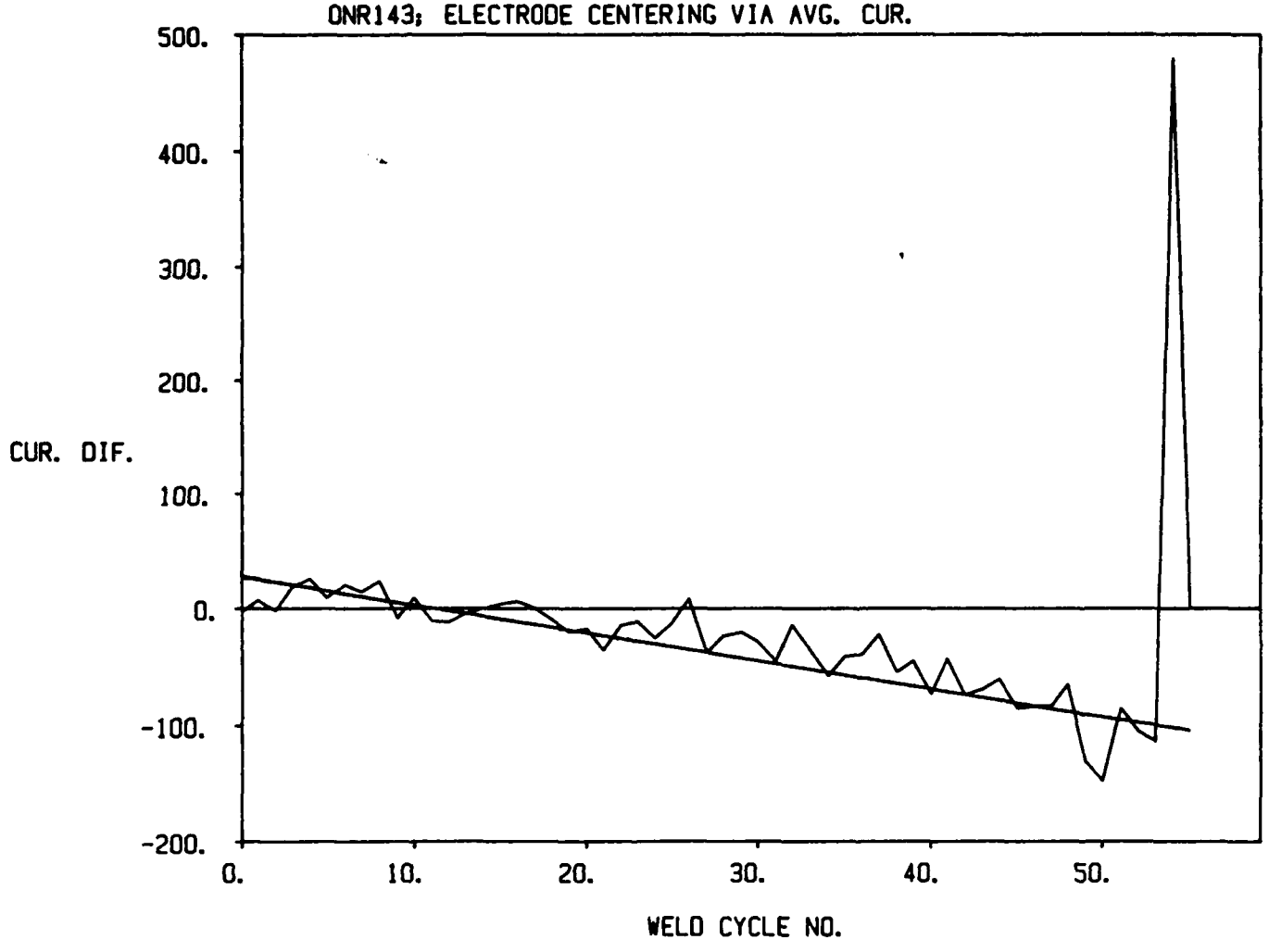

Fig. 66. Average current difference between left and right measurements for skewed joint test.

waveform prior to integration. The resulting waveform is a measure of the deviation from the nominal center value and yields a smaller integrated value to compare against the fixed reference.

Algorithms Based On Integration of Weighted Current Waveform Over Full Half Cycle

To reduce the effect of random changes in the welding current near the center of oscillation, the current wavefrom may be weighted by the cross-seam position signal, as shown in Figure 67. As can be seen, the current waveform near the extremes of the oscillation excursion are weighted more heavily than the current values near the center of the oscillation. As before, the average value of the integrated current waveform on the left side of the oscillation cycle may be compared with the average value on the right side to produce a centering correction signal as depicted in Figure 68 for the weld sample number 14, pass 3. As can be seen by comparing this result with the results shown in Figures 64 and 66, this approach is roughly equivalent to the other algorithms, at least, for this specific test.

The algorithm described in this section may be modified by normalizing the weighting function (the cross-seam oscillation signal) to unit peak magnitude. This will result in the same weighting factor, independent of the oscillation width. As before, the computational burden may be reduced by using the integral of the weighted current waveform rather than the average value of the waveform.

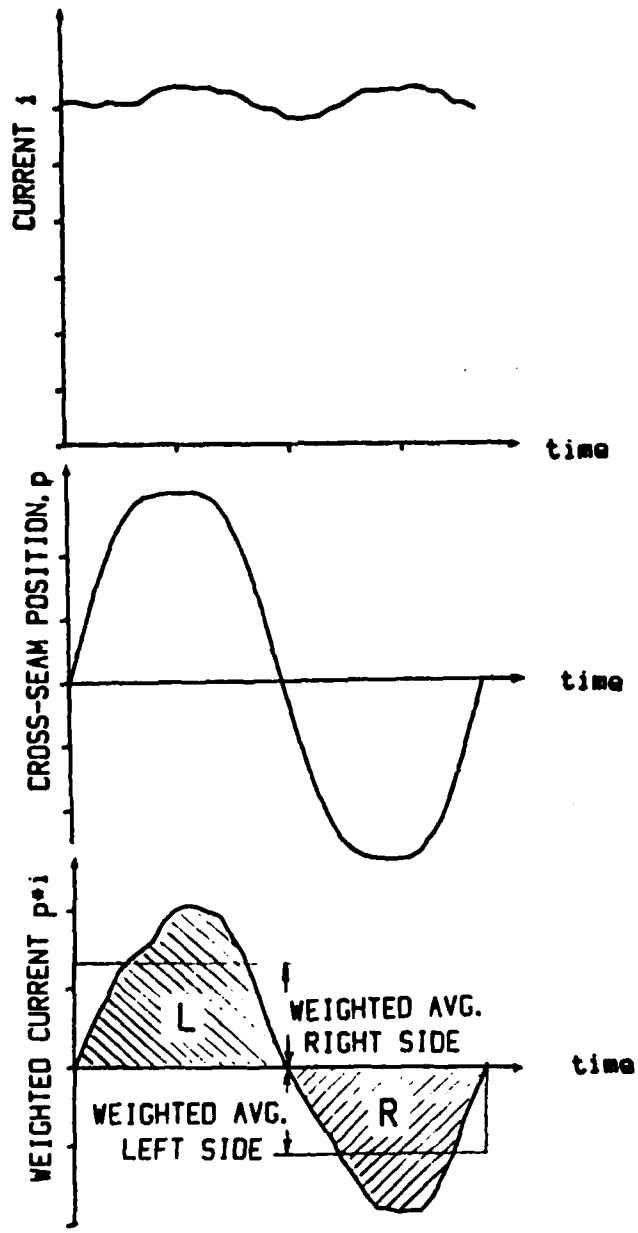

Fig. 67. Weighted current average over full half cycle.

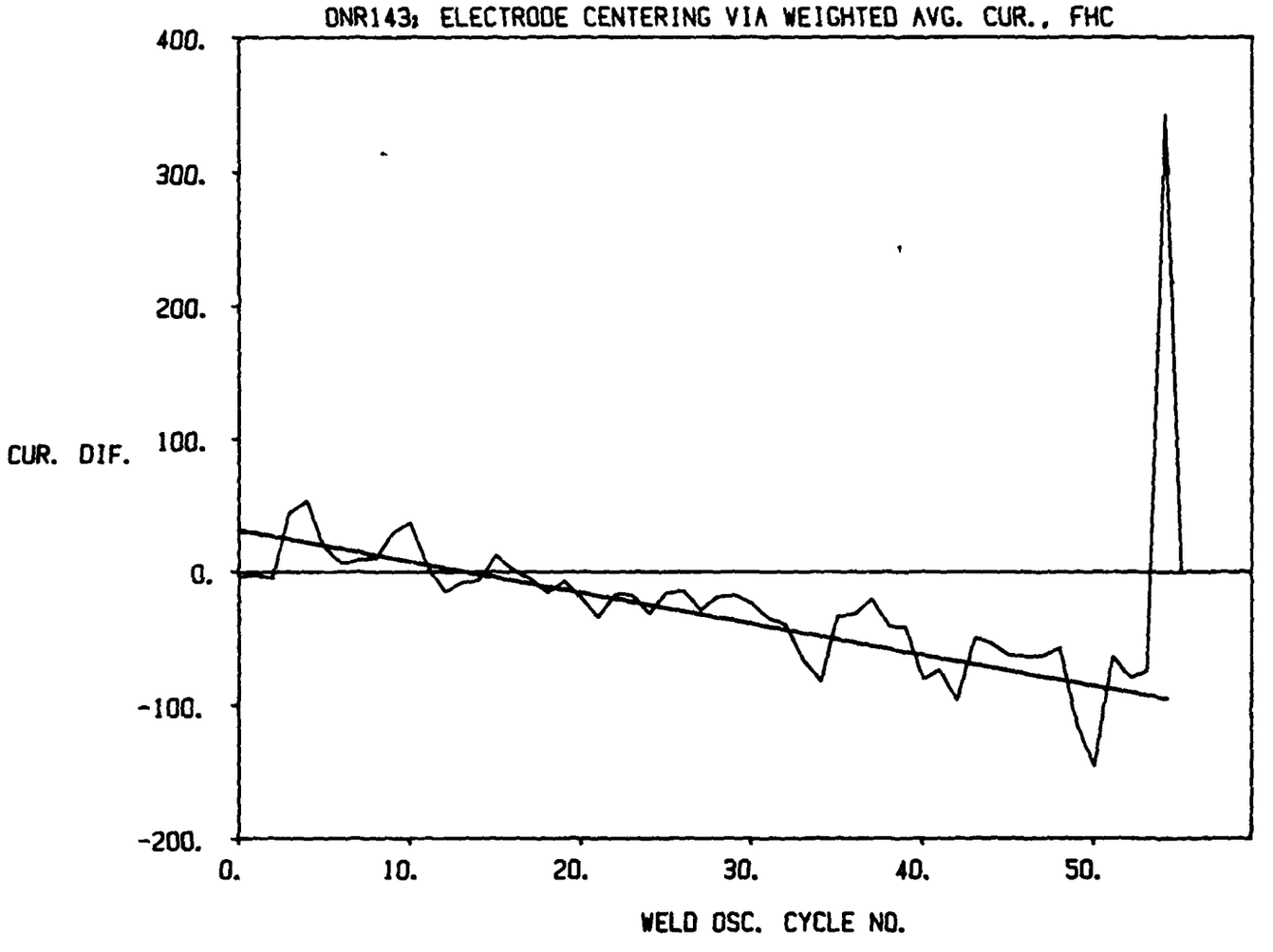

Fig. 68. Weighted average current difference between left and right measurements for skewed joint test.

Algorithms Based On Integration Of Current Waveform Over Less Than A Full Half Cycle

The algorithms described in the previous section attempted to reduce the effect of random variations in the current waveform near the center of oscillation by weighting the waveform more heavily near the oscillation extremes than near the center. The measured current values near the extremes of the oscillation cycle may be weighted even more heavily by only considering those values near the oscillation extremes. This is depicted in Figure 69. This approach is equivalent to multiplying by a window that is of unit magnitude near the oscillation extremes and is of zero magnitude otherwise. An added advantage of this approach is that there is time near the center of the oscillation cycle when the control computer may be used for other calculations.

To correct for CTWD variations and width variations as well as variations in the electrode centering, the current may be measured and averaged at the center of oscillation, as shown in Figure 70. The averaged current on the left side and the averaged current on the right side may be compared with the averaged current at the center of oscillation to determine whether a change in the oscillation width is called for. The averaged current at the center of oscillation may be compared with a fixed reference value to determine necessary corrective actions in the CTWD. Finally, the averaged current on the left side may be compared with the averaged current on the

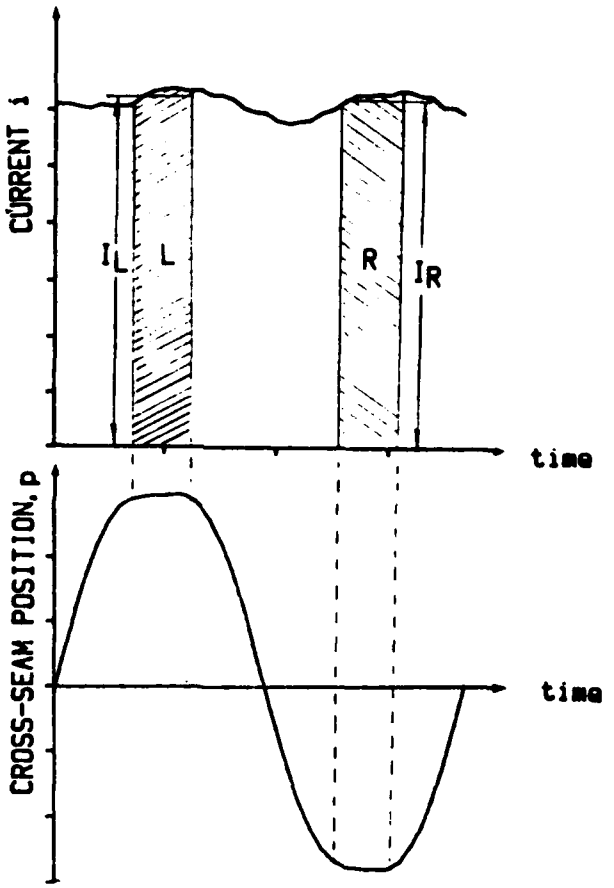

Fig. 69. Current average over less than full half cycle.

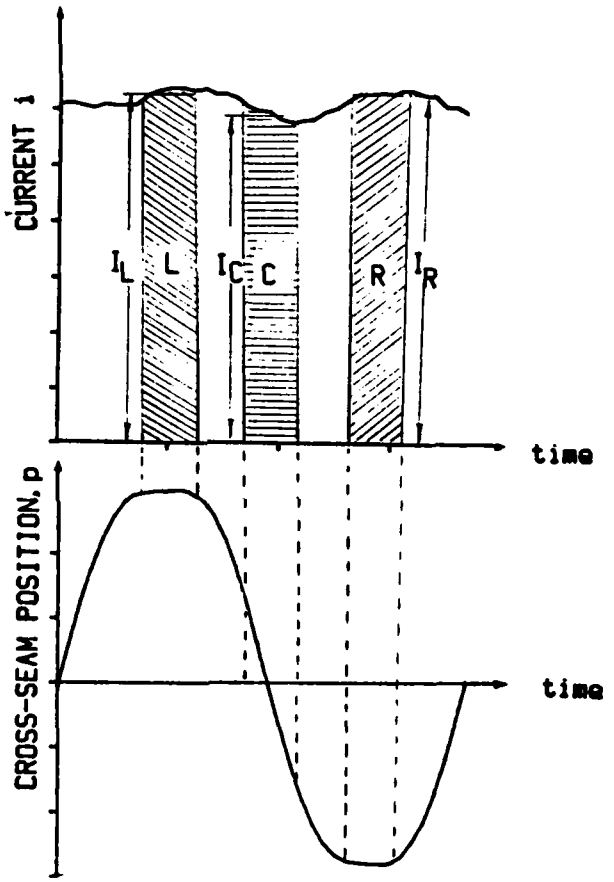

Fig. 70. Current average on left- and right-hand side plus current measurement at center of oscillation cycle.

right side to determine necessary corrective actions in the electrode centering. The result of computing the averaged current difference signal of a cycle-by-cycle basis is shown in Figure 71. The result shown is based on data corresponding to weld sample 14, pass 3. As before, the data used was that obtained after filtering and decimation to a 50 Hz sampling rate. The averaging is done over six samples. These results may be compared with those shown in Figures 64, 66, and 68. Once again, for this specific test, the results are comparable.

Algorithms Based On Integration of Delayed Current Waveform Over Less Than A Full Half Cycle

The algorithm described in the previous section is based on the assumption that the current variation is in phase with the instantaneous cross-seam position of the electrode. To determine the accuracy of this assumption the cross-seam oscillation signal was crosscorrelated with the current waveform. The result of doing this is shown in Figure 72 for weld sample 14, pass 3. It can be seen that the peak in the crosscorrelation curve occurs at approximately 20 ms. This corresponds to the time delay between the cross-seam position signal and the current waveform for this specific test.

The manner in which the time delay is taken into account is depicted in Figure 73. The average value of the delayed current samples on the left are compared with those on the right to determine the electrode centering. The result of doing this is shown in Figure 74. As can be seen, the results

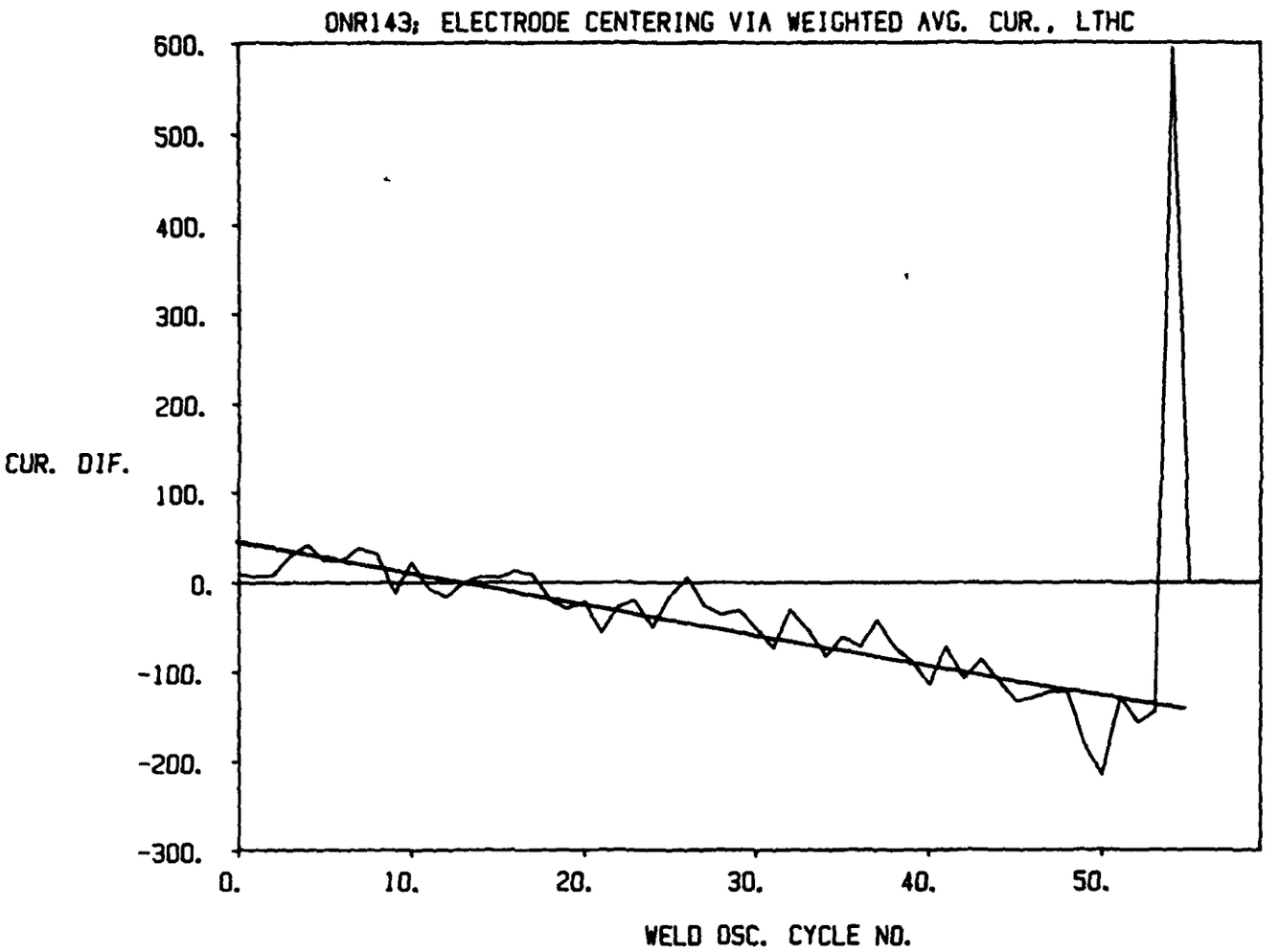

Fig. 71. Average (less than full half cycle) current difference between left and right measurements for skewed joint test.

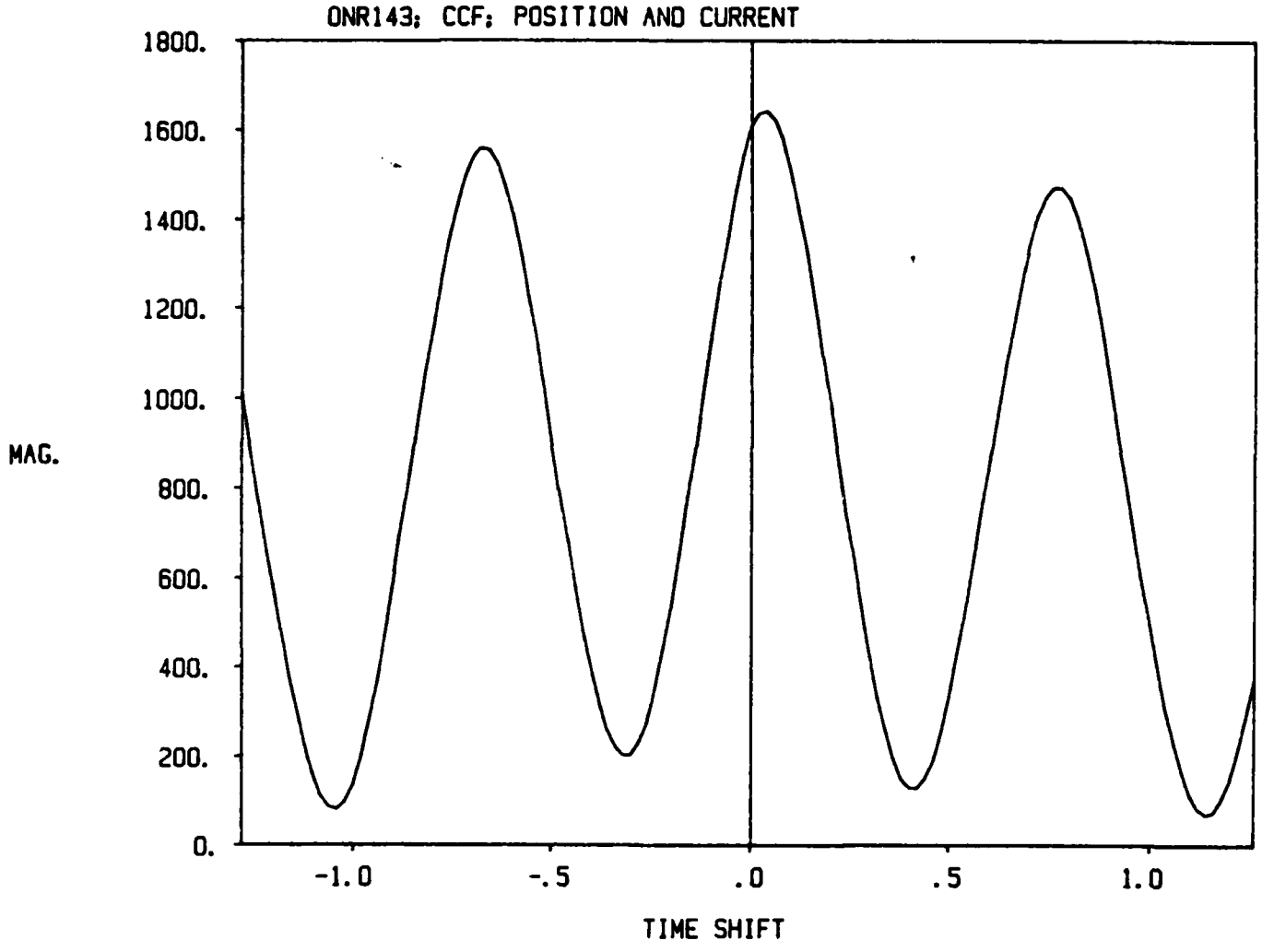

Fig. 72. Cross-correlation between cross-seam position and current for skewed joint test.

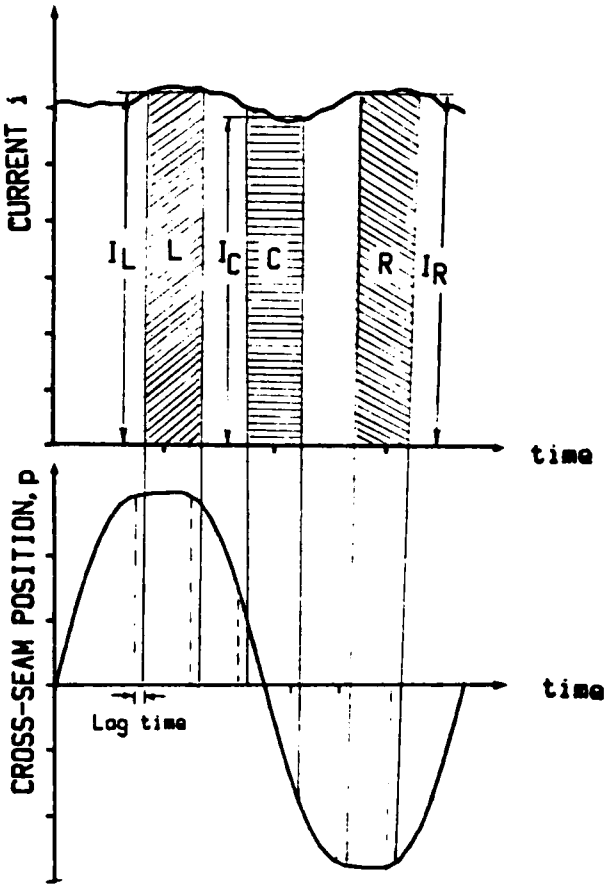

Fig. 73. Delayed current average for skewed joint test.

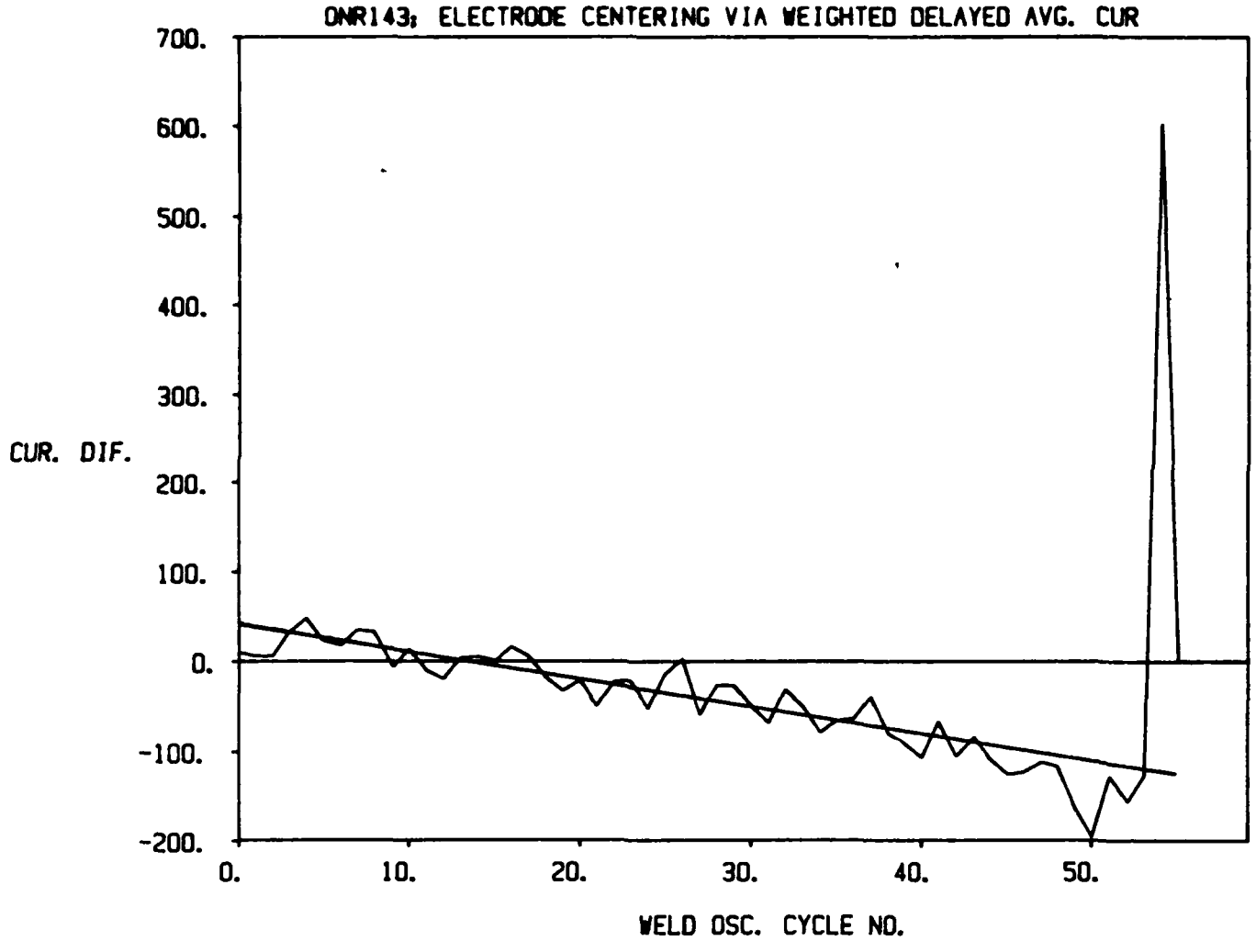

Fig. 74. Delayed average current difference between left and right measurements for skewed joint test.

show an improvement over those obtained without accounting for the time delay.

Algorithms Based On Power and Impedance Waveforms

The four generic algorithms discussed in the sections above were repeated for waveforms of instantaneous power and instantaneous impedance. The results of applying the four algorithms to the instantaneous power waveform for weld number 14, pass 3, are shown in Figures 75-78.

In Figure 75, the difference between the minimum power during the left-hand cycle and the minimum power during the right-hand cycle is plotted versus the weld oscillation cycle number. (As previously described in the section on feature recognition, the power function exhibits a minimum at either extreme of the oscillation excursion rather than a maximum as exhibited by the current signal.) As before, only one data point per cycle is actuallly computed. The points are shown connected simply for convenience in using the plotting routine available with the statistical analysis package. The curve shown in Figure 75 does indeed show a progressive change in the correction needed to bring the electrode back into alignment with the joint. The result is not considered as reliable, however, as the other methods based on integration (or averaging) of the waveform.

The result shown in Figure 76 is based on taking the difference

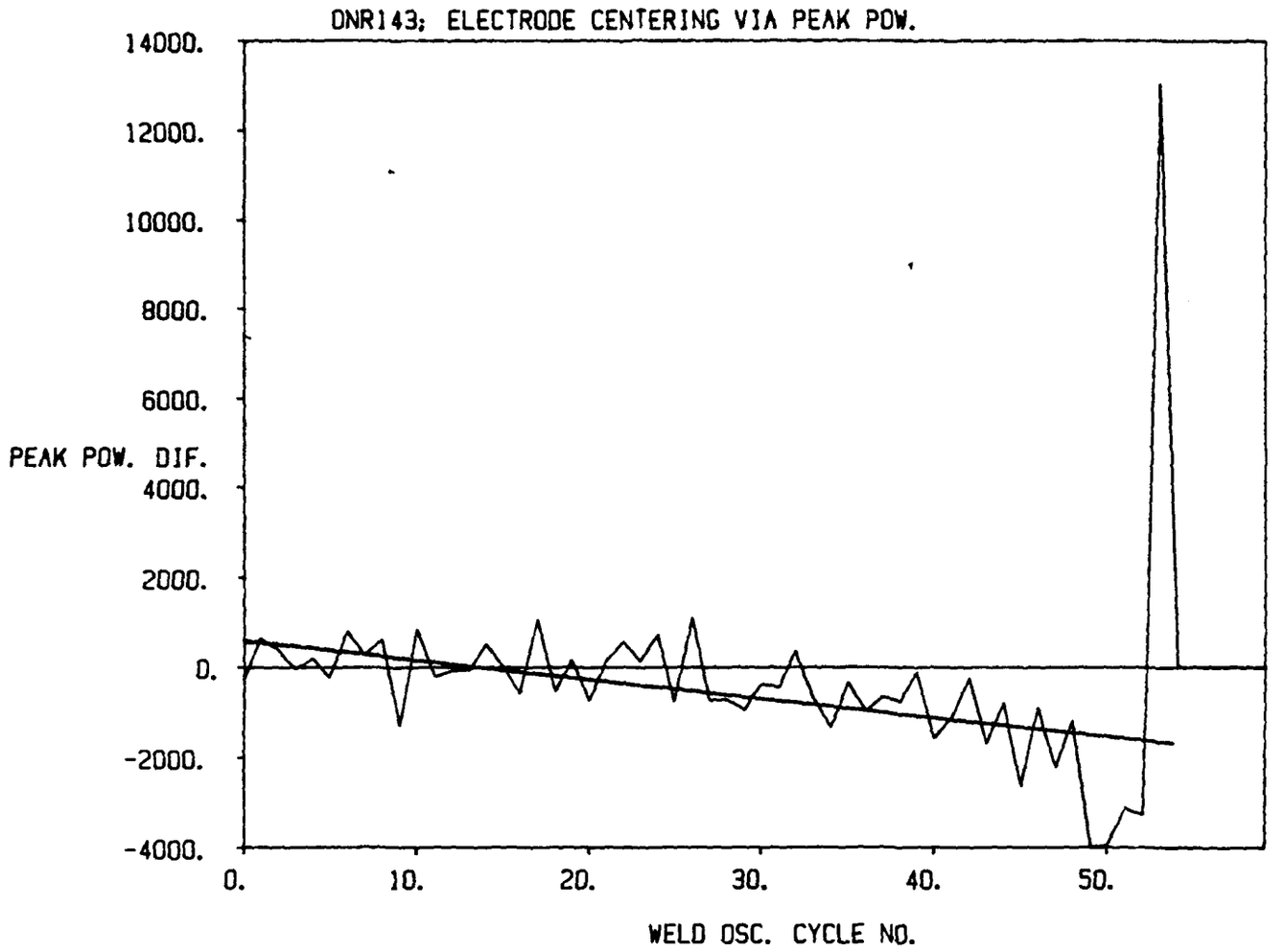

Fig. 75. MInimum power difference between left and right sidewall measurements for skewed joint test.

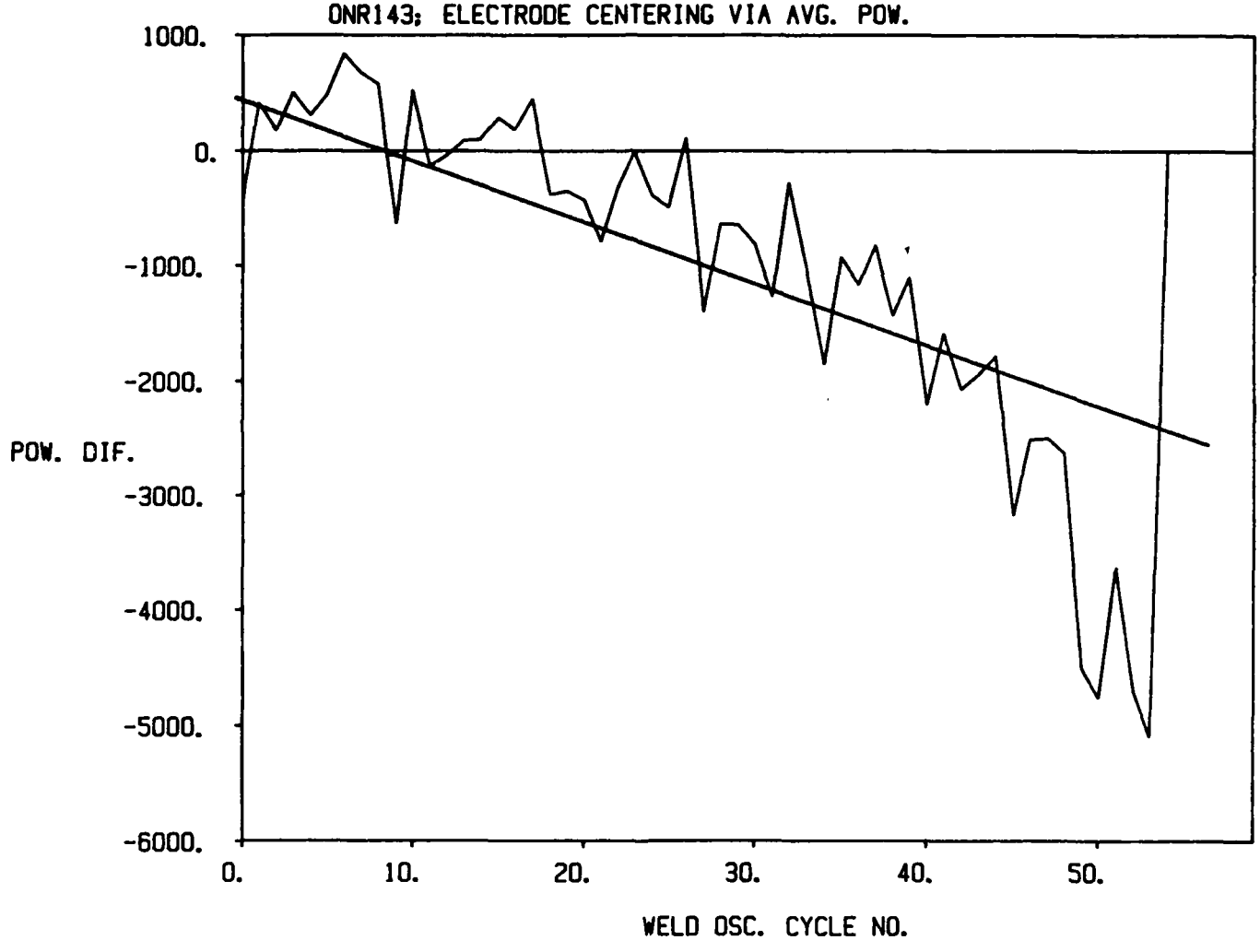

Fig. 76. Average power difference between left and right sidewall measurements for skewed joint test.

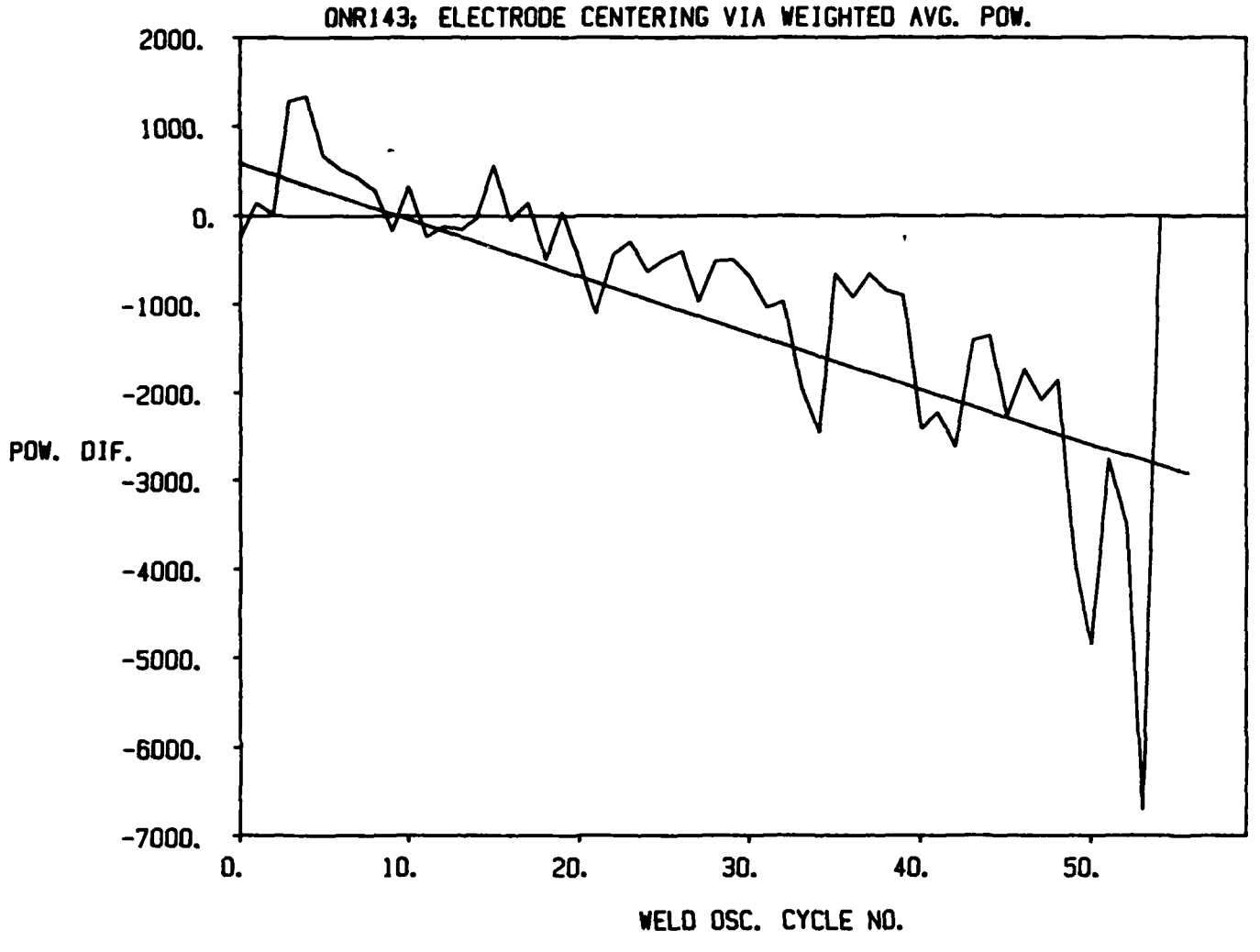

Fig. 77. Weighted average power difference between left and right sidewall measurements for skewed joint test.

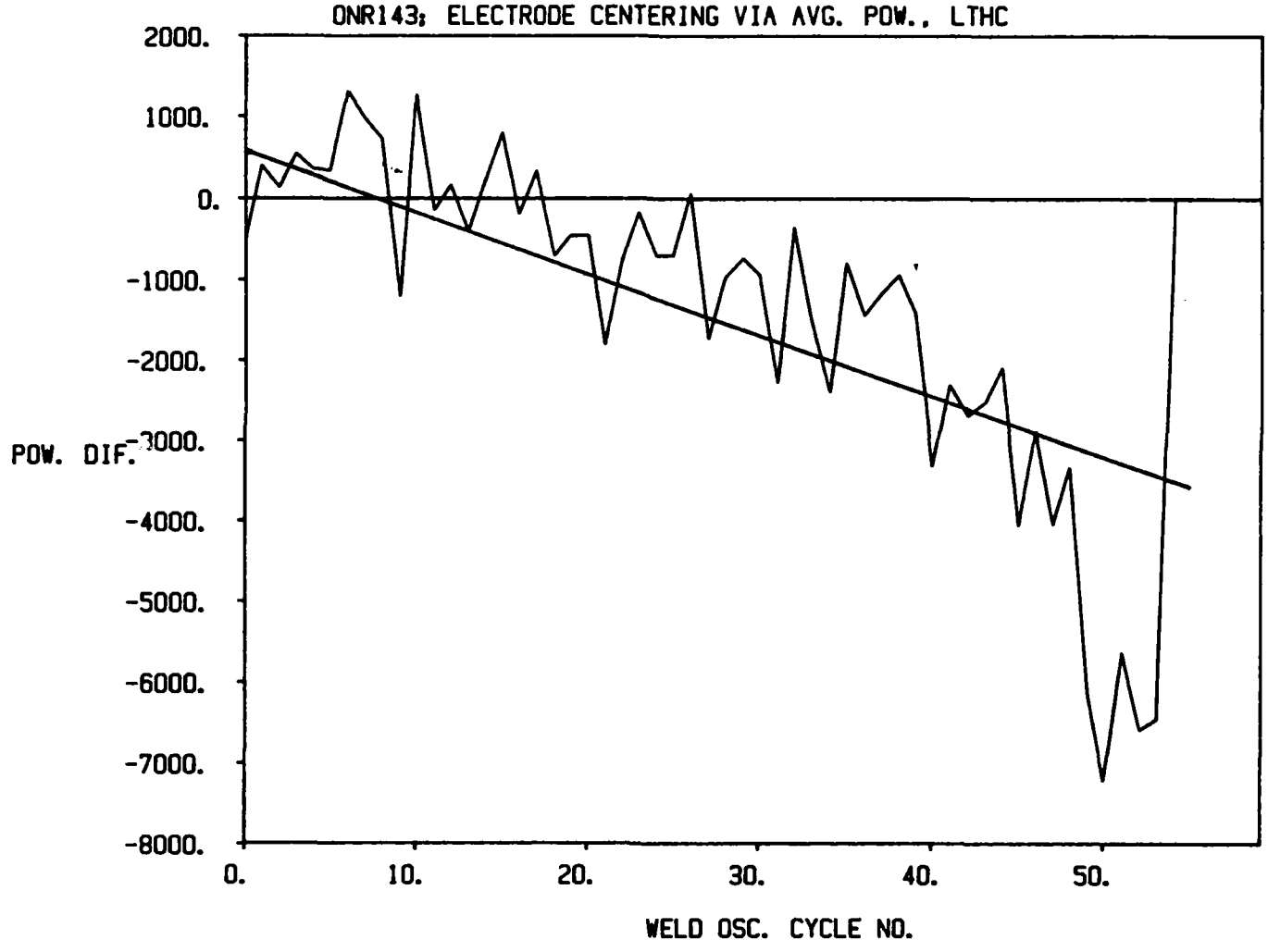

Fig. 78. Average (less than full half cycle) power difference between left and right sidewall measurements for skewed joint test.

between the average of the power waveform over a full half cycle on the left and the average over a full half cycle on the right. As can be seen, the signal is robust and comparable to the method applied to the current waveform.

Figure 77 shows the result of using a weighted average taken over full half cycles, and Figure 78 shows the result of using an average over less than a full half cycle. Both of these results compare favorably with those obtained based on the current waveform.

The results of applying the four algorithms to the instantaneous impedance are shown in Figures 79-82. Once again, as described in the section on feature recognition, the impedance waveform exhibits a minimum at either extreme of the oscillation excursion. The result of searching for the impedance minimum on the left- and right-hand sides and taking the difference is shown in Figure 79. The result does not show the expected skew between the electrode travel and the joint centerline, as exhibited with the other methods. It is anticipated, however, that the result would be improved if the impedance waveform were further smoothed prior to searching for the peak. The need for further smoothing is perhaps due to the impedance function decreasing for both a decrease in voltage and an increase in current. This makes the impedance function more sensitive than the power signal or the current signal taken alone. This greater sensitivity is desirable from a feature recognition standpoint. However, greater care

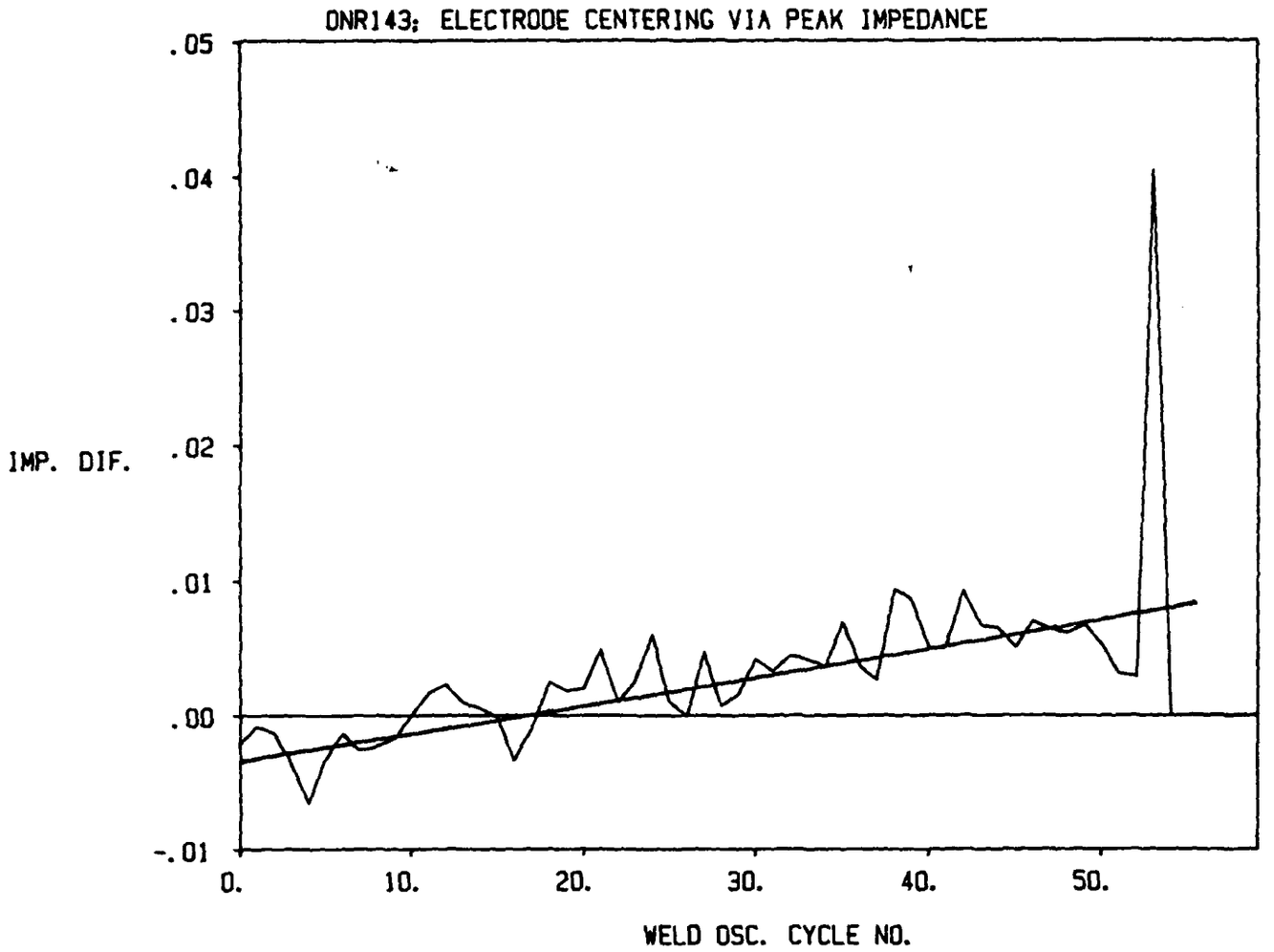

Fig. 79. MInimum impedance difference between left and right sidewall measurements for skewed joint test.

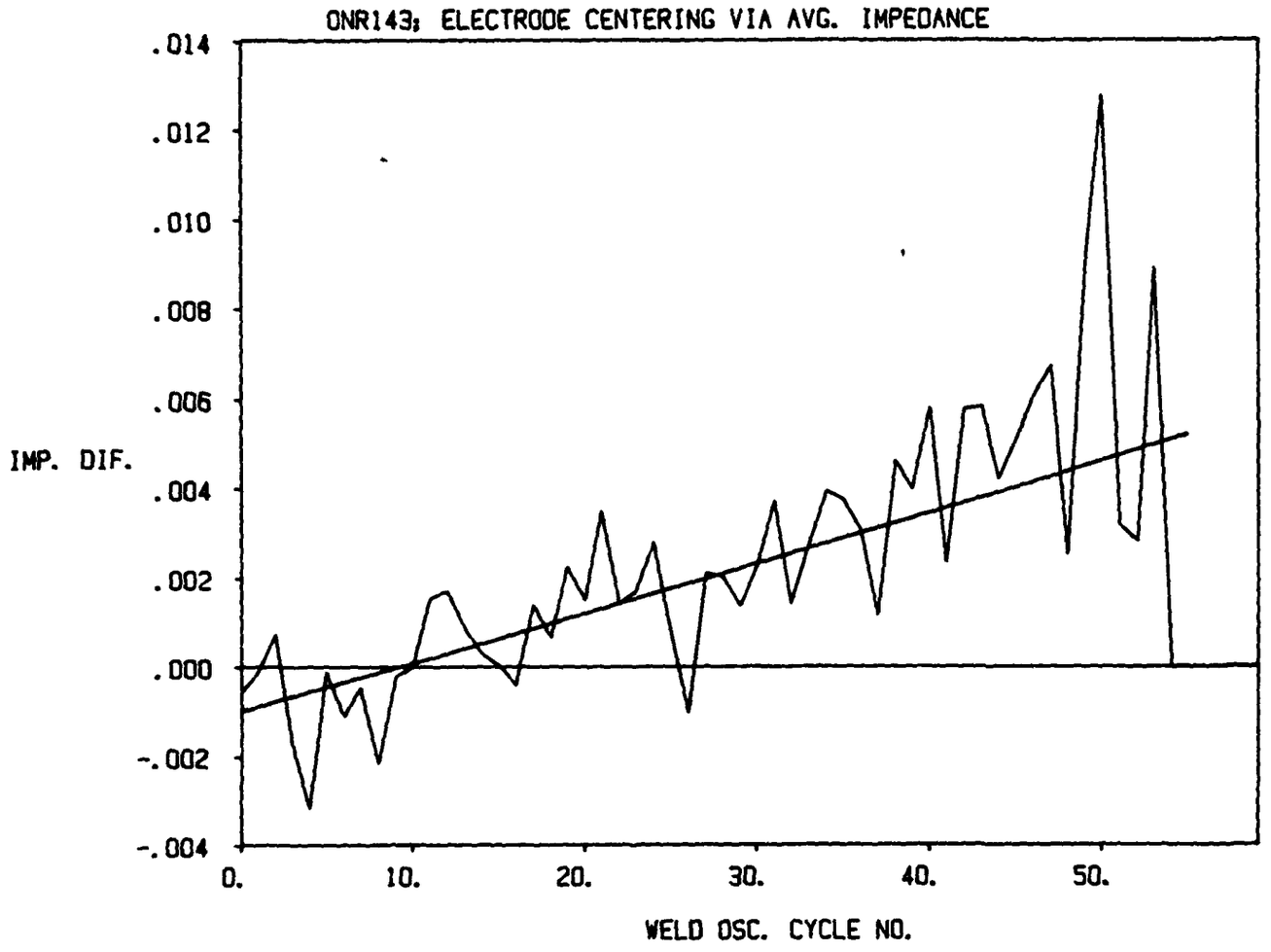

Fig. 80. Average impedance difference between left and right sidewall measurements for skewed joint test.

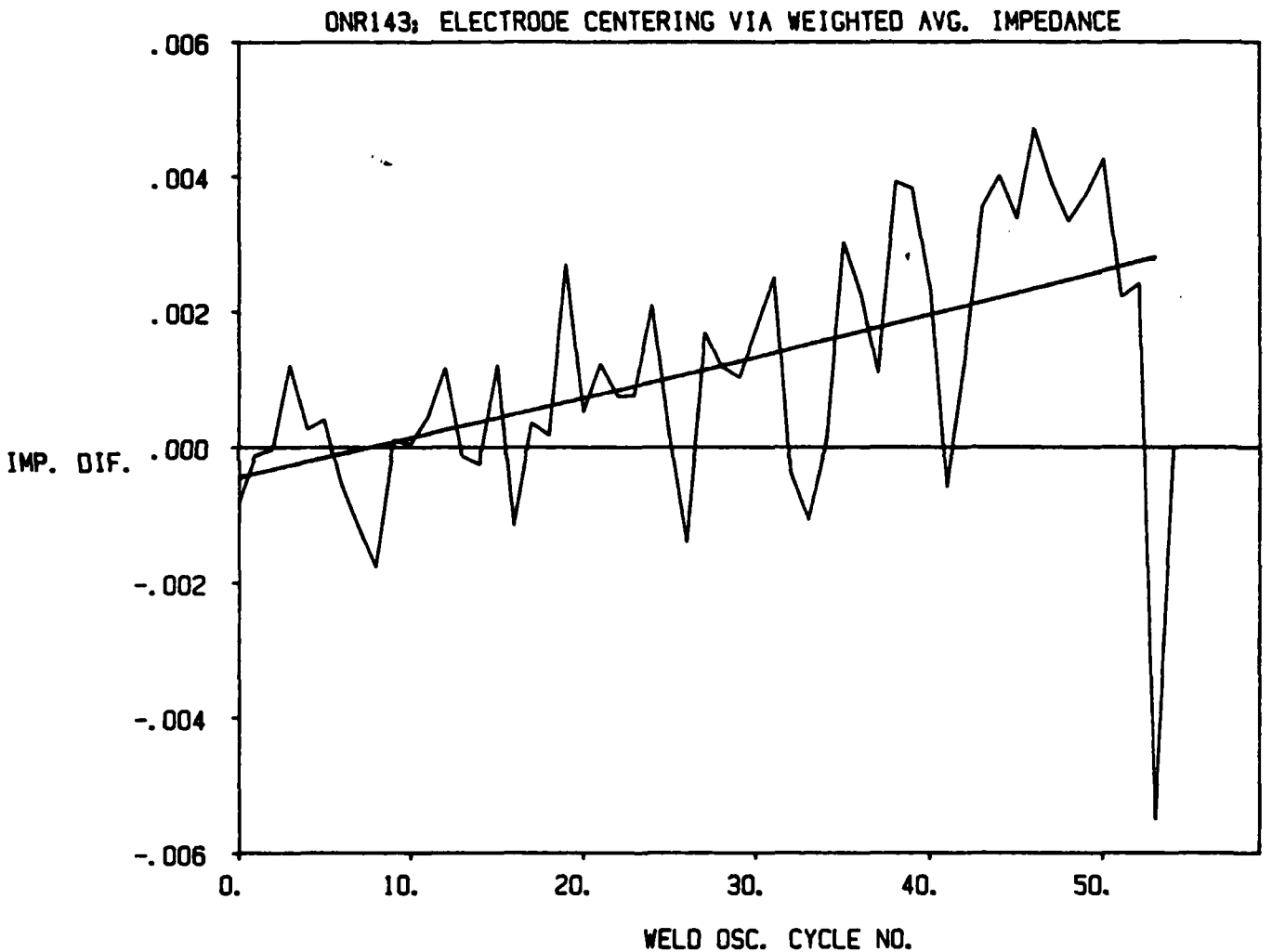

Fig. 81. Weighted average impedance difference between left and right sidewall measurements for skewed joint test.

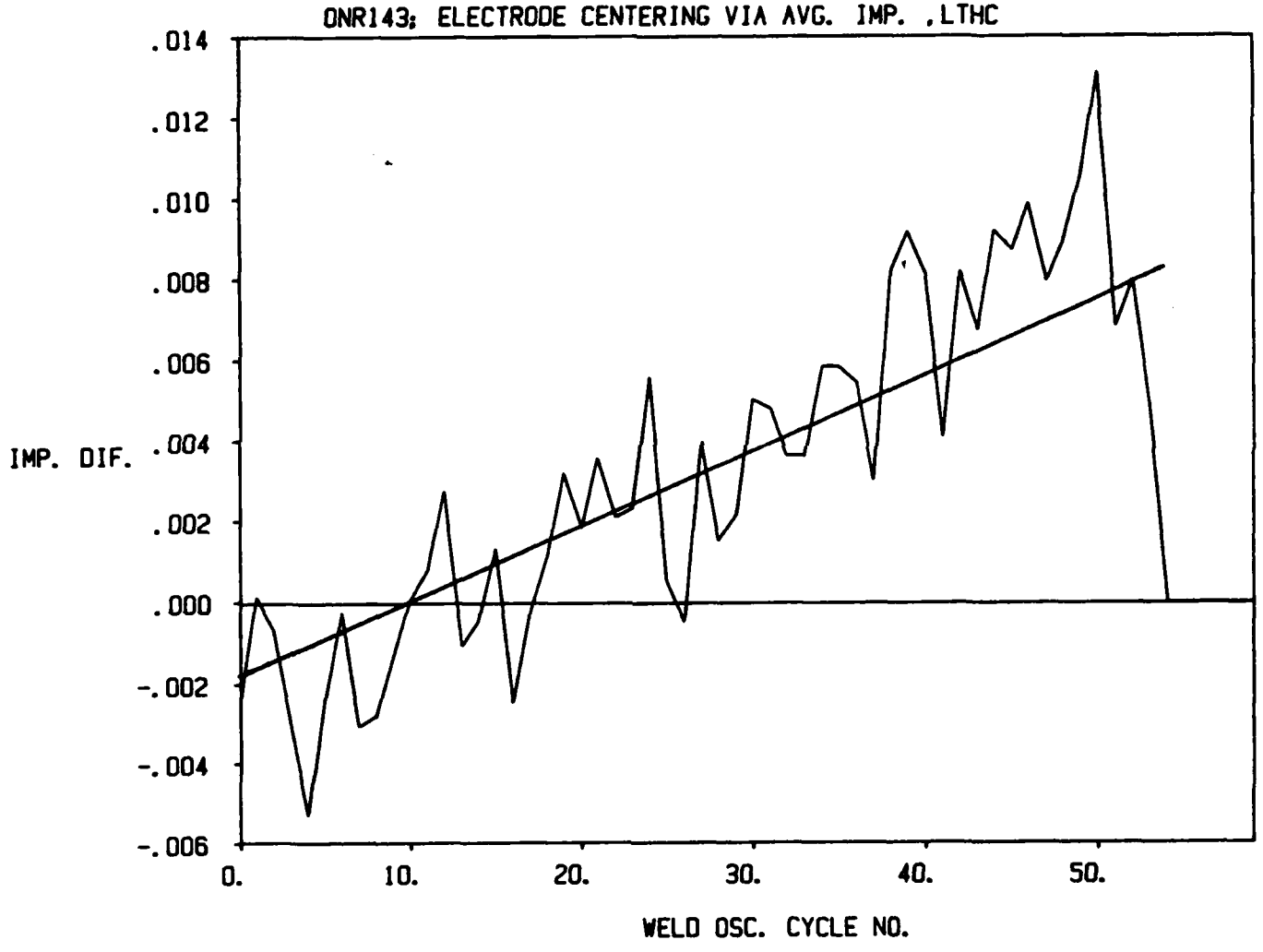

Fig. 82. Average (less than full half cycle) impedance difference between left and right sidewall measurements for skewed joint test.

must be exercised in smoothing the impedance waveform because it is more susceptible to large excursions due to noisy variations in the voltage or current waveforms.

The results of applying the averaging algorithms to the impedance waveform are shown in Figures 80-82. These results are comparable to those obtained from the current waveform, however they appear more noisy again suggesting that better smoothing methods may be needed if the impedance waveform is chosen for processing and control.

Metallographic sections taken from weld number 14 are shown in Figures 83-85. The metallographic section shown in Figure 83 was taken from the first third of the weld, the section shown in Figure 84 was taken from the middle third of the weld, and the section shown in Figure 85 was taken from the last third of the weld. Even though the electrode's path of travel was skewed with respect to the centerline of the torch from one end of the weld to the other, the fusion characteristics can be seen to be quite good for all three sections of the weld. This serves to demonstrate quite well, the robustness and excellent sensitivity of the through-the-arc signal analysis methodology. The signal analysis clearly showed that there was a skew between the electrode path and the joint centerline, even when the skew was well within tolerance levels that would normally be taken as adequate for producing sound welds.

Demonstration of Centering Control Based on Current Waveform

The arc signal variations, as a function of variations in the CTWD, were

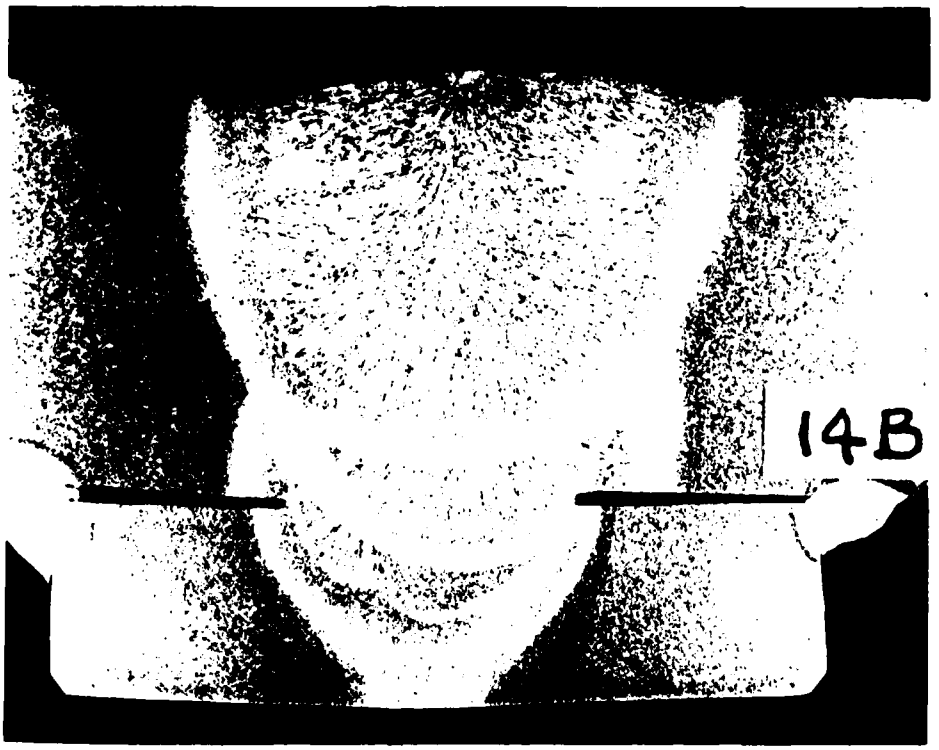

Figure 83. Photomacrograph of first third of weld number 14.

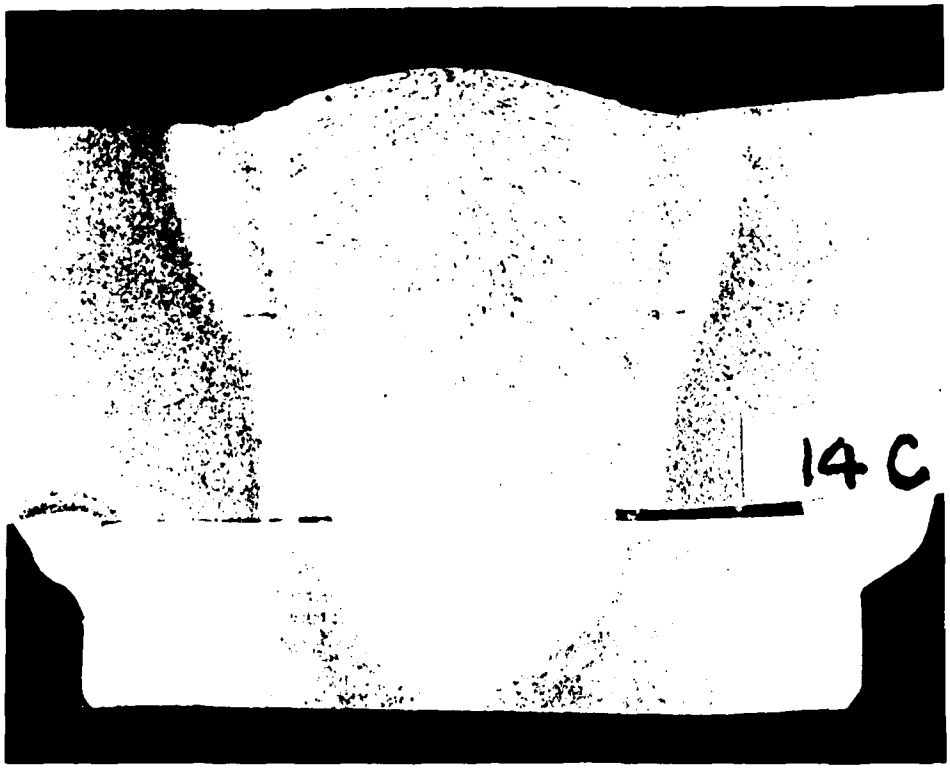

Figure 84. Photomacrograph of middle third of weld number 14.

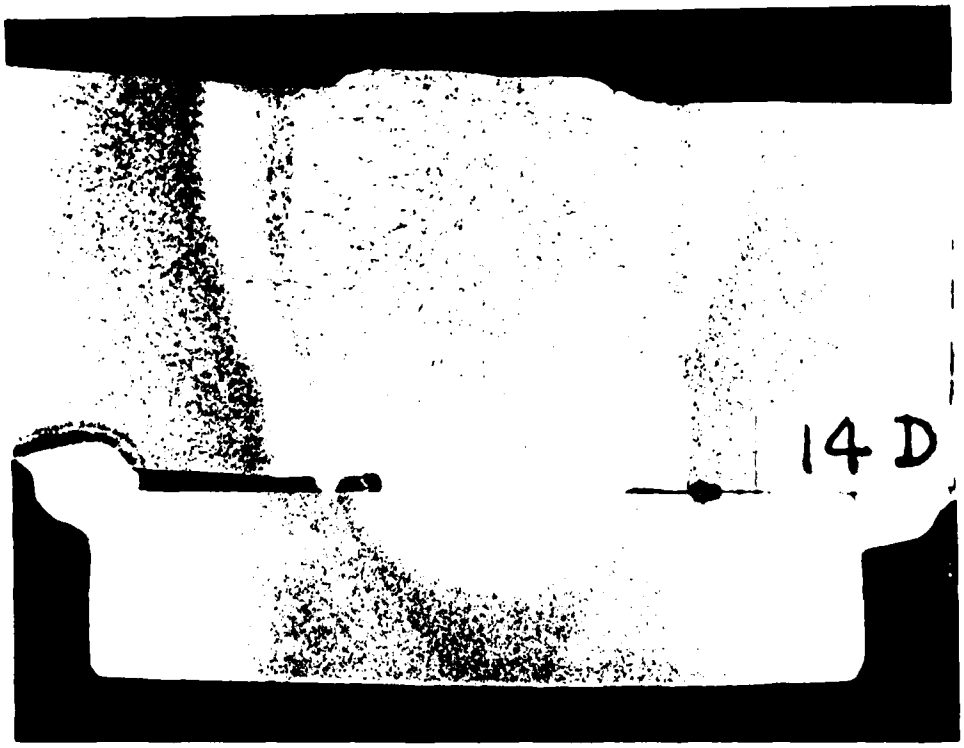

Figure 85. Photomacrograph of final third of weld number 14.

found to be so robust for the SAW process that is was possible to easily maintain centering by observing the current waveform. To demonstrate this, welds were made with centering adjustments manually made in real-time based on the observed current waveform variation. The digitally recorded waveforms of one such weld are shown in Figure 86. The voltage waveform is labeled #1, the current waveform #2, the cross-seam position #3, and the wire speed #4. These waveforms were obtained from the raw data, which was sampled at a rate of 1000 samples per second, by a filtering and decimation process that reduced the number of samples per second to 50. (The filtering and decimation process is described in the section, Data Acquisition and Signal Preprocessing Considerations.) The manual corrections that were made in real-time were not based on these waveforms, but instead on strip chart recordings with an approximate 100 Hz rolloff frequency. Hence, the waveforms used for the real-time observations and control were more noisy than those shown in Figure 86.

The weld test number for the weld corresponding to the waveforms shown in Figure 86 was 15, pass 4. On this weld pass, the nominal current was 540 amperes, the nominal voltage was 31 volts, the CTWD was 12.7 mm, the wire speed was 3,875 mm/min, the travel speed was 175 mm/min, the oscillation width was 12.5 mm peak-to-peak, the oscillation frequency was 0.7 Hz (as evident from the power spectrum plot of the cross-seam position signal in Figure 87), and the right and left dwell times were 0.33 seconds.

The basis for making the manual adjustments to the electrode centering was that, under conditions of proper centering, the current waveform should

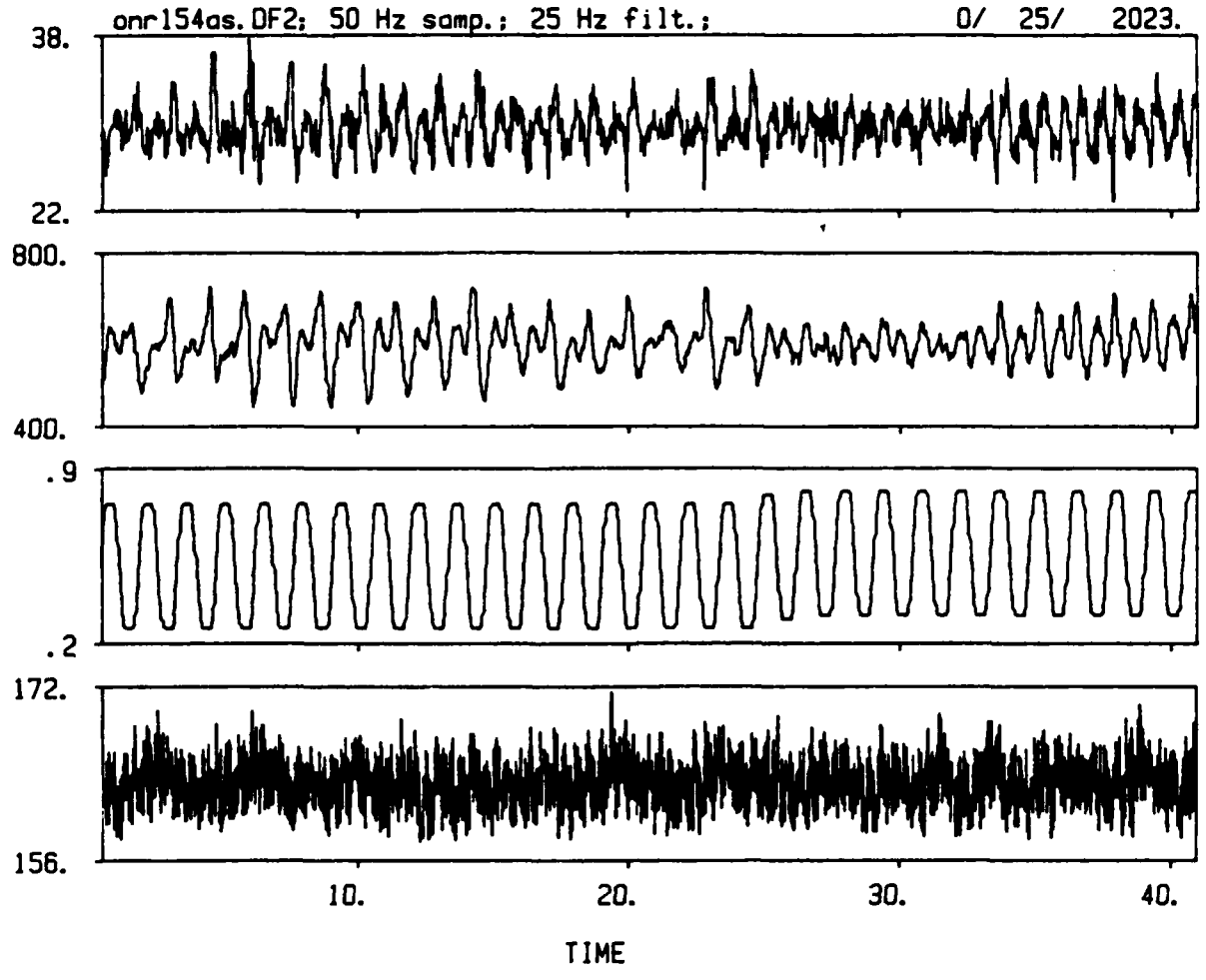

Fig. 86. Waveform of voltage (1), current (2), position (3), and wire speed (4) of weld with manual correction in centering.

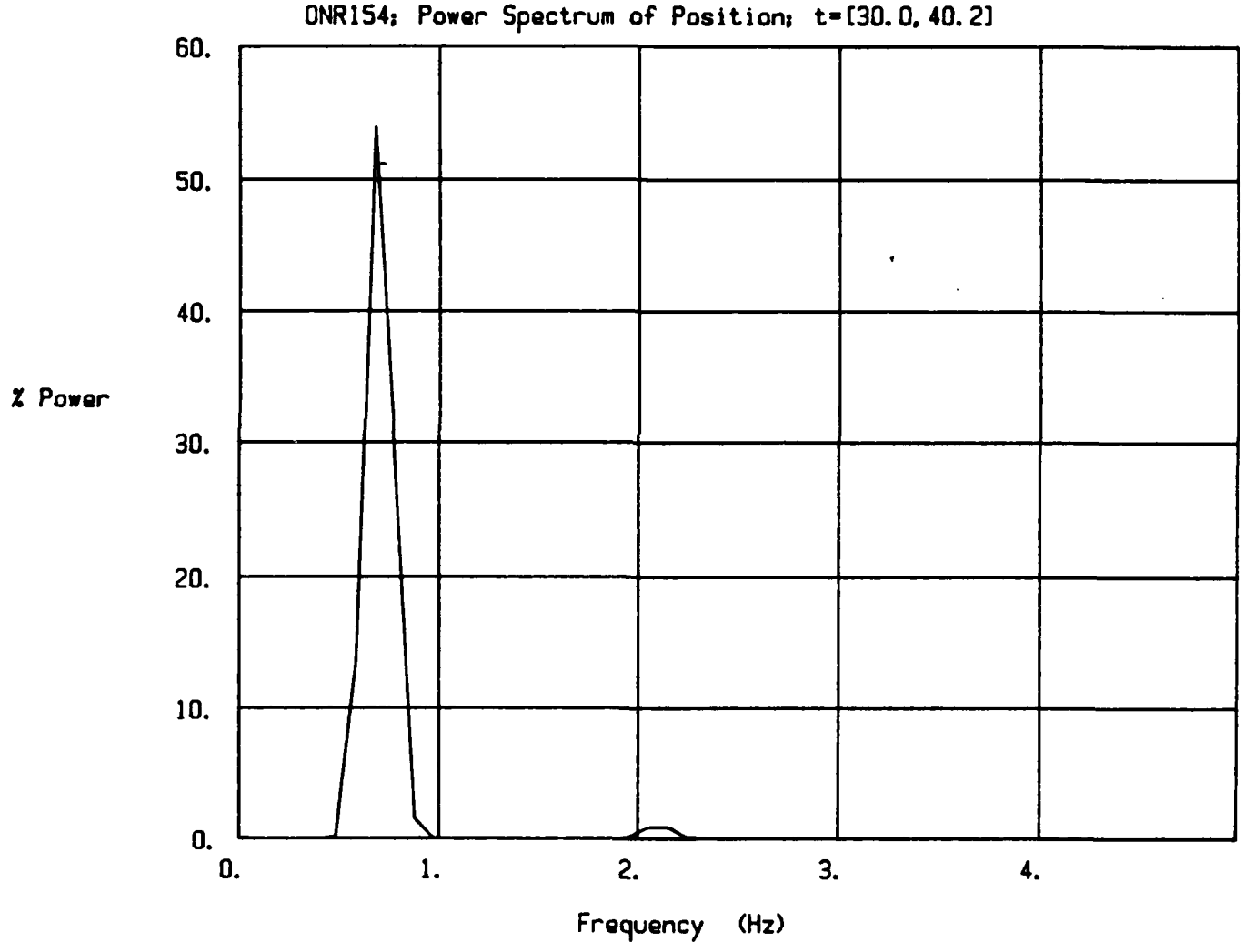

Fig. 87. Power spectrum of cross-seam position signal for weld made with manual correction in centering.

show a peak at either extreme (left-most excursion or right-most excursion) of the cross-seam position. Hence, when the electrode is correctly centered in the symmetrical joint the frequency of the fundamental current variation should be exactly twice that of the cross-seam oscillation frequency.

Referring to Figure 86, a single correction was made at approximately 25 seconds. This is clearly evident by the upward offset in the cross-seam position (waveform number 3). Prior to making the correction, the current waveform shows a considerable unbalance between the current peak on the right and the current peak on the left. (An expanded view of the waveforms between approximately 5 and 15 seconds is shown in Figure 88.) It was based purely on this observation that a correction was made at 25 seconds. Following the correction it can be seen that the balance in the current peaks on the left and right are much more evident. (An expanded view between 30 and 40 seconds is shown in Figure 89.)

To provide an analytical check on these observations of the waveforms, power spectra were computed for the voltage, current, power, and impedance waveforms between 5 and 15.2 seconds and between 30 and 40.2 seconds. The former time span corresponds to the condition prior to making the correction, and the latter time span corresponds to the condition after making the correction. Ideally, for perfect centering, the power spectra should show a substantial percentage of the total power concentrated at a frequency equal to twice the cross-seam oscillation frequency. Under conditions of improper electrode centering, the power spectra would be expected

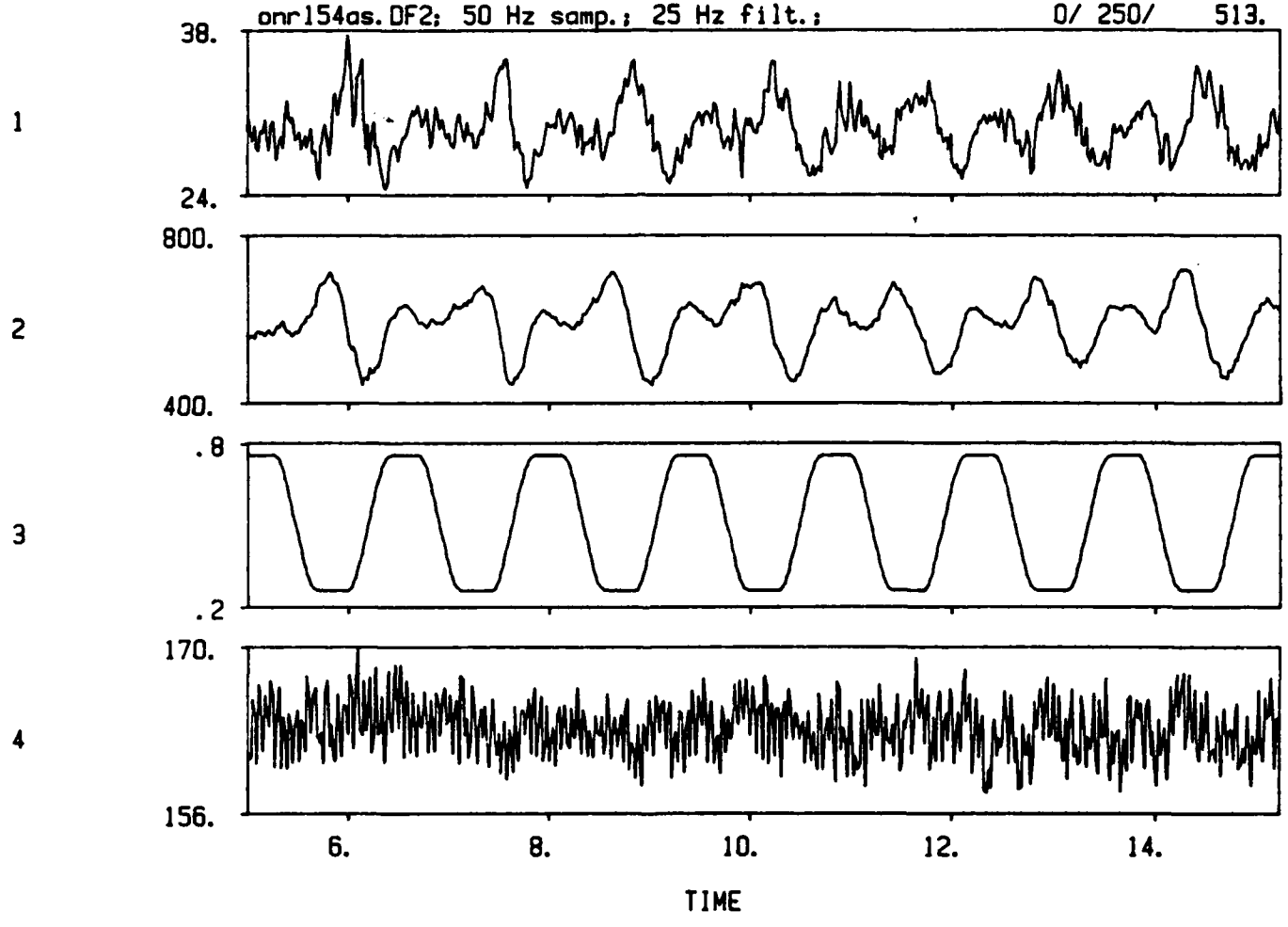

Fig. 88. Waveform of voltage (1), current (2), position (3), and wire speed (4) of weld with manual correction in centering. (time duration 5 - 15 seconds.)

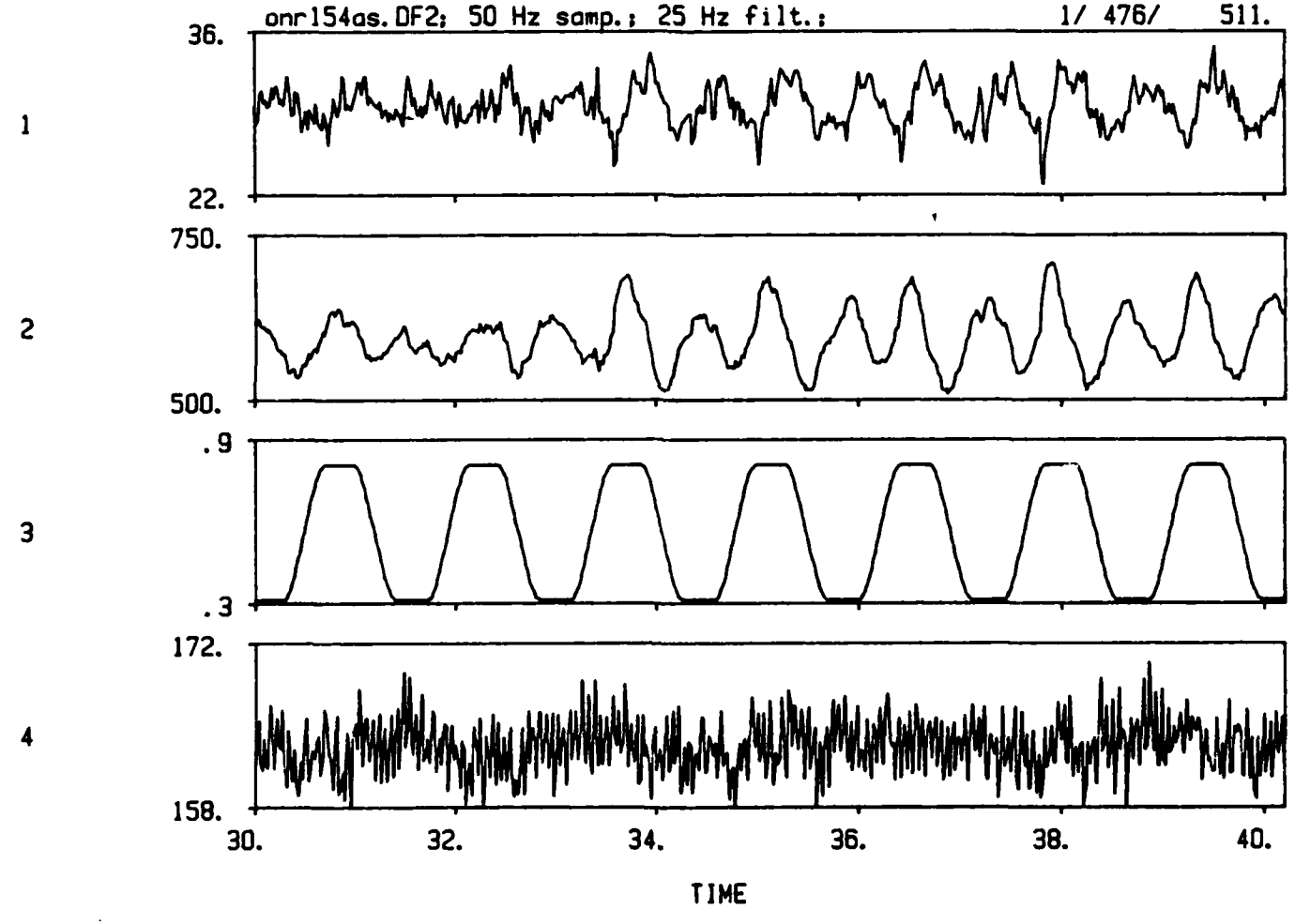

Fig. 89. Waveform of voltage (1), current (2), position (3), and wire speed (4) of weld with manual correction in centering. (time duration 30 - 40 seconds.)

to show significant power components at both the fundamental frequency of the cross-seam oscillation and twice this frequency, with the relative amounts of each dependent on the level of centering offset.

The power spectra for the voltage, current, power, and impedance waveforms between 5 and 15.2 seconds are plotted in Figures 90-93. To provide an easier basis for comparing these plots, the total power under each curve was computed and used to compute the percent power contained in each of the 512 frequency bands (the power spectra were computed by means of 512 point Fast Fourier Transforms.) Hence, the ordinate in each plot is percent total power. As predicted, these power spectra show substantial power peaks at both the fundamental frequency of the cross-seam oscillation as well as at twice the fundamental frequency. This clearly shows that an unbalance existed between the left and right excursions of the cross-seam position relative to the left and right sidewalls of the joint. That is to say, a correction in the cross-seam centering of the electrode was indeed being called for.

The power spectra for the voltage, curent, power, and impedance waveforms between 30 and 40.2 seconds (i.e., after the cross-seam correction had been made) are shown in Figures 94-97. As can be seen, in each of these plots the predominant percentage of the power is concentrated at twice the oscillation frequency, i.e., 1.4 Hz. Hence, the correction, based on simple visual analysis of the current waveform, did indeed result in proper centering of the electrode in the joint.

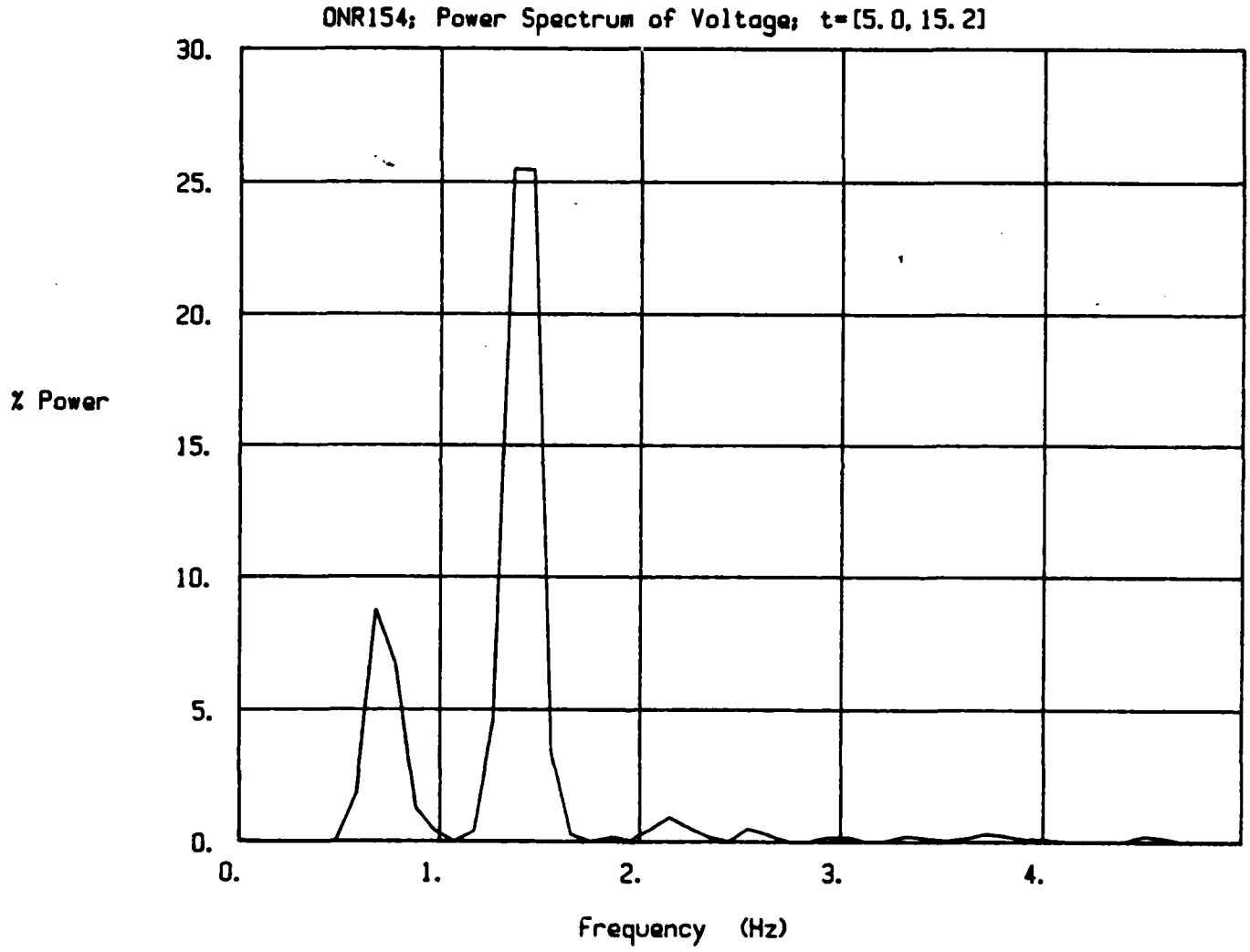

Fig. 90. Power spectrum of voltage waveform taken from data segment between 5 and 15.2 seconds; prior to making correction in centering.

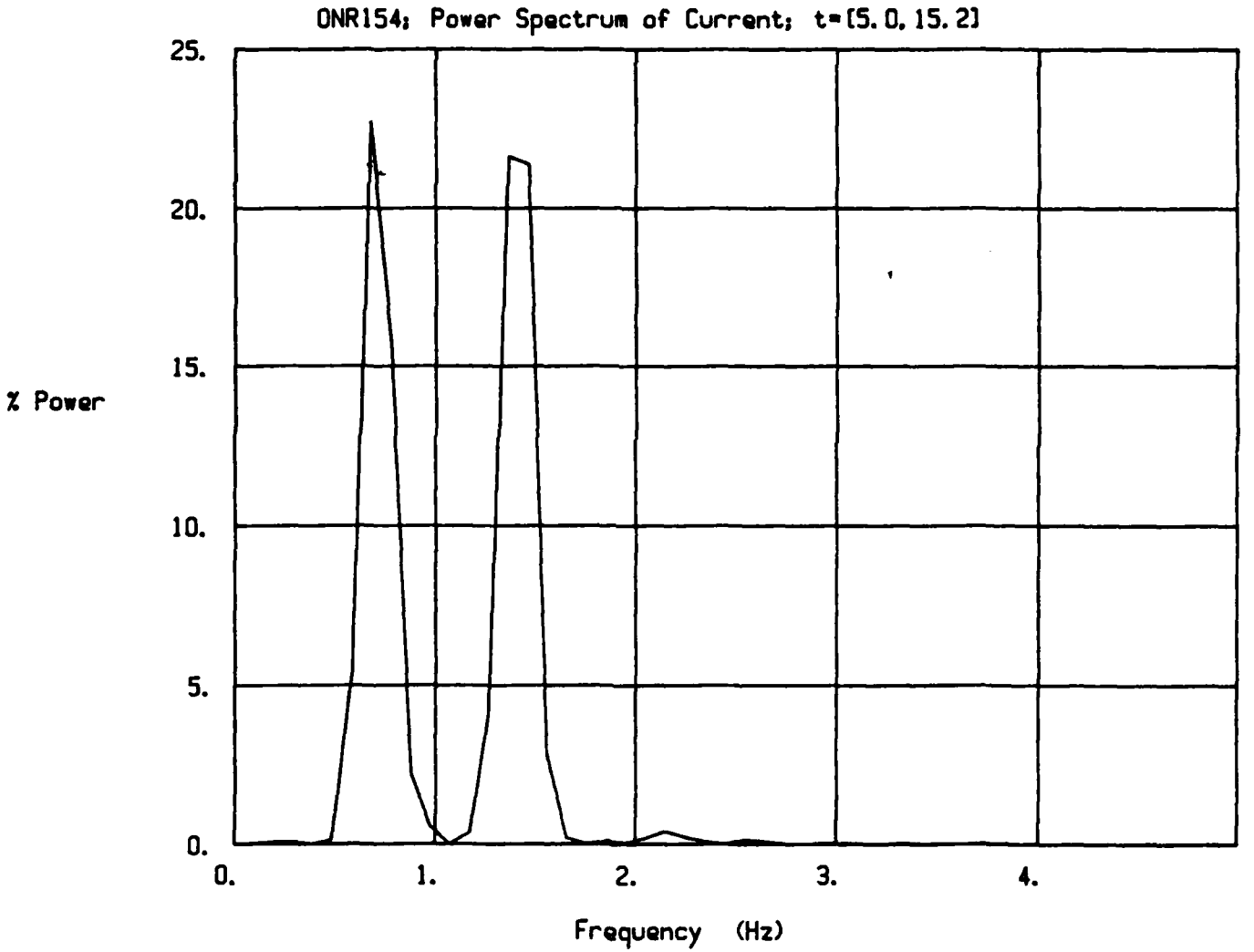

Fig. 91. Power spectrum of current waveform taken from data segment between 5 and 15.2 seconds; prior to making correction in centering.

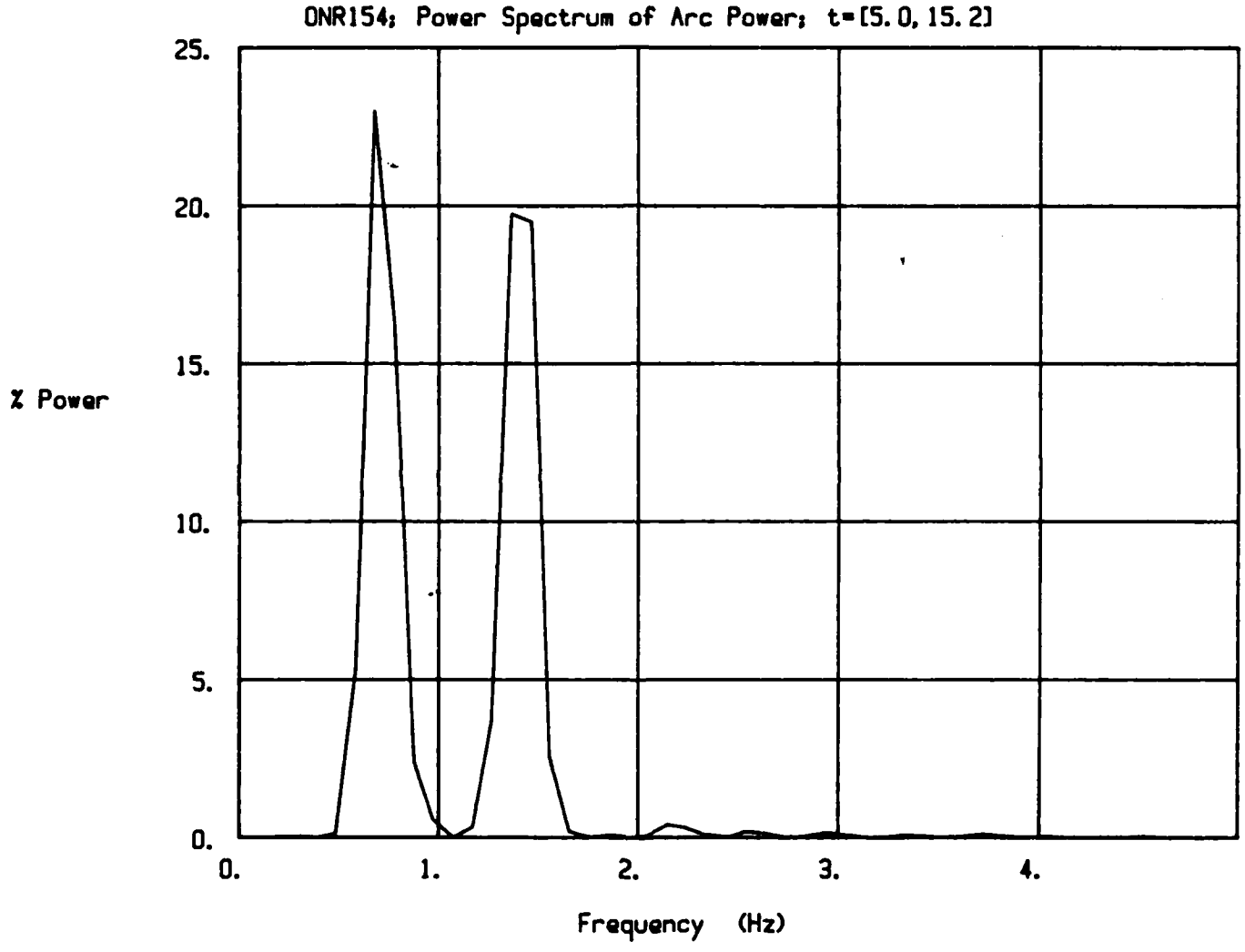

Fig. 92. Power spectrum of instantaneous power waveform taken from data segment between 5 and 15.2 seconds; prior to making correction in centering.

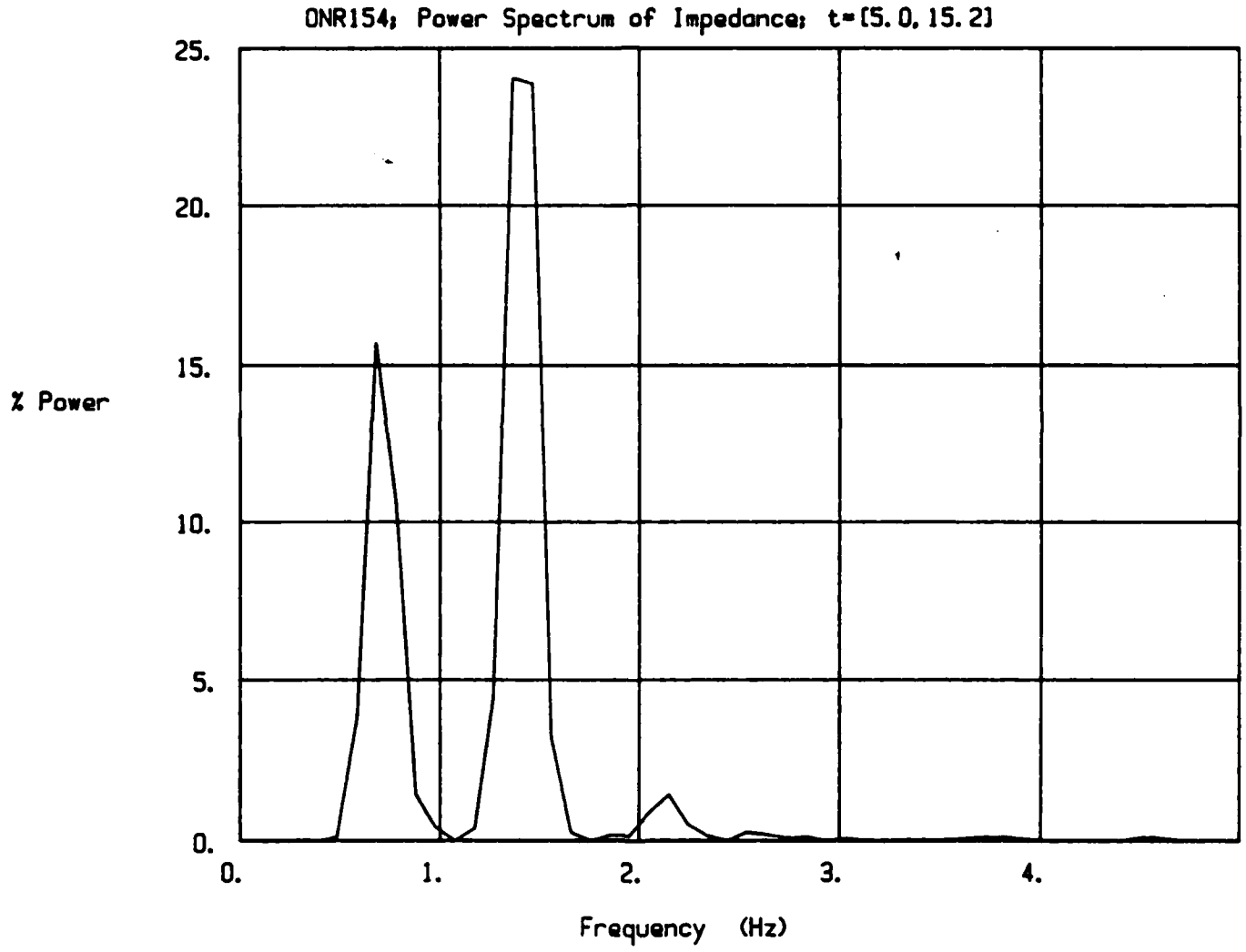

Fig. 93. Power spectrum of instantaneous impedance waveform taken from data segment between 5 and 15.2 seconds; prior to making correction in centering.

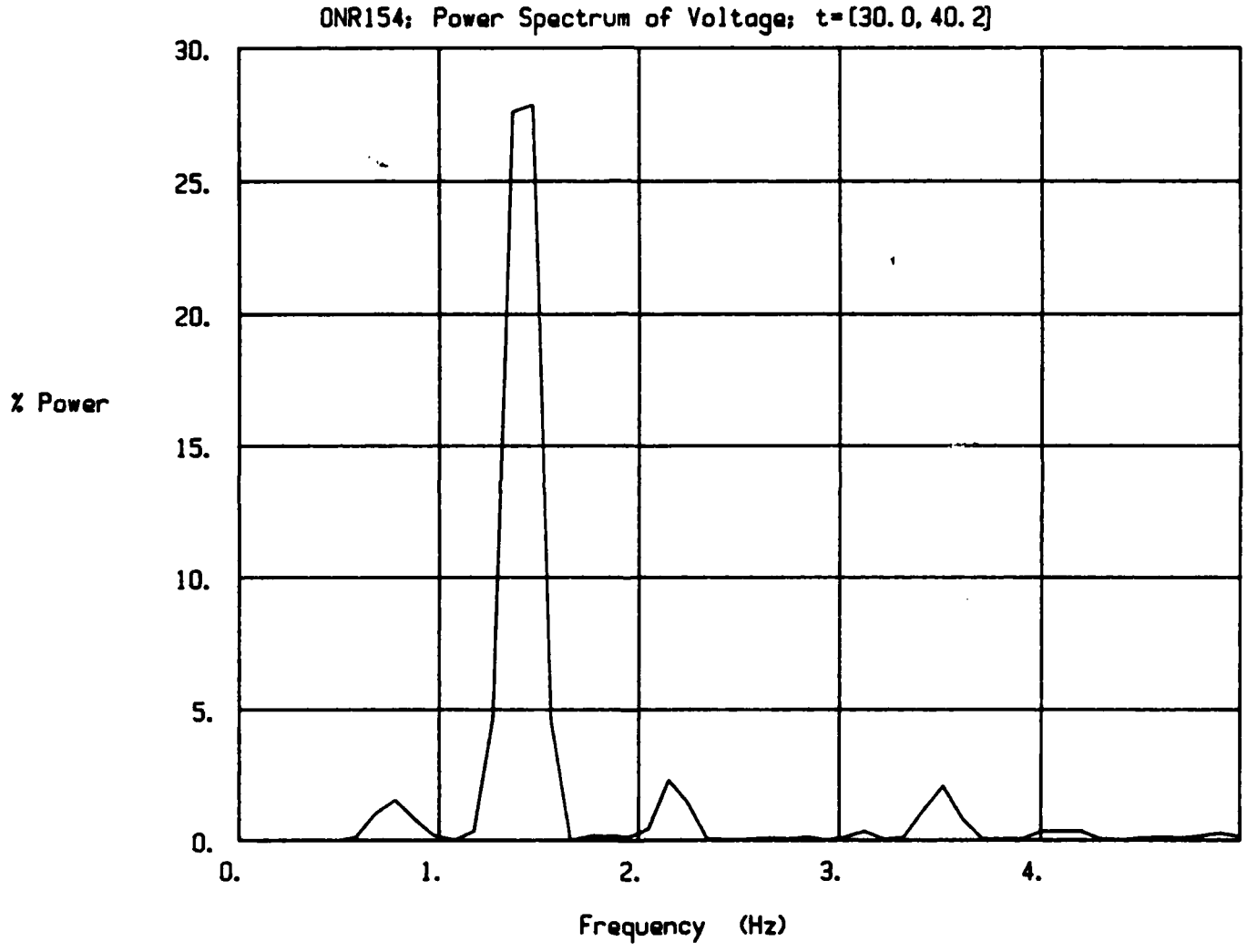

Fig. 94. Power spectrum of voltage waveform taken from data segment between 30 and 40.2 seconds; after making correction in centering.

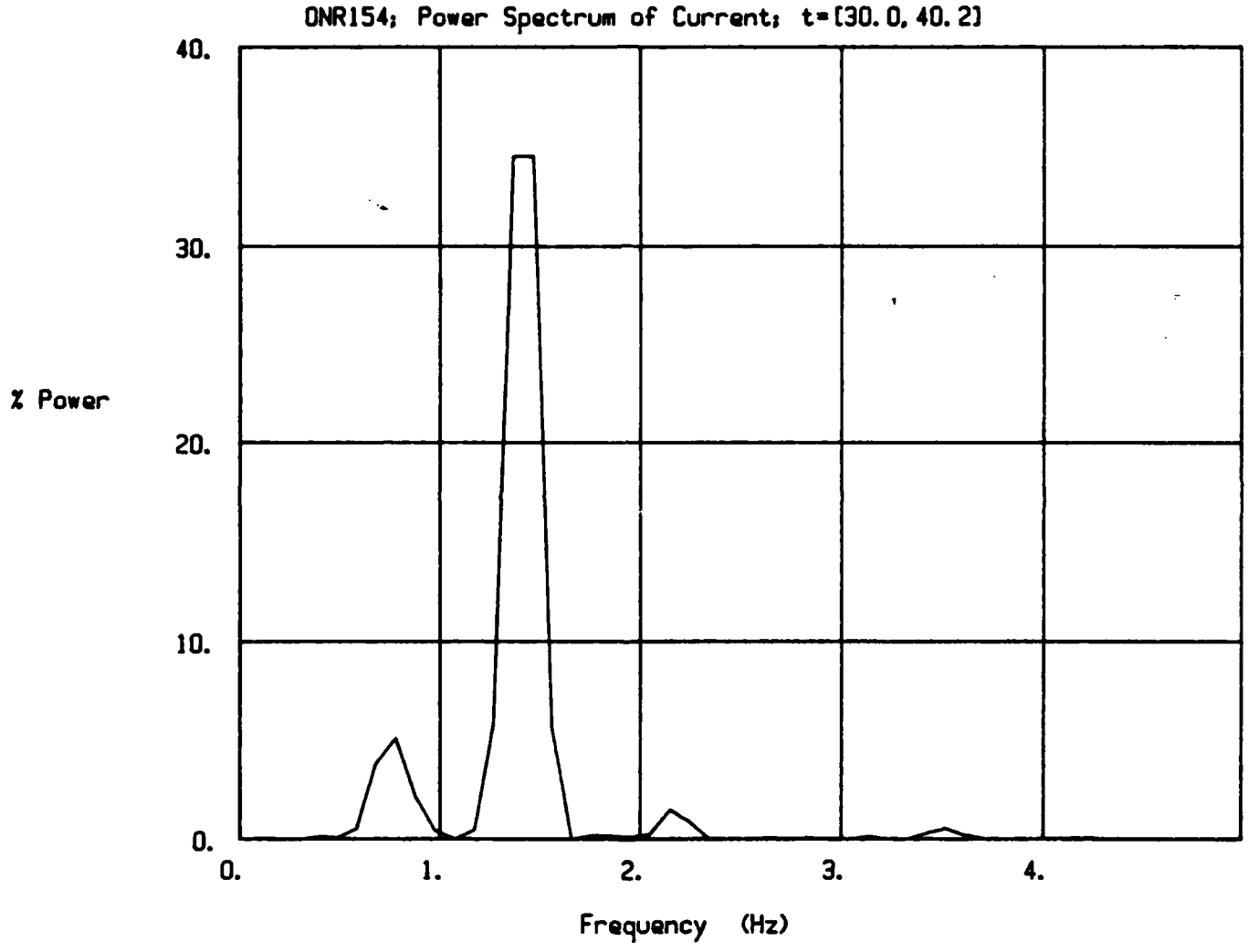

Fig. 95. Power spectrum of current waveform taken from data segment between 30 and 40.2 seconds; after making correction in centering.

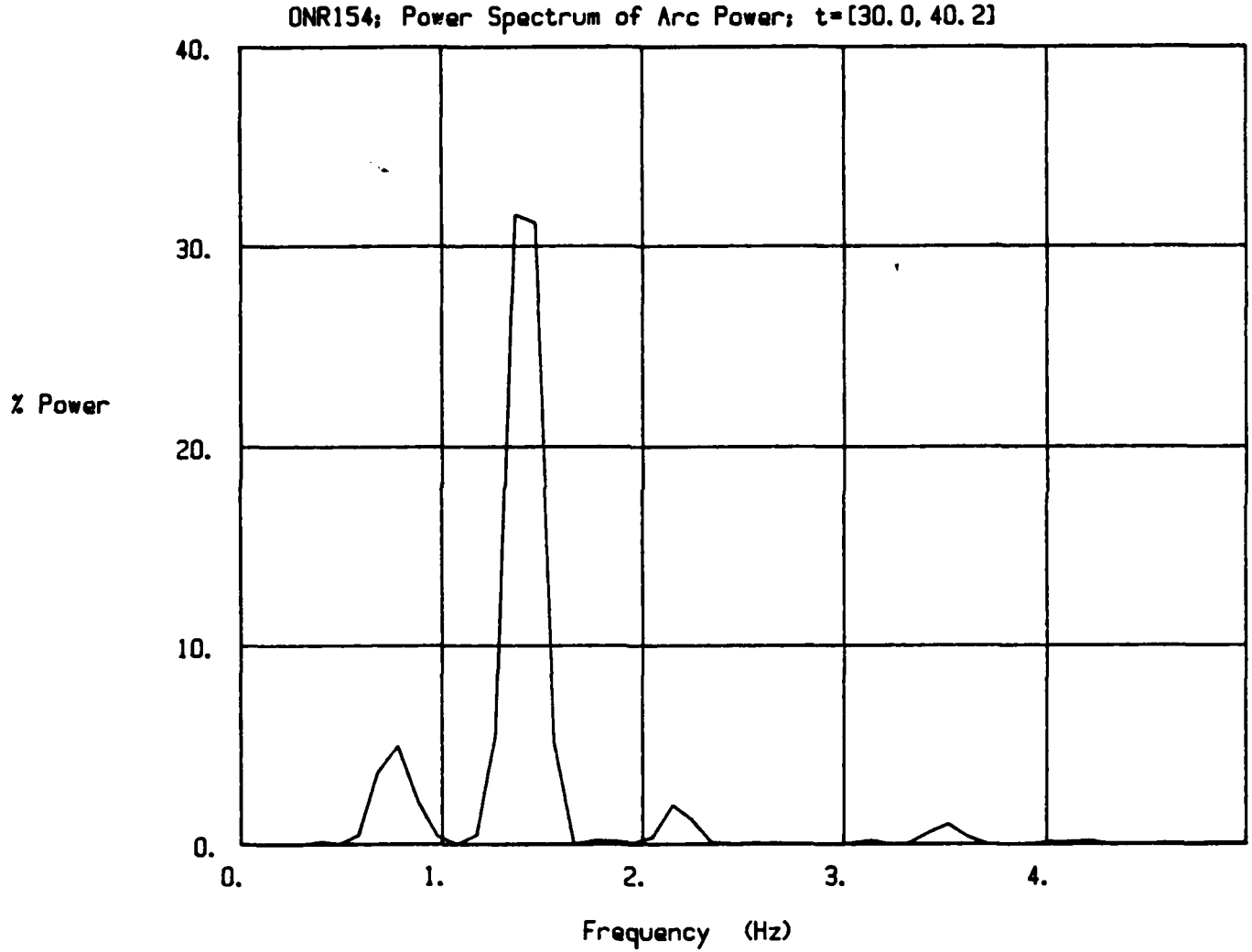

Fig. 96. Power spectrum of instantaneous power taken from data segment between 30 and 40.2 seconds; after making correction in centering.

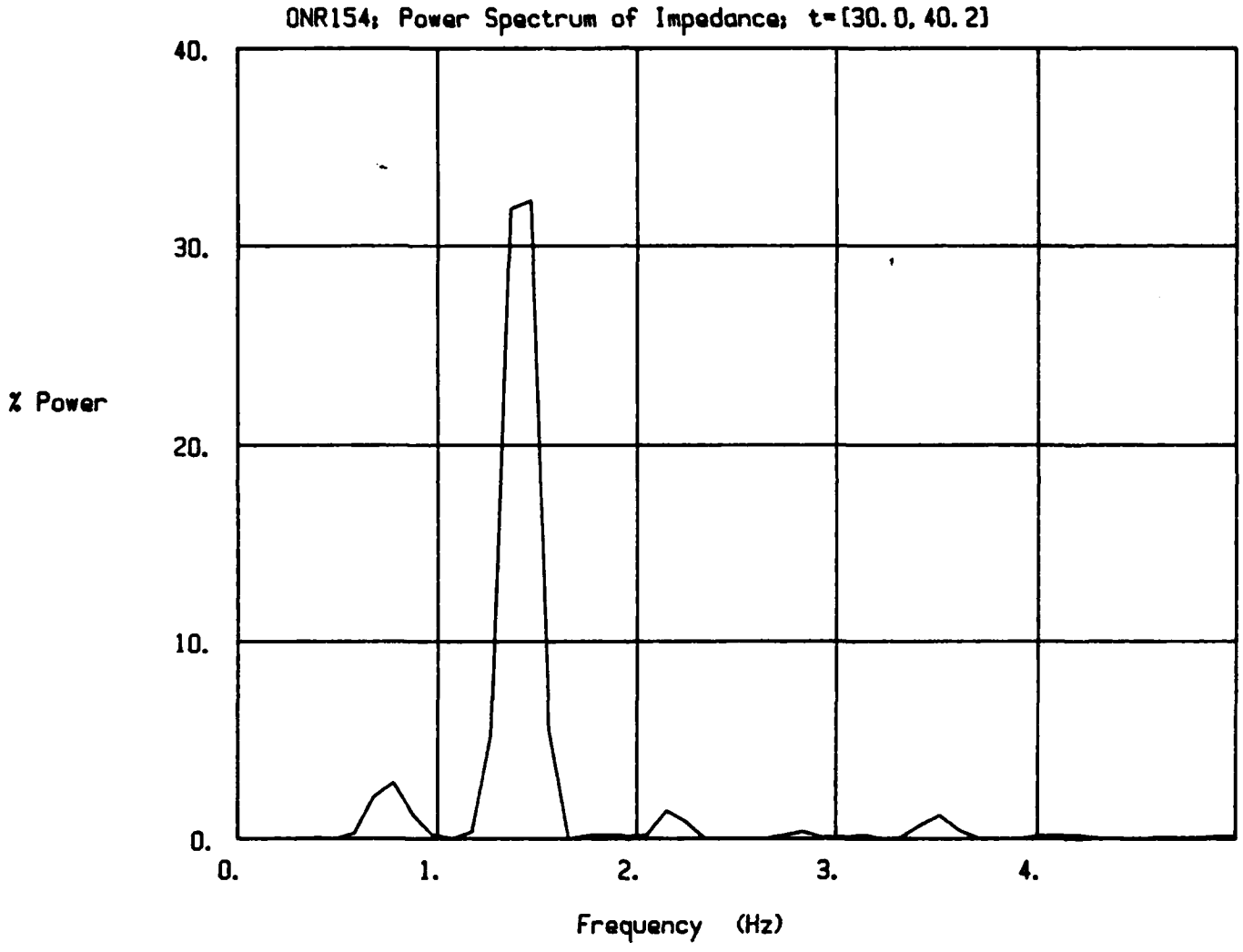

Fig. 97. Power spectrum of instantaneous impedance waveform taken from data segment between 30 and 40.2 seconds; after making correction in centering.

It should also be pointed out that the total correction made in the centering was only 1.13 mm, which is approximately half of the electrode diameter. Normally, tolerances of +/- one-half to one wire diameter in the eletrode centering are considered adequate for assuring a sound weld. Hence, the centering deviation that was detected and corrected was less than an amount normally considered as needing correction!

A metallographic section taken from the weld prior to making the cross-seam correction is shown in Figure 98. A section taken from the weld after the correction was made is shown in Figure 99. Comparing these two figures, it can be seen that the weld was slightly skewed to the right prior to the correction and is centered quite well after the correction.

The purpose of the test weld discussed in this section was to demonstrate the robustness of the arc signal variations versus changes in the CTWD for the SAW process. Obviously, much more sophisticated signal analysis will be used in the actual real-time, computer-controlled system. This should produce even more dramatic results.

Process And System Modeling

Preliminary modeling and simulation work has been done, aimed at identifying and qualitatively assessing major differences between SAW and GMAW processes from the standpoint of arc signals produced by torch oscillation.

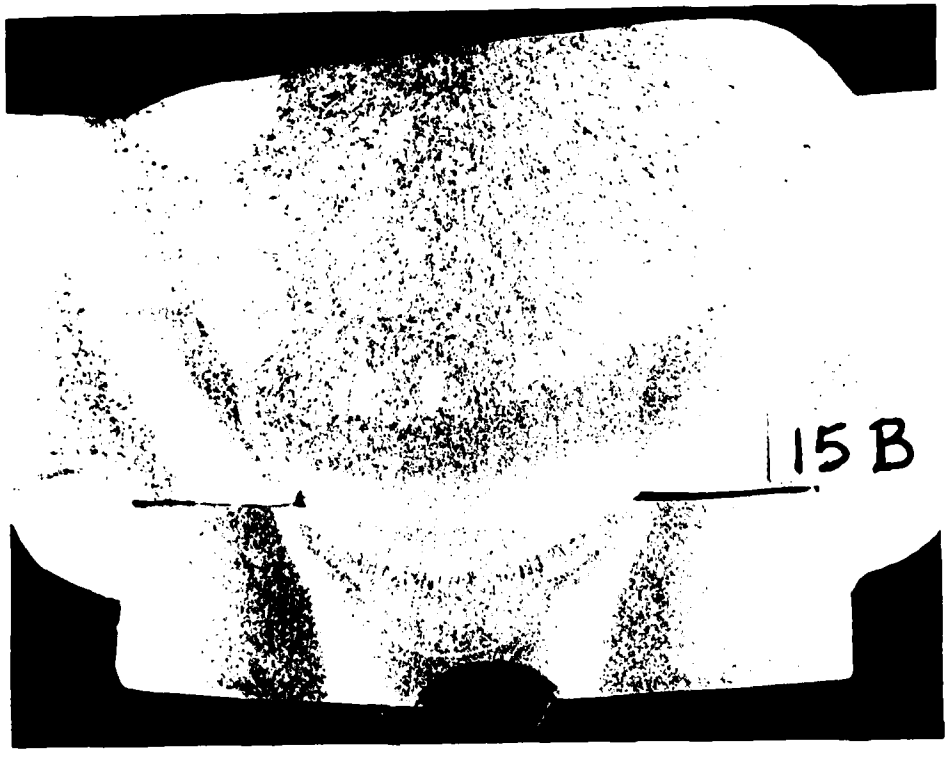

Figure 98. Photomacrograph of weld number 15 prior to making correction in centering.

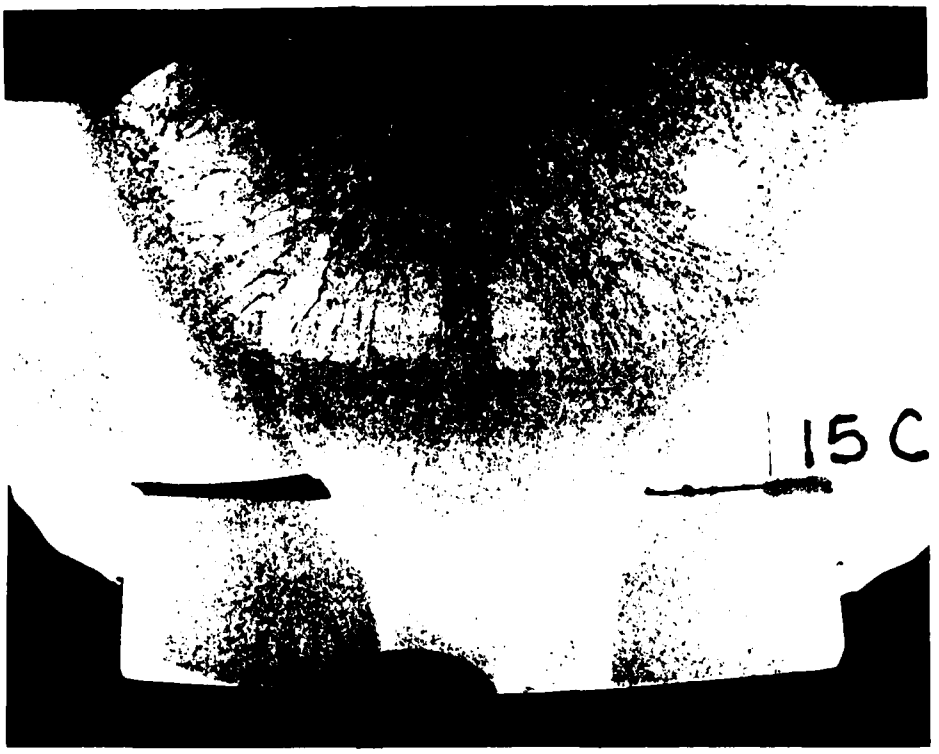

Figure 99. Photomacrograph of weld number 15 after making correction in centering.

The modeling deals with the self-regulation phenomenon in consumable-electrode welding processes; it is the dynamics of electrode burnoff rate in response to a change in CTWD which produce the arc signals observed as a result of torch oscillation.

Background

Work done by Wilson et el. [1], Lesnewich [2], Amson [3], Manz [4], and Halmoy [5], has addressed the burnoff rate of a consumable electrode as a function of process parameters during steady-state conditions. The main parameters involved are current, electrode diameter and composition, work-piece composition, and shielding gas. The results of the past work are expressions relating wire burnoff rate (equal to feed rate in steady-state) to welding current, involving constants based on the other parameters.

Halmoy [5] presents the equation

$$v_b = k_1 J + k_2 L J^2 ,$$

where v_b is the burnoff rate, J is the current density in the electrode, L is the stickout length, and k_1 and k_2 are constants of the process and materials. The first term, linear in J, represents heat input to the electrode through the constant effective anode potential, and varies directly with welding current. The quadratic term represents I^2R heating in the stickout, and may be dominant or insignificant, depending on the process parameters.

Motivation

Based on the Phase I feasibility research program, it is our contention that the current density in the electrode extension is a fundamental difference between typical SAW and GMAW processes. A GMAW process using 0.9 MM wire at a welding current of 250 amperes has a current density of 403 A/mm^2; an SAW process with 2.4 mm wire at 600 amperes has a current density of 135 A/mm^2. One result of this difference is that the I^2R term is much less significant (a factor of three, in this example) for the SAW process. Consequently, the k_1J term dominates, and for a fixed feed rate, the welding current is less sensitive to stickout length than the GMAW process.

A further consequence involves changes in welding current in response to CTWD changes. If CTWD is decreasing at some velocity, the electrode extension must "burn back" at that velocity to maintain constant arc length. In practice, some arc length change must occur to increase current to the level necessary to produce the needed burnback velocity. To match a given CTWD velocity, however, requires a much larger relative current change in a low current-density process. The burnback velocity is the difference between burnoff rate and feed rate; if the feed rate is low (as with SAW), then a much larger relative change in burnoff rate is required for a given CTWD velocity. Since burnoff rate is increased by increasing current, a much larger relative current change results.

Modeling

All of the models developed to date for burnoff rate are valid only in steady-state: i.e. when current and stickout are not time-varying. The models assume that the temperature distribution along the stickout is not changing, and that the I^2R heating at the electrode tip is a function only of current, and not time. If the current had just increased, however, the electrode metal at the tip will not have been exposed to the higher current density for long enough to have acquired the heat predicted by the steady-state model, which assumes it experienced the higher current density throughout its travel along the stickout. The steady-state model incorrectly models burnoff rate for time- varying current. There is significant need for a comprehensive dynamic model of the arc self-regulation process. This will be developed as part of the Phase II research program.

For preliminary investigation, it was decided to use the best existing model for burnoff rate and to incorporate it into a simulation of of the self-regulation process. A voltage loop equation for the welding circuit was written. The power source was modeled as a constant voltage in series with a resistance and inductance. Lesnewich's steady-state relation for burnoff rate was combined with a linear model of the arc characteristics, and these were used with the power source model to simulate system performance on a VAX 11/780 computer.

Using the simulation model described, the CTWD was varied sinusoidally and the corresponding variations in current were plotted. The result of doing this for several different values of frequency are shown in Figure 100 for the GMAW process. As can be seen, below a frequency of approximately 3 Hz, the system is in a steady state condition and the sensitivity is roughly 3.5% of the nominal current per mm change in CTWD. As the frequency increases, the sensitivity begins to increase rapidly at approximately 3 Hz and continues to increase to about 10 Hz. The low-frequency steady-state results of this simulation agree closely with results that have been cited by Cook [6-10]. The simulation result shows that more robust signals would be obtained at faster oscillation rates, i.e., on the order of 10 Hz. For many applications this is excessively rapid, however, and cannot be practially achieved. Therefore, most GMAW and FCAW applications of through-the-arc sensing are based on the steady-state, low frequency conditions shown in Figure 100.

Preliminary simulation work with the SAW process indicates that it will exhibit a response characteristic similar to that shown in Figure 100, only the break frequency will be lower by nearly an order of magnitude. This is an extremely significant observation and must be confirmed by more thorough and accurate modeling of the system dynamics in the Phase II research effort. The low frequency breakpoint predicted for the SAW process as compared to the GMAW and FCAW processes means that the SAW process will exhibit substantially more robust arc signals at reasonable, low frequency oscillation rates. This is exactly what has been observed in the

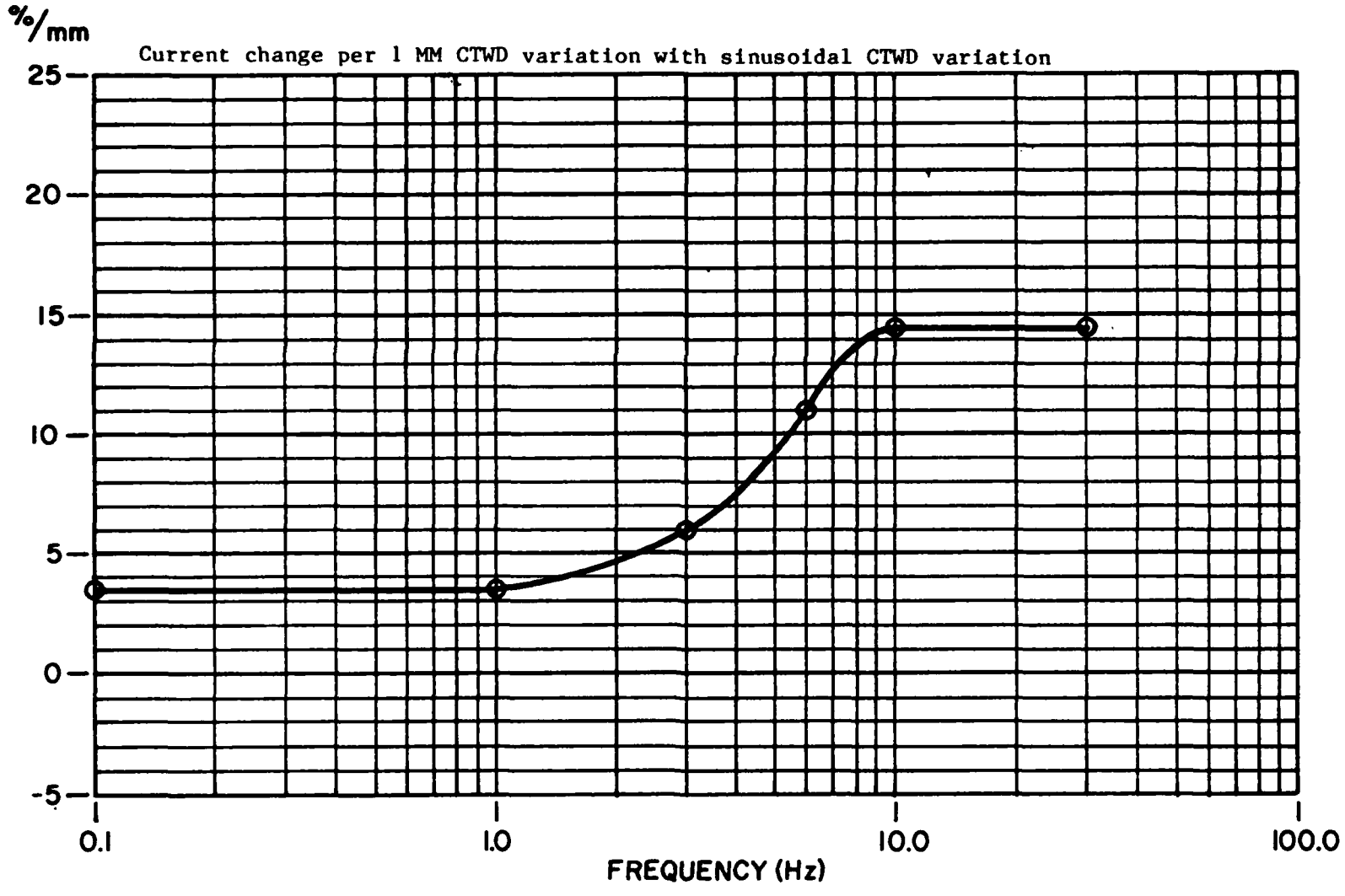

Fig. 100. Frequency response plot obtained from computer simulation for GMAW process.

limited testing of this Phase I feasibility research program. The signals obtained are strong, excellent indicators of joint geometry and electrode position relative to the joint.

Metallographic Sections of Selected Welds and Results

Conventional submerged arc welding does not use electrode oscillation. Consequently, it was important to determine if the oscillation of the electrode necessary for through-the-arc tracking would create lack-of-fusion or other defects in the weld, particularly in the Narrow Gap joint design. To investigate this concern, welds 6 and 7 were deposited in Narrow Gap joints. Weld 6, shown in Figure 101, did not use electrode oscillation. Weld 7, shown in Figure 102, used an electrode oscillation of 3.3 mm. All other welding parameters used in depositing the welds were identical.

It can be seen that both welds are well formed, symmetrical, and have good sidewall fusion. Weld 7 is wider at the root than weld 6 by 3 mm, the width of the oscillation. The other welds deposited in the 45-degree included angle joints using oscillation also showed good sidewall fusion and no adverse effects of oscillation.

DISCUSSION

While the tests conducted in this Phase I feasibility study have been limited in scope, and hence, not within themselves, necessarily indicative

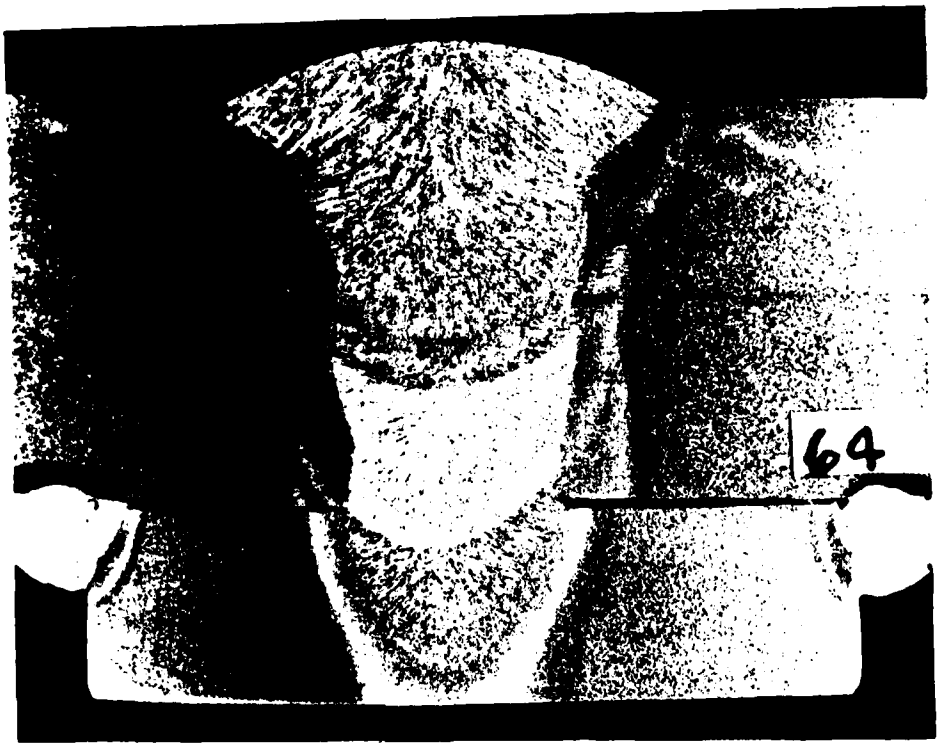

Figure 101. Photomacrograph of weld number 6.

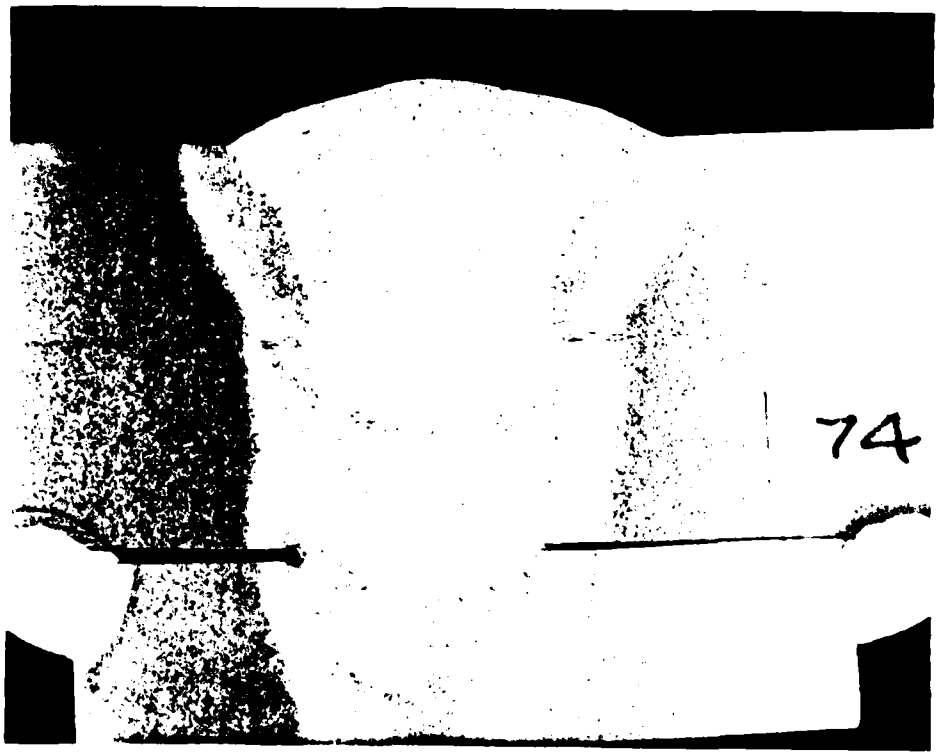

Figure 102. Photomacrograph of weld number 7.

of general results, the knowledge that has been gained points to through-the-arc sensing as an excellent tool for SAW. The dynamics of the SAW process are substantially different from the other consumable electrode welding processes, and the difference makes the through-the-arc sensing methodology much more easily applied to SAW than the other processes for which it has already been proven successful.

On all of the tests conducted, the signal analysis proved to be capable of predicting the need for corrections in electrode centering, oscillation width, and CTWD well in advance of when they would be considered necessary by conventional rules of thumb for acceptable tolerances. Such exellent sensitivity was not anticipated at the beginning of the research effort. Indeed, it was felt that if the signal variatons of the SAW process simply proved to be as good as that of the other consumable electrode processes, then the research effort would be quite successful. Having found the SAW process to exhibit much greater sensitivity than expected has simply magnified the success of the program.

The discovery of the substantial difference in the SAW process dynamics, as compared to the other consumable electrode processes, point to the urgent need for more fundamental understanding of process dynamics than currently exists. This, along with expanding the scope of the test variables, will be a major thrust of the Phase II research effort.

As a by-product of the Phase I findings, the data acquisition, reduction, and analysis method developed have proven to be excellent diagnostic tools

for better understanding, monitoring, and controlling of the SAW process. For example, for tests set up under conditions that would normally be considered quite adequate for producing sound welds, the analysis methods clearly showed large variations in the electrode straightness, that would otherwise go undetected until after the fact. While, perhaps within the acceptable tolerance range for conventional joint designs, such a condition would likely result in frequent lack of sidewall fusion in more critical narrow gap welding. It is further predicted that statistical analysis of the signals acquired will be correlatable with various defect causes such as moisture in the flux or on the electrode, or minor element variations in the electrode or workpiece. These topics will also be explored in the Phase II research effort.

CONCLUSIONS

Based on the limited scope of effort possible with the Phase I feasibility research program, it can be concluded that lateral cross-seam oscillation of the electrode does not have a detrimental effect on the SA weld; instead, it may offer advantages in terms of bead geometry, sidewall fusion, and perhaps strength and toughness. The current and voltage signal variations that result from the lateral cross-seam oscillation are very robust and quite indicative of weld joint geometry and electrode placement relative to the joint.

The dynamics of the SAW process are substantially different than the dynamics of the other consumable electrode processes. As a result, the

voltage and current variations as a function of changes in the CTWD are greater by nearly an order of magnitude as compared to the other processes.

Digital data acquisition and analysis of the current and voltage signals can serve as an excellent diagnostic tool for better understanding, monitoring, and control of the SAW process.

Unlike the other consumable electrode processes, process dynamics plays a major role in the operation of the SAW process with through-the-arc sensing for purposes of monitoring and control. While steady-state conditions have been discussed at length in the literature, the dynamic characteristics and development of dynamic models of the SAW process have not been previously addressed.

RECOMMENDATIONS

The limited research effort of the Phase I research program has shown that through-the-arc sensing and control methodology offers excellent promise for the SAW process. Indeed, the results achieved suggest that through-the-arc sensing will be potentially more powerful as a diagnostic and control tool for the SAW process than the other consumable electrode processes, where it has already met with high success. However, it is the very reasons why the SAW process may prove to be the most applicable for through-the-arc methodologies, that additional research is necessary and very important.

Listed below are the research extensions believed necessary to fully exploit the results of the Phase I feasibility research effort.

1. Thorough and accurate models of the process dynamics must be developed. These models must be applicable to the range of power sources normally employed with the SAW process. The fundamental knowledge gained from this effort will not only lead to full understanding of what is required for optimum SAW process control, but it will fill a gap that exists in the knowledge of other consumable electrode processes, as well.

2. The limited research conducted in the Phase I program must be extended to include a full range of electrode sizes, materials, joint designs, fluxes, multiple-electrode configurations, and ac and dc power sources.

3. Based on the more extensive data base determined in item 2, continued research must be conducted to evaluate the effect of lateral oscillation on the SA weld, and to establish the relationship between lateral oscillation and the other process variables and the weld bead geometry.

4. The extended data base determined in item 2, must be used to continue the necessary research to identify the optimum waveform features for pattern recognition, to determine the best pattern recognition algorithms, and to determine and evaluate the optimum control strategies.

5. Both hardware and software must be developed to test and demonstrate the methodologies devised in the previous steps. This must be done over a broad and representative range of SAW conditions.

6. As a by-product of the Phase I findings, the data acquisition and analysis system developed should be used to conduct statistical analysis of the acquired signal waveforms for the purpose of detecting and correcting the occurrence of process faults, such as moisture in the flux or on the electrode, or surface contaminates on the workpiece or electrode. It is believed that the methodologies proposed for further research will not only lead to an adaptive SAW system capable of modifying its parameters to maintain electrode centering, optimum joint fill, and optimum heat input, but one that is capable of detecting and correcting, in real-time, many process fault conditions that would otherwise occur.

REFERENCES

1. Wilson, J.L., et al., "The Effect of I^2R Heating on Electrode Melting Rate," Welding Journal, Vol. 35, No. 1, pp 1s - 8s, 1956.

2. Lesnewich, A., "Control of Melting Rate and Metal Transfer in Gas-Shielded Metal-Arc Welding, Part I - Control of Electrode Melting Rate," Welding Journal, Vol. 35, No. 8, pp 343s - 353s, 1958.

3. Amson, J.C., "An Estimate of the Voltage Fall Along the Electrode Stick-out in the Consumable-Electrode Arc System," IIW Doc 212-202-70.

4. Manz, A.F., "Hot Wire Welding and Surfacing Techniques," WRC Bulletin 223.

5. Halmoy, E., "Wire Melting Rate, Droplet Temperature, and Effective Anode Melting Potential," Arc Physics and Weld Pool Behavior, The Welding Institute, Cambridge, England, May, 1979.

6. Cook, G.E., "Adaptive Positioning Control for Arc Welding: Noncontact Sensing Via the Arc," NSF Workshop on Assembly and Inspection, Ed.: J. Boothroyd, AMherst: U. of Mass., 1981, 5 pgs.

7. Cook, G.E., "Through-the-Arc Sensing for Arc Welding," Proc.: Tenth Conf. on Production Research and Technology, NSF, ISBN 0-89883--087-7, March 1983, pp 141-151.

8. Cook, G.E., "Through-the-Arc Sensing: Positioning Control for Robotic Arc Welding," Proc. of the First Annual International Robot Conf., Los Angeles: Tower Conf. Management Co., June 1983, pp 79-94.

9. Cook, G.E., "Position Sensing With An Electric Arc," Conf. Proc., 13th International Sym. on Industrial Robots and Robot 7, Vol. 1, Soc. of Man. Engrs, April 1983, pp 6-46 - 6-69.

10. Cook, G.E. and Levick, P.C., "Advances in Through-the-Arc Sensing for Adaptive Control," Developments and Innovations for Improved Welding Production, Ed.: G.R. Salter, Cambridge: Welding Institute, Sept. 1983, pp P11-1 - P11-9.

END

DTIC

5-86